DESIGN AND APPLICATION OF MICROFLUIDIC PLATFORMS FOR INTEGRATED ADIPOCYTE PERFUSION AND SECRETION ANALYSIS BY ENZYME ASSAY AND MASS SPECTROMETRY

by

Colleen Elisabeth Dugan

A dissertation submitted in partial fulfillment
of the requirements for the degree of
Doctor of Philosophy
(Chemistry)
in the University of Michigan
2016

Doctoral Committee:

Professor Robert T. Kennedy, Chair
Professor Kristina Hakansson
Professor Ormond A. MacDougald
Associate Professor Stephen Maldonado

To my family

ACKNOWLEDGEMENTS

I first want to sincerely thank my advisor, Dr. Robert Kennedy. I am so grateful to have had the opportunity to work in your lab and learn from such an accomplished scientist. While working on a project that somewhat deviated from the rest of the group, you were very supportive and encouraged my pursuits. You allotted me the freedom to be creative in my chip designs and plan my experimental directions, which has really helped me hone my research skills; and you could also recognize when I was stuck on a particular challenge and would offer great advice.

I would also like to thank my dissertation committee. I am very appreciative to Dr. Ormond MacDougald for meeting with me to discuss my progress and offering insight into the biological side of my results. I really learned a lot from those discussions and collaboration. Thank you Dr. Kristina Hakansson and Dr. Stephen Maldonado for offering many great research suggestions during my committee meetings; getting your input helped me address different aspects and perspectives of my projects.

Thank you to the MacDougald lab for sharing your lab space for cell culture. I especially want to thank Will for culturing adipocytes for me when I was first getting started with my project, and also Sebastian for training me to do cell culture once I started needing adipocytes more frequently. It has been a great skill to learn and helped me better bridge the chemistry and biology aspects of my projects.

I want to thank the Kennedy lab members that I have had the pleasure to worked with, past and present. Maojun and Jing got me started working with microfluidics and

trained me in all the fabrication and assembly techniques. Jim helped immensely throughout the whole process of the chip-MS project—we didn't make our initial timeframe goal, but we got it working! So many people from lab have helped me throughout my research, from troubleshooting software, helping to fix an instrument mid-experiment or just offering great advice, discussion and encouragement.

I want to thank all of the amazing friends that I have made here at Michigan. We navigated through grad school together, were a constant support system for each other and celebrated so many accomplishments and milestones together. Thank you for the years of wonderful memories, laughs, and countless adventures. A special shout-out to the 'square' – Wendi, Casey and Laura, we have been through it all together and I am so glad to have your friendship and support.

Finally, I would like to thank my family. You have taught me to be true to myself and shoot for the stars, and always remind me that I can accomplish whatever I set my mind to. Words cannot express my gratitude for your constant encouragement and support. It truly means the world to me and I wouldn't be where I am today without it.

TABLE OF CONTENTS

DEDICATION ii

ACKNOWLEDGEMENTS iii

LIST OF FIGURES vii

LIST OF APPENDICES xvi

ABSTRACT xvii

CHAPTER 1: INTRODUCTION 1

Microfluidics 1

Microfluidic Cell Perfusion 11

Adipocyte Metabolism 16

Dissertation Overview 20

CHAPTER 2: MULTIPLEXED MICROFLUIDIC ENZYME ASSAYS FOR SIMULTANEOUS DETECTION OF LIPOLYSIS PRODUCTS FROM ADIPOCYTES 30

Introduction 30

Experimental 33

Results & Discussion 42

Conclusions 53

Supplementary Information 54

CHAPTER 3: MONITORING CELL SECRETIONS ON MICROFLUIDIC CHIPS USING SOLID-PHASE EXTRACTION WITH MASS SPECTROMETRY 61
Introduction 61
Experimental 65
Results and Discussion 70
Conclusions 80
Supplementary Information 81
CHAPTER 4: MICROFLUIDIC DUAL ASSAY CHIP FOR MONITORING ADIPOCYTE LIPOLYSIS PRODUCTS 88
Introduction 88
Experimental 91
Results & Discussion 97
Conclusions 104
CHAPTER 5: DISSERTATION SUMMARY 108
Future Directions 111
APPENDICES 124

LIST OF FIGURES

Figure 1.1: PDMS channel filled with 10 µM rhodamine B at time 0, 1 and 4 hrs. Over time the analyte absorbs into the PDMS bulk, as visualized by fluorescence. 3

Figure 1.2: PDMS chip fabrication procedure. A high-resolution CAD transparency is printed with the channel features (a). Photoresist is spun on a Si wafer (b). Transparency is positioned over wafer and UV light is exposed (c). Photoresist is developed and only channel features remain on the wafer (d). PDMS pre-polymer is cast over the mold and cured (e). The PDMS can be peeled away from the wafer with the channel features embedded in the polymer (f). 5

Figure 1.3: Surface chemistry of PDMS in the native state and with exposed surface silanol groups. 6

Figure 1.4: Schematic of diffusive mixing and Taylor dispersion in a microchannel. As fluids from 2 streams are joined in one channel, there is minimal mixing initially. At longer times the chemical species undergo lateral diffusive mixing. Additionally, due to the parabolic flow profile in microchannels, Taylor dispersion is observed over time. 9

Figure 1.5: Demonstration of microfluidic integration; an entire PCR is completed on one µTAS device. 10

Figure 1.6: An integrated microfluidic device, containing a cell chamber, chemical assay reaction channels and an on-line detection method. 13

Figure 1.7: A system devised to couple on-chip cell perfusion with MS detection. Cells are incubated in chambers and media is flowed from the chamber onto a packed SPE bed in a subsequent chip. That chip is then disconnected from the cell chamber chip, the SPE bed is washed and analyte is eluted continuously into the MS ESI source..... 15

Figure 1.8: Graphic representation of lipolysis and NEFA recycling in adipocytes. 17

Figure 1.9: Multilayer glass chip developed to perfuse 3T3-L1 adipocytes on-chip followed by integrated enzyme assay reaction channels to continuously measure secreted NEFAs. 20

Figure 2.1: Design of the 3 different fabricated layers in the PDMS multi-layer chip. The control layer (a), the reaction channel layer (b), and the base chamber layer (c) fabrication patterns are shown. The fluorogenic dye, Amplex UlraRed, is abbreviated as AUR. The blue circles in (a) represent the points where access holes were punched through the PDMS, and the red line in (b) indicates the portion of the design that was fabricated with AZ photoresist. 35

Figure 2.2: Side view of chip slice showing fabrication layers and direction of flow. The dotted lines represent the interfaces between layers that were irreversibly bonded. 36

Figure 2.3: The assembled chip in compression frame. Blue food dye is being perfused through one of the valves for better visualization. The arrows highlight the capillary connections and the direction of fluid flow. 40

Figure 2.4: COMSOL modeling of the dual chip. (a) The velocity of laminar flow at the flow split allowed the ratio of cell perfusate that would be directed into each assay reaction channel to be determined. (b) The mixing efficiency could be measured at a reagent inlet by injecting a 5 µM chemical species at the flow split and a blank solution at the reagent inlet, and finding the point in which complete diffusion has occurred across the width of the channel. (c) A concentration gradient moving through the cell chamber when a 5 µM chemical species was injected was modeled to show the profile of flow across the width of the chamber. 44

Figure 2.5: Dual chip calibration. (a) Detector trace (plotted as relative fluorescence units, RFU) from step changes of glycerol and NEFA standards in the dual chip, which are simultaneously detected. The resulting calibration curve for the glycerol assay (b) for 4 replicate experiments show a linear response through 112 µM, a LOD of 5 µM and R^2 of 0.998. The fatty acid assay (c) is linear through 150 µM, and has a LOD of 6 µM and R^2 of 0.999 for 4 replicate experiments..... 46

Figure 2.6: Step changes on glycerol assay independent chip from high to low concentration standards without (a) and with (b) fabricated valves. 48

Figure 2.7: NEFA calibration curves illustrate the improved assay sensitivity with daily SDS modification (a). The real-time traces of on-line switching from low to high concentration are shown in (b). Assay 1 was performed immediately after SDS modification. Assay 2 was run a subsequent day without prior SDS modification, and a lower sensitivity is observed. The original sensitivity can be restored; SDS modification was done before assay 3 and improved signal is seen. All 3 assays were performed on the same chip. 50

Figure 2.8: Representative traces of simultaneous detection of NEFA and glycerol secretion from adipocytes and trends in day-to-day experiments. Traces were collected during basal secretion and during lipolysis stimulation by the application of isoproterenol, represented by the black bar. (a) Cells day 14 post-induction (PID). (b) Cells day 35 post-induction. (c) The NEFA/glycerol ratio decreased for basal secretion the longer the adipocytes remained in culture. (d) As the cells matured, the ratio of average isoproterenol-stimulated cell response to the average basal response increased for the NEFA assay and decreased for the glycerol assay. 53

Figure 2.9: Calibration curves for the glycerol (a) and NEFA (b) assays, performed on the respective single assay chips. The error bars are the standard deviations of the averaged time points. 56

Figure 3.1: PDMS mold layers. Each box indicates a different fabricated layer; (a) lower cell chamber, (b) fluidic layer, and (c) valve control layer. The numbers in (c) indicate the valves that are operated together on the same solenoid valve. 67

Figure 3.2: Schematic of chip connection to SPE column and ESI components. 69

Figure 3.3: Operation modes for the injection loop chip. Closed valves are black and open valves are white. (a) Loop fills with perfusate from cell chamber (red) and flows to a waste outlet, while the wash solvent (blue) bypasses the loop and is directed towards the SPE bed. (b) The cell perfusate is flushed out of the loop and onto the SPE bed by the wash solvent. Flow from the cell chamber is directed towards a waste outlet upstream of the loop. (c) Valves are in the same mode as (a), but wash solvent is replaced with elution solvent (green). Elution solvent bypasses the loop and is flowed onto the SPE bed, while the loop fills with cell perfusate again..... 73

Figure 3.4: Calibration curve of palmitoleic acid (POA) standard, performed in duplicate. POA was dissolved in basal buffer and perfused through the chip at the inlet upstream of the cell chamber. Standard filled the loop, was loaded onto the SPE bed, washed and eluted to the MS in an on-line format..... 76

Figure 3.5: Full scan analysis of m/z ranging from 200-320 was performed for all experiments on a QQQ-MS. (a) Mass spectrum of on-line elution profile from 3T3-L1 adipocytes. Adipocytes were loaded in the cell chamber and stimulated with isoproterenol/forskolin in this example spectrum. Perfusate was loaded onto the on-line SPE bed. The SPE bed was subsequently washed and sample was eluted to the MS. Peaks are labeled with the NEFAs that associate with the appropriate m/z. (b) Mass spectrum of direct injection of elution buffer, showing background signal of 16:0 and 18:0. 78

Figure 3.6: Averaged peak area of various NEFAs detected by MS from on-chip adipocyte secretion under basal and isoproterenol/forskolin (iso/fsk) stimulation. Data is average of 3 cell experimental replicates ± standard deviation, statistical significance determined by paired, 2-tailed Student's t-test, * $P < 0.1$, ** $P < 0.05$, *** $P < 0.01$. 80

Figure 3.7: Extracted ion chromatogram of 8 NEFAs in adipocyte conditioned buffer, measured with HPLC-TOF-MS (a) along with the associated mass spectra of the most abundant NEFAs (b). 83

Figure 4.1: Overview of microfluidic chip design. Arrows indicate inlet and outlet channels, with the respective reagents flowing through each. 96

Figure 4.2: Basal and isoproterenol-stimulated (ISO) measurements plotted as a function of NEFA/GLY release from 3T3-L1 adipocytes. Statistical significance determined by paired (between BASAL and ISO for each technique) or unpaired (between bars of the same color) Student's t-test. * $P < 0.01$, ** $P < 0.0001$, $n = 10$. 99

Figure 4.3: Simultaneous detection of NEFA and glycerol (GLY) release from 3T3-L1 adipocytes. Cells are perfused with basal buffer and then stimulated with 20 µM isoproterenol as indicated by the black bar. (a) Isoproterenol stimulation of 6 min. (b) Isoproterenol stimulation of 50 s and 60 s in the same experiment. 101

Figure 4.4: Mechanisms of adipocyte lipolysis: pathway of stimulated lipolysis by an adrenergic agonist (a) and possible variations in protein action with acute or prolonged stimulation (b). 103

Figure 5.1: Microfabricated fluorescence fiber optic probe (a) and calibration step plots of on-chip glycerol enzyme assay, measured with the probe (b)..... 113

Figure 5.2: Moat design for on-chip SPE packing. (a) Schematic of channel dimensions and (b) 20 µm particles packed in a PDMS channel..... 115

Figure 5.3: Proposed injection loop chip design with added valve at the wash/elution solvent inlet. 116

Figure 5.4: Schematic of adipocyte with different chemical stimuli regulatory action on fatty acid (FA) storage/lipolysis. Insulin promotes FA re-esterification into the lipid droplet, and inhibits lipolysis. Adenosine and a-catecholamines also inhibit lipolysis, whereas b-catecholamines, growth hormones promote lipolysis..... 121

Figure A.1: Set-up and operation diagram for dual assay chip..... 127

Figure C.1: Experimental reaction scheme modeled with COMSOL. Diffusion of GLN and GLU through microdialysis probe was simulated along with theoretical neuronal turnover of GLN to GLU. 131

Figure C.2: Modeling of microdialysis probe *in vivo*. (A) Diagram of COMSOL model with reaction domain highlighted in the legend. (B) Flux of infused GLN across dialysis membrane and concentration profile across regions, with varied brain 'consumption' reaction rates. (C) Measurement of concentration profiles for infused GLN, and GLU formed outside the probe (k1 = 10, k2 = 100, k3 = 100 s^{-1}). 142

Figure D.1: Velocity plot of flow through dual assay chip..... 146

Figure D.2: Flow split analysis of dual assay chip. (A) Diagram of chip and measurement points. (B) Flow velocity at points A & B were monitored while glycerol reagent flow rates were varied. 147

Figure D.3: Step change plot of dual assay chip. Top inlet flow rate changed from 0 to 0.5 mM (other inlets remained at 0 mM, hence the varying maximum concentrations). 148

Figure D.4: On-chip reagent mixing efficiency. (A) Pictoral representation of 2 concentrations of a chemical species mixing at a reagent inlet on the dual assay chip. (B) Concentration of the chemical species was measured across the width of the channel at various distances from the reagent inlet. 149

Figure E.1: A) Recovery for probe with 30% porosity and B) for 0.9% porosity..... 156

LIST OF APPENDICES

APPENDIX A: FABRICATION AND OPERATION TIPS 124

APPENDIX B: OFF-LINE ASSAY PROTOCOLS.....128

APPENDIX C: COMSOL MODELING OF MICRODIALYSIS PROBES 130

APPENDIX D: COMSOL MODELING OF DUAL ASSAY CHIP 143

APPENDIX E: COMSOL MODELING OF MICROFABRICATED PROBE.....150

ABSTRACT

DESIGN AND APPLICATION OF MICROFLUIDIC PLATFORMS FOR INTEGRATED ADIPOCYTE PERFUSION AND SECRETION ANALYSIS BY ENZYME ASSAY AND MASS SPECTROMETRY

by

Colleen Elisabeth Dugan

Chair: Robert T. Kennedy

Microfluidic chips enable integration of many components onto one miniaturized platform, creating highly automated devices with the potential for increased throughput of chemical analysis processes. Chips can be adapted to load and perfuse cells; the continuous flow principle of these devices is more biomimetic to the *in vivo* cellular environment, and allows collection and analysis of secreted metabolites with greater temporal resolution. To learn more about their cellular function, polydimethyl siloxane (PDMS) microfluidic devices were developed to perfuse 3T3-L1 adipocytes and measure secreted lipolysis products. A chip was constructed that contained a cell perfusion chamber with integrated fluorescent enzyme assay reaction channels to simultaneously monitor adipocyte release of non-esterified fatty acids (NEFAs) and glycerol. This multiplexed analysis was measured with laser-induced fluorescence (LIF) detection. The NEFA assay had a limit of detection (LOD) of 6 μM and the glycerol assay had a LOD of

5 µM; both assays had sufficient linear dynamic ranges to measure the secreted products at a flow rate of 0.75 µL/min. Initial studies monitored the secretion of lipolysis products under basal and stimulated conditions. With simultaneous detection, NEFA recycling could be inferred, based on the ratio of secreted NEFAs to glycerol. Further studies compared on-line perfusion and analysis to conventional off-line techniques in terms of NEFA recycling; initial findings suggest there is less NEFA recycling with on-chip cell perfusion. Additionally, pilot studies investigated the kinetics of lipolysis regulation by applying brief pulses of chemical stimuli.

A second chip was developed to couple on-line adipocyte perfusion with mass spectrometry (MS) detection to learn more about the identities of secreted NEFAs. As the enzyme assay only permits measurement of total NEFA concentration, MS allows multiplexed analyte detection. An injection loop was integrated downstream of a cell perfusion chamber, operated with multilayer pneumatically-actuated valves. The injection loop acted to isolate the cells from the back pressures generated from the solid phase extraction (SPE) bed coupled to the chip, which was necessary to improve electrospray ionization (ESI)-MS efficiency. Eight NEFAs secreted from adipocytes were monitored under basal and lipolysis-stimulated conditions using this chip.

CHAPTER 1

INTRODUCTION

Miniaturization and automation of chemical analysis tools has become a pinnacle aim of recent scientific research and discovery. The advancements of microfluidic techniques have been pivotal in achieving this objective. Generally hailed for their small footprint and reduced reagent consumption, these devices (chips) have immense attributes that extend much further. Microfluidic applications are incredibly broad and can extend many disciplines, bridging chemistry and biology, and have assisted in bringing advances to our knowledge on myriad topics.

One microfluidics application that has become momentous in recent years is the capability to perfuse cells on-chip. The ability to constantly flow media over cells creates an environment that mimics physiological nutrient circulation *in vivo*, and is one of many advantages that have been harnessed. In this dissertation novel microfluidic platforms that integrate on-chip cell perfusion coupled to automated, on-line analysis methods are described and along with their application to monitoring adipocyte metabolite secretion.

Microfluidics

The essential basis of microfluidic technology is the control of fluid flow on a miniaturized platform. Through photolithography fabrication processes, enclosed microchannels are created on the order of tens to hundreds of microns. Geometries and designs of the channels vary depending on application and chosen substrate, often

offering unparalleled spatiotemporal control. Due to the reduced size of microfluidic flow paths, a substantial reduction of reagent/solvent use is achieved, minimizing cost and waste. Chips can be used repeatedly for experiments, creating an economical alternative to larger scale techniques. Furthermore, the sample size requirement for applications is significantly reduced, making it an ideal tool when limited sample volumes are available.[1.1-3]

Microfluidic Substrates

A number of substrates can be used to create microfluidic chips based on matching the most suitable properties to the application of interest. The type of fabrication process used to create the microchannels is also dependent upon the substrate used. Possible options range from silicon to glass to plastics, each with their own merits. Silicon was commonly used when microfluidics was initially conceived because microelectronic machining fabrication techniques were clearly established. However, the associated expense, fragility and opacity were major deterrents of its extended use. Glass has become the cornerstone substrate for microfluidic capillary electrophoresis (CE) with its inherent chemical resistance and ability to be easily modified. Additionally, glass is optically transparent making it compatible with many detection techniques; however, fabrication of glass chips is accomplished through an isotropic hydrofluoric acid wet etching process and cannot be readily produced in bulk. A variety of plastics have become popular for use as microfluidic devices: polydimethyl siloxane (PDMS), poly(methylmethacrylate), cyclic olefin polymers, and polystyrene, to name a few.[1.4] The latter 3 plastics can be made with injection molding and hot embossing methods, which is favorable for bulk manufacturing. For the remainder of the dissertation, PDMS

microfluidic techniques and devices will be discussed, as that was the substrate utilized in all the dissertation chapters.

PDMS is the most widely used plastic microfluidic substrate, owing to a number of advantages. PDMS is transparent, allowing optical detection techniques to be accomplished on-chip. Optical transparency is also beneficial for general visualization of features on-chip, monitoring flow patterns, and checking for problems like bubbles or fabrication errors. PDMS is inherently elastomeric, allowing for reversible sealing and integrating valves (merits of which will be described in more detail in following chapters). PDMS is gas permeable, making it an ideal substrate for applications where cells or tissue are loaded on-chip. The one disadvantage of PDMS is the hydrophobic surface chemistry is not very chemically resistant. PDMS swells in organic solvents, and biomolecules and hydrophobic analytes can adsorb onto the channel walls or absorb further into the bulk. Figure 1.1 shows that when native PDMS channel is filled with a hydrophobic fluorescent dye, the chemical absorbs into the PDMS bulk over time.[1.5]

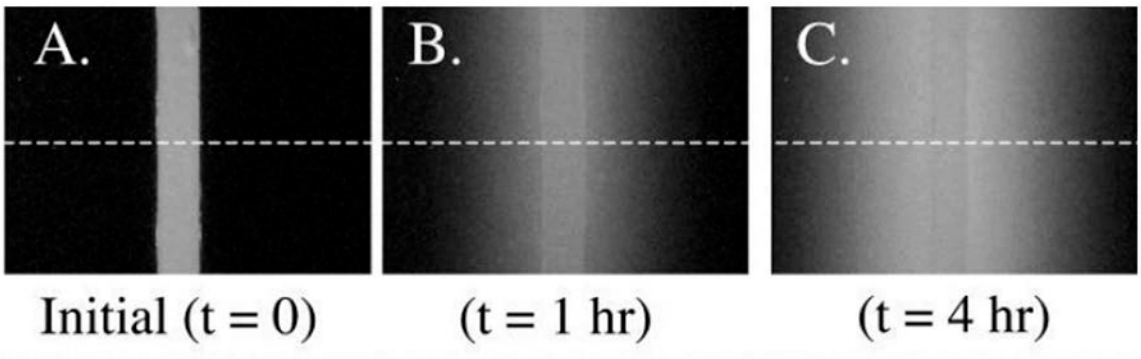

Figure 1.1: PDMS channel filled with 10 µM rhodamine B at time 0, 1 and 4 hrs. Over time the analyte absorbs into the PDMS bulk, as visualized by fluorescence. Reprinted (adapted) with permission from Roman, G. T.; Hlaus, T.; Bass, K. J.; Seelhammer, T. G.; Culbertson, C. T., *Anal. Chem.* 2005, *77*, 1414-1422. Copyright 2005 American Chemical Society.[1.5]

PDMS Chip Microfabrication

PDMS is fabricated through soft lithography; a master mold is made via photolithography and PDMS prepolymer can be recast on the mold repeatedly, making it compatible with large-scale production.[1.6, 7] Silicon wafers act as the template base for forming the channels. Positive or negative photoresists are used to create the channels. Depending on the type of photoresist used, a clear- or dark-field transparency with the aerial channel design is created through a computer-aided design (CAD) program. Photoresist is spun on the Si wafer, hardened by baking, and the transparency is placed on the wafer. UV light exposure crosslinks the negative photoresist through the clear areas on a dark-field mask, however the areas of positive photoresist exposed to UV light become soluble. The last step of the mold fabrication process is to develop the photoresist, leaving only the rectangular channel features. This process of creating the PDMS mold is shown in Figure 1.2, steps a-d.

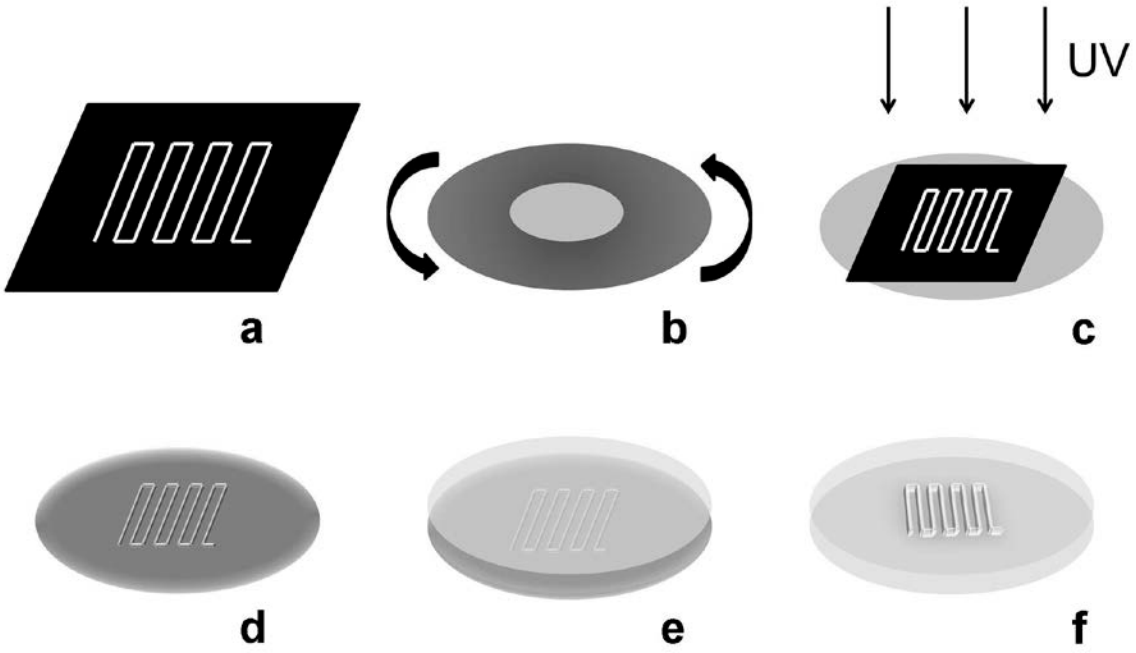

Figure 1.2: PDMS chip fabrication procedure. A high-resolution CAD transparency is printed with the channel features (a). Photoresist is spun on a Si wafer (b). Transparency is positioned over wafer and UV light is exposed (c). Photoresist is developed and only channel features remain on the wafer (d). PDMS pre-polymer is cast over the mold and cured (e). The PDMS can be peeled away from the wafer with the channel features embedded in the polymer (f).

A viscous PDMS prepolymer is made by mixing a base reagent and curing agent. The most typical ratio used is 10:1 (base:curing agent), however greater amounts of the curing agent compared to base reagent will create a firmer polymer upon baking (and conversely using less curing agent will result in a softer product). The PDMS prepolymer forms bubbles during mixing, but after degassing, the mixture is poured onto the mold on the Si wafer and baked to cure (Figure 1.2e). The PDMS can be peeled away from the wafer (Figure 1.2f) and irreversibly bonded to other pieces of PDMS or glass by changing the surface chemistry from silane to silanol groups[1.8], as shown in Figure 1.3. This surface chemistry change can be achieved by exposing areas to be bonded to oxygen

plasma, corona discharge or strong oxidizing agents like Pirahna solution (3:1 H_2SO_4:H_2O_2). The exposed silanols revert back to siloxy groups if left unbound.

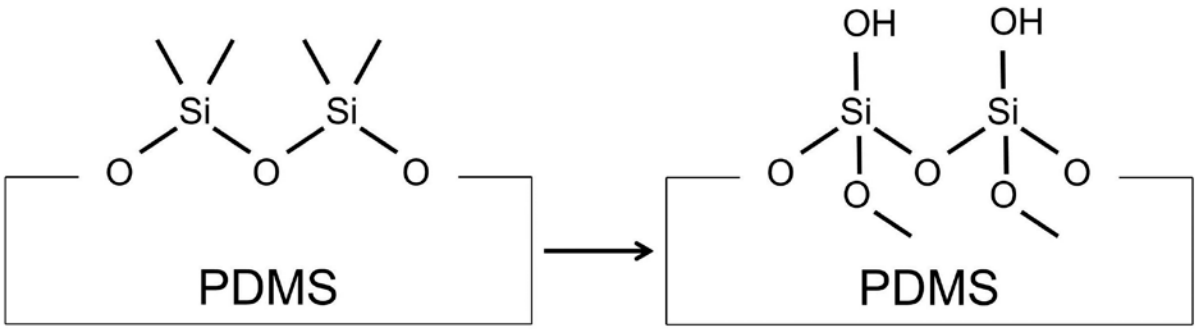

Figure 1.3: Surface chemistry of PDMS in the native state and with exposed surface silanol groups.

PDMS Surface Modifications

As previously mentioned, PDMS is often incompatible with many analytes, but extensive research has gone into developing surface modifications to combat those challenges. These strategies range in time and complexity, but the modification method is typically chosen based on the application goals of the chip. The main approaches for PDMS surface modification rely on passive perfusion of a solution that physically interacts with the surface or chemically changing the surface through covalent linkages.[1.9-11] Passive modification techniques generally involve pumping a solution through the chip that will temporarily interact with the channel walls. Commonly used procedures involve the use of charged surfactants or biomolecules that won't interfere with the on-chip assay. Sodium dodecyl sulfate (SDS) is a surfactant with a negatively-charged head group and hydrophobic tail that can interact with the hydrophobic PDMS. Pumping a solution of 1 mM SDS was shown to increase the wettability of the PDMS microchannels[1.12, 13] and increase the EOF efficiency.[1.14] Polyelectrolyte multilayers can

be formed on channel walls through layer-by-layer deposition. Alternately charged polyelectrolyte solutions can be deposited on the microchannel creating a hydrophilic surface and preventing analyte absorption into the bulk PDMS.[1.15] While these methods require short modification times, they can also be less stable and need to be frequently refreshed. Although generally having more complex procedures, covalent modifications offer greater longevity and stability. A few examples of covalent modifications preventing PDMS analyte absorption include sol-gel formation[1.16] and linking polyethylene glycol or amine terminal groups to the wall via silanization reactions.[1.8]

Fluid Flow through Chip Microchannels

Fluid movement in microfluidic devices can be controlled in a number of ways.[1.17] Gravity driven flow is the most basic form, not requiring any external equipment, making it ideal for maintaining a small footprint. Fluid is filled in an open reservoir and is wicked through the channels until the outlet reservoir is the same height as the inlet. Media can be manually replaced at the inlet (or extracted from the outlet) however it's not an automated process and does not maintain a consistent flow rate. Vacuum or pressure driven flow are the more commonly used methods employed by researchers. Tubing and a vacuum pump can be connected to the outlet of the chip and draw fluid through the channels at a set, constant velocity. Pressure driven flow can be accomplished through the use of a syringe or peristaltic pump. Peristaltic pumps can be built on-chip and operated through the expansion of overlaid channels by adding gas pressure[1.18] or an electric Braille module.[1.19] While potentially reducing the footprint of the system, peristaltic pumping results in pulsatile flow, whereas a syringe pump produces stable flow over time.

Flow through microchannels is sufficiently slow that it is in the laminar flow regime, wherein flow profiles can be adequately defined.[1.20] As a result of laminar flow, two joining fluid streams will only mix laterally (across the width of the channel) by molecular diffusion, illustrated in the left portion of Figure 1.4a. Complete diffusion (mixing) in wider, straight microchannels can be difficult, although for some applications like particle sorting, this property can be advantageous. A variety of channel design schemes have been produced that result in more rapid mixing of parallel fluid streams, with their efficiency often depending on fluid properties and flow rate. Passive mixers like serpentine networks are often the simplest to implement, but may not provide as rapid of mixing compared to an externally controlled active mixer.[1.21] Additionally, in microchannels, flow along the walls is slower than in the center of the channel creating a parabolic profile, and resulting in Taylor dispersion[1.22], shown in the right portion of Figure 1.4a. This phenomenon can cause band broadening and increased temporal resolution for on-chip assays. Droplet microfluidics is a possible circumvent for these problems. As shown in Figure 1.4b, this approach involves creating discrete sample plugs in the channel, separated by oil or air; within these droplets, temporal information can be retained and rapid mixing is observed.[1.23, 24]

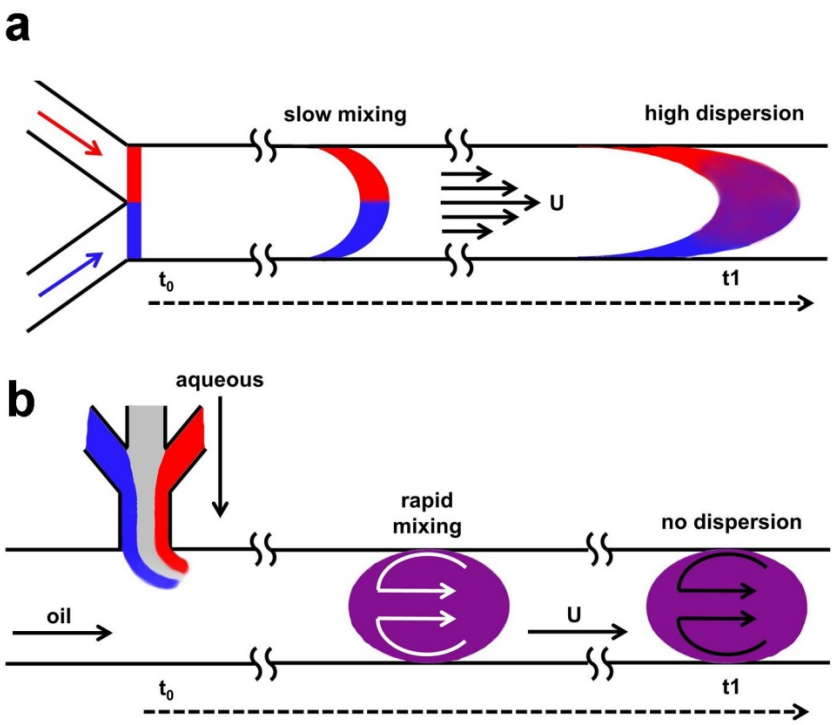

Figure 1.4: Schematic of diffusive mixing and Taylor dispersion in a microchannel. As fluids from 2 streams are joined in one channel, there is minimal mixing initially. At longer times the chemical species undergo lateral diffusive mixing. Additionally, due to the parabolic flow profile in microchannels, Taylor dispersion is observed over time. Adapted with permission from John Wiley & Sons, Inc.[1.23]

Computer modelling programs like COMSOL Multiphysics can be extremely beneficial when designing microfluidic devices.[1.25-27] Exact chip designs can be imported into the program, and different physics models can be applied to simulate flow or chemical species movement. Complex channel networks can be optimized in terms of geometric proportions and flow rate.

Integration

Microfluidic devices have the immense capacity to join multiple analytical components onto one platform, creating a 'lab on a chip' or micro total analysis system (μTAS).[1.4, 28] This component integration vastly increases automation of a technique, scale of data acquisition, and multiplexing potential. Countless examples of microfluidic

integration have been demonstrated, ranging from on-chip detection[1.29] to performing an entire polymerase chain reaction (PCR) procedure (depicted in Figure 1.5)[1.30]. An integrated component repeatedly used in this dissertation was on-chip pneumatically-actuated valves, which allow automated manipulation of fluid flow. First described by Unger, et al., a multilayer PDMS chip design with overlaid channel networks is constructed for the valve operation.[1.31] Gas pressure is applied to an upper layer channel, causing expansion of the elastomeric polymer and constricting a lower fluidic channel. Computer programs can control the activation of the gas pressure. The integration of cells or biological tissue on-chip was another key milestone in the complete integration of scientific laboratory techniques on one device and will be described further in the following section.

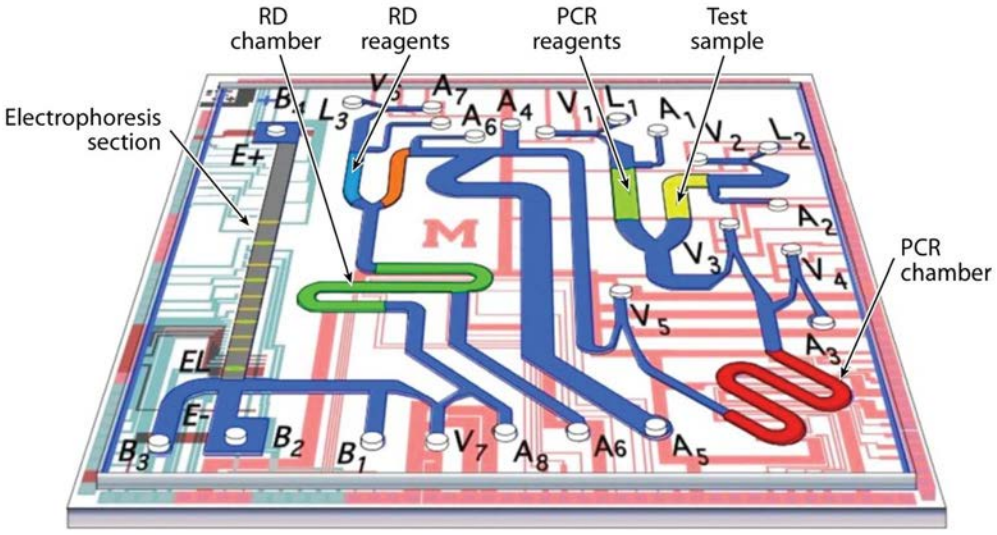

Figure 1.5: Demonstration of microfluidic integration; an entire PCR is completed on one µTAS device. Reprinted with permission from Annual Reviews.[1.32]

Microfluidic Cell Perfusion

Joining biological cell analysis with microfluidic technology has created many advances in the understanding and diagnosis of physiological events. In addition to all the benefits of microfluidics, like reduction in sample/reagent consumption and increased automation, there are many more reasons that integrating cells on-chip is advantageous. The essential foundation of fluid flow with microfluidics can be equated to the circulatory system *in vivo*, constantly transporting nutrients and secreted products or waste.[1.33] Therefore, compared to conventional static culture, perfusion of cells creates more physiologically relevant conditions.[1.26] Fresh media can be continuously added or recirculated depending on application.[1.34] Additionally, with microfluidics, spatial or temporal gradients can be generated in relation to media transport, allowing a wide variety of parameters to be tested on one platform.[1.35, 36]

Perfusion systems in water-jacketed columns have been employed, but require large volumes of media and number of cells (flow rates on the order of hundreds of μL/min and millions of cells).[1.37, 38] With microfluidics, cells can be loaded onto chips and cultured for extended periods of time, and in much smaller quantities than required for the column perfusion or static culture. Groups have even reported the capability of capturing and analyzing single cells, well suited in the dimensions of microchannels, potentially gaining understanding of their autocrine signaling.[1.39] There are a few different methods of introducing cells into a microfluidic perfusion channel or chamber, but it generally depends on the properties of the cell line. Cells can be suspended, pumped into the chip, and then flow is briefly stopped, wherein the cells adhere to the surface of the chip.[1.25] Flow is then resumed for the culture or perfusion experiment.

Another method is culturing cells on a substrate through conventional methods, and then transferring that material with attached cells to a chamber.[1.40, 41]

Geometry, microfluidic substrate and flow design of cell chambers greatly varies depending on cell type and application.[1.42] The first consideration when fabricating chambers on-chip is size of the cell line used. The height should be sufficiently greater than the size of the cell, but not so high that nutrients and waste are properly transported[1.43]; Kim et al. report suggested chamber heights for a variety of cell lines.[1.26] The width of the chamber will control how many cells can be seeded in a 2D monolayer format. Flow rates are generally optimized to a given application. Higher flow rates create shear stress on the cells, which can be biologically relevant to a certain point, but when increasingly elevated can result in morphological changes.[1.44] PDMS is the most widely used substrate for implementing cells on-chip, as it is gas permeable and biocompatible, however use of other substrates have been reported.[1.26, 45]

Traditional studies performed on cell cultures often require lengthy incubation times (on the order of hours), which makes it difficult to gain any kinetic information about the system. Manual addition and removal of media is required for all static cell experiments, followed by off-line analysis and detection methods to identify or quantify an analyte of interest. Microfluidic integration of analysis techniques allows direct, automated assays to be performed.[1.46, 47] Continuous flow allows more real time data to be acquired with on-line detection, as demonstrated in Figure 1.6.[1.48] A new field of study has been coined ‘secretomics’, which is the study of secreted proteins from cells.[1.49] This process can be easily adapted to microfluidic devices and expanded to monitor a variety of metabolites; different stimuli or drug treatments can be added and the secreted

products can be directly and continuously monitored to learn more about their physiology.[1.48, 50, 51] Many groups have demonstrated the utility of on-line analysis of microfluidic cell perfusion, exemplified in Table 1, however much of the work in the field of integrating cells on-chip still focusses on the engineering aspects of design and optimization of microfluidic devices, while utilizing them to understand the biological aspects of the cell is lacking.

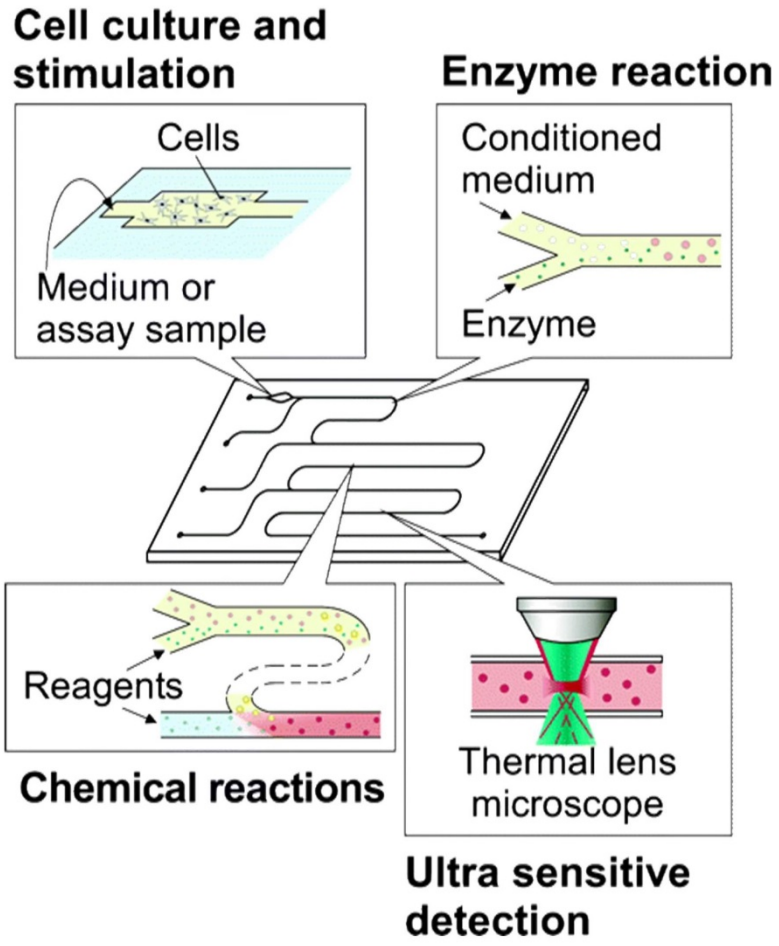

Figure 1.6: An integrated microfluidic device, containing a cell chamber, chemical assay reaction channels and an on-line detection method. Reprinted with permission from Goto, M.; Sato, K.; Murakami, A.; Tokeshi, M.; Kitamori, T., *Anal. Chem.* 2005, *77*, 2125-2131. Copyright 2005 American Chemical Society[1.48]

Table 1: Examples of microfluidic cell perfusion and secretion analysis.

Cell	Substrate	Analysis	Detection
3T3-L1 Adipocyte[1.40, 41, 52]	Glass, PDMS	NEFA & glycerol secretion, on-chip enzyme assay	Laser-induced fluorescence (LIF)
Islet[1.53-55]	Glass	Insulin[1.53, 54] or glucagon[1.55] secretion, on-chip immunoassay	LIF
Chromaffin[1.56]	PDMS	Catecholamine secretion	Electrochemical
PC12[1.57]	PDMS	Glutamate secretion	MS
Macrophage[1.48]	Glass	NO secretion, on-chip bioassay	Laser-induced thermal lens microscope
Erythrocyte[1.58]	PDMS	ATP secretion, on-chip enzyme assay	Chemiluminescence

Detection Methods

Laser-induced fluorescence (LIF) detection methods are a popular choice for measuring secreted metabolites from cells. Fluorescent assays can be integrated onto the chip and resulting fluorophores can be detected immediately with high sensitivity and low detection limits.[1.53, 55, 59] Given that most microfluidic substrates are optically transparent, chips can be positioned on an inverted microscope or optics set-up. Insulin secretion from islets of Langerhans has been measured via an on-chip fluorescent immunoassay and detected with LIF.[1.54] The pulsatile release of insulin phases is possible to measure with this microchip; 6 s injections were made, and the system had a detection limit of 0.8 nM. A follow-up to this study demonstrated the potential of microfluidics to allow parallel sampling of islets from 15 cell chambers on the same platform.[1.60]

Mass spectrometry (MS) is an alternative detector for coupling to microfluidic devices.[1.61] The electrospray ionization (ESI) source allows continuous flow into the MS,

which allows for rapid, sensitive, and multiplexed detection of secreted cellular metabolites. Unlike LIF, MS has the advantage that no fluorescent tag is necessary. Groups have reported direct, on-line microfluidic connection to MS, but generally involve cell lysis or biological samples that have been pre-processed off-chip (cite).[1.62-65] However, cell perfusion buffers contain high salt content, which is not amenable with ESI, which has been a challenge in creating cell chip-to-MS systems. Salt leads to ion suppression and decreased signal intensity of the analyte of interest.[1.66, 67] Pretreatment or clean-up methods incorporated between the sampling region and MS is a way around this challenge.[1.66] One group has reported incorporating a solid phase extraction bed into a microfluidic system to monitor glutamate release from neurons under different concentrations of stimuli.[1.57] Secreted metabolites from the cells in the chamber load onto the SPE bed, the bed was washed to remove salts and other interfering media components, and the analyte was eluted to the MS (pictorial schematic shown in Figure 1.7). This method is not completely on-line as manual connection and movement of tubing is necessary during the course of the experiment, but was a demonstration of microfluidic cell perfusion to MS.

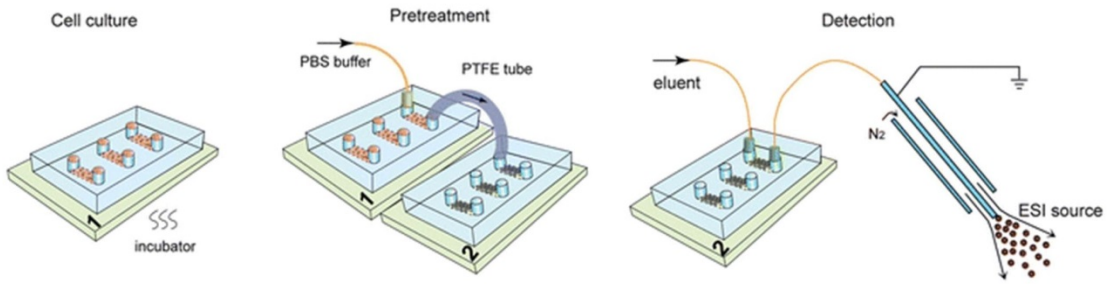

Figure 1.7: A system devised to couple on-chip cell perfusion with MS detection. Cells are incubated in chambers and media is flowed from the chamber onto a packed SPE bed in a subsequent chip. That chip is then disconnected from the cell chamber chip, the SPE bed is washed and analyte is eluted continuously into the MS ESI source. Reproduced with permission from The Royal Society of Chemistry.[1.57]

Adipocyte Metabolism

As previously discussed, the extent and versatility of microfluidic cell culture and analysis has grown in recent years, but little research has delved into monitoring adipocytes on-chip. Dysfunction of adipocyte metabolism can lead to various obesity-related disorders like type 2 diabetes[1.68-71], which have a huge economic impact on the healthcare industry. Researchers are still continuing to understand the complexities of this tissue and how different factors lead to these conditions. Therefore in this dissertation, novel microfluidic devices have been developed to learn more about the secretion of metabolites from adipocytes.

Mammalian fat stores reside in adipocytes, where the majority of the cell volume is a lipid droplet.[1.68] The adipocyte lipid droplet is comprised mainly of triglyceride molecules; a glycerol backbone with 3 attached fatty acid moieties.[1.68] An intrinsic metabolic process in adipocytes is lipolysis, the catabolism of the triglyceride molecule into glycerol and non-esterified fatty acids (NEFAs). Glyercol is secreted by the adipocyte and transported predominantly to the liver; however, depending on energy requirements of surrounding tissues, NEFAs can be released from the adipocyte or recycled back into the adipocyte for continued storage, as shown in Figure 1.8.[1.68, 72] This process, known as NEFA re-esterification or recycling, is vital in moderating energy distribution.[1.73, 74] Both lipolysis and NEFA re-esterification are highly regulated functions of cellular homeostasis, responding to (and secreting) a variety of signaling molecules, making adipose tissue a central entity of the endocrine system.[1.75-77]

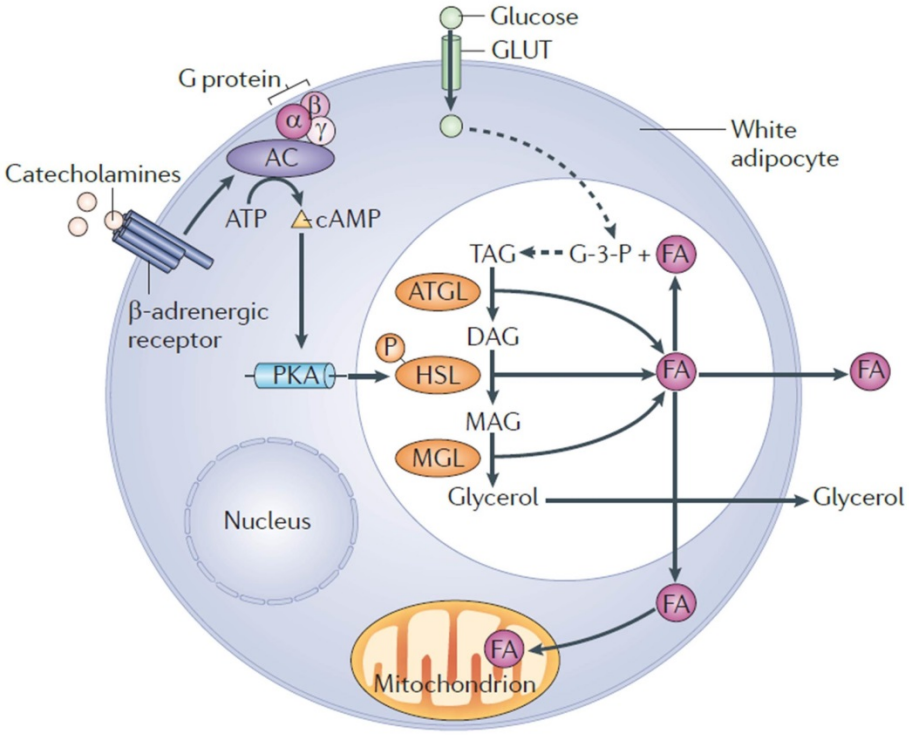

Figure 1.8: Graphic representation of lipolysis and NEFA recycling in adipocytes. Reproduced with permission from Nature Publishing Group.[1.78]

During energy excess or postprandial states, enzymatic and hormonal signaling molecules promote increased exogenous fat storage and NEFA recycling, and decreased lipolysis.[1.69, 70, 79] Contrastingly, during fasting states, lipolysis rates are elevated.[1.69, 79, 80] *In vitro* or *ex vivo* experiments use secreted glycerol concentration as an indicator of lipolysis rate; due to the lack of glycerol kinase in the adipocyte, glycerol cannot be directly re-esterified into a triglyceride molecule like NEFAs.[1.72] The rate of NEFA recycling can be inferred by measuring the secreted concentration of NEFA and comparing to the amount of glycerol release; complete lack of any NEFA recycling would result in a 3:1 concentration ratio of released NEFAs to glycerol. Physiologically that ratio isn't observed as 30-40% of NEFAs are immediately recycled into the lipid droplet.[1.73, 76] Glycerol-3-phosphate (G3P) is necessary to generate new triglyceride

molecules through NEFA re-esterification. Since glycerol is generally not a source of G3P in the adipocyte, other precursors are utilized: predominantly glucose during the fed state and glyceroneogenic precursors (i.e. pyruvate, lactate, amino acids) in fasting states.[1.80, 81]

Secretion of glycerol and NEFAs from adipocytes has been sampled through a few different methods: sampling supernatant media in static culture[1.82, 83], perfusing cells in a large-scale column[1.37, 38, 84], and collecting blood aliquots via catheterization[1.85, 86]. The latter method has the benefit of *in vivo* measurement (i.e. adipocytes are exposed to the matrix, vasculature and signaling molecules of their native environment), however there is less control of external parameters and it only provides a systemic evaluation. Sampling from static culture is the standardized approach and comparisons can easily be made to literature reports from other groups, but it doesn't offer any kinetic information and the extracellular environment is less biomimetic than a flow system. Perfusion of cells in a column incorporates the principle of fluid circulation, but large cell numbers and reagent volumes are required, and manual fraction collection is necessary. Therefore, microfluidic technology can be beneficial for understanding more of the fundamental aspects of lipolysis and NEFA recycling.

A variety of adipocyte cell types can be used to understand more about adipose biological mechanisms *in vitro*. As a cultured murine cell line, 3T3-L1 adipocytes are one of the most frequently used type due to their ease of culture/differentiation, aptitude to adhere to surfaces and ability to passage numerous times in the pre-adipocyte stage. Since they are so frequently employed for *in vitro* experimentation, vast literature sources provide comparison to experimental data. In terms of representing human adipose tissue,

3T3-L1 cells contain multilocular lipid droplets and are aneuploid in nature (containing a different number of chromosomes and missing genes)[1.87, 88] and therefore not always the most ideal model. Murine stem cells can also be used, when induced to commit to the adipogenic lineage.[1.89] Ear mesenchymal stem cells (eMSCs) can be obtained from mouse ear punches, and have the advantage of carrying the same genetic model as the host mice (ie. knockout lines).[1.90] Primary adipocytes are the third commonly used cell type, as they are derived from a fat pad in a host animal and are therefore contain the most physiologically relevant qualities.[1.91] They are comprised of unilocular lipid droplets and can be collected from a variety of fat depots, allowing differences in function among the depots to be monitored.[1.88] However, primary cells can be more difficult to handle as they float in media.

3T3-L1 adipocytes will be used as the cell model line in all of the dissertation chapters, due to the relative simplicity of culturing, handling and incorporation into a microfluidic cell chamber. Despite the fact that 3T3-L1 cells are easier to adapt to on-chip adipocyte perfusion studies, care must still be taken to ensure the cells maintain their normal function under continuous flow. This entails creating the appropriate chamber design and flow rate parameters that are amenable with their inherent fragility and buoyancy. Furthermore, in comparison to other types of cells, adipocytes have lengthy culture durations, necessary to accumulate sufficient lipid. This creates a challenge when integrating on-chip; cells must be able to be cultured on-chip for that period of time or transferred once mature.

Previously, chips have been developed that integrate an adipocyte cell perfusion chamber with on-line enzyme assay and LIF detection to measure secreted concentrations

of glycerol or NEFAs.[1.40, 41] Adipocytes were grown using conventional static culture procedures on pre-cut glass coverslips prior to loading on-chip. Because of this, the chip needed to have a reversibly-sealed cell chamber. These experiments were conducted in glass chips, which were advantageous because of their chemical resistance, however creating an efficient and reproducible seal of the glass layers was challenging. The multilayer device with reversibly-enclosed cell chamber is shown in Figure 1.9. Furthermore, only one assay could be performed on these designs.

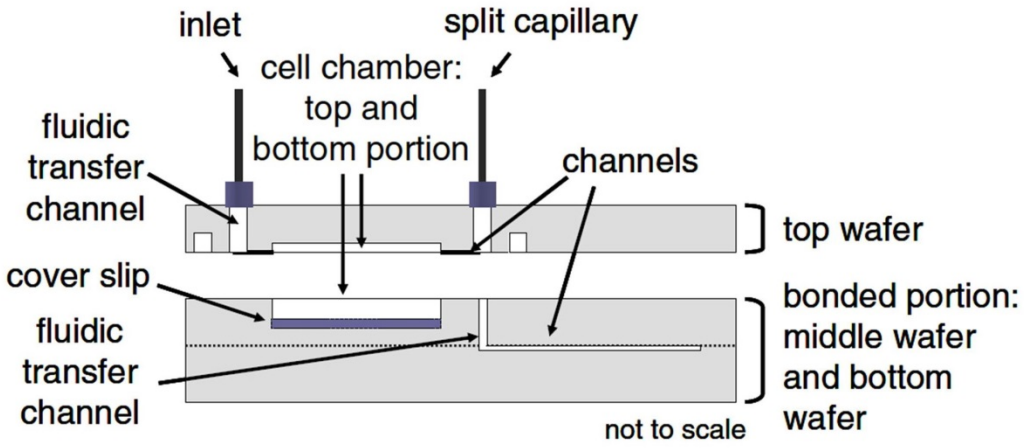

Figure 1.9: Multilayer glass chip developed to perfuse 3T3-L1 adipocytes on-chip followed by integrated enzyme assay reaction channels to continuously measure secreted NEFAs. Reproduced with permission from Springer.[1.40]

Dissertation Overview

In this dissertation, novel PDMS microfluidic devices have been developed with integrated cell chambers coupled to on-line detection techniques to monitor secreted metabolites. These systems allow continuous, automated analysis of cellular secretion, not possible with traditional techniques. Adipocytes were used herein as the model cell line, with the goal of learning more about secreted lipolysis products, glycerol and

NEFAs. Furthermore, the technology developed may have application to measuring the chemical environment around other cells that are grown on microfluidic chips.

Chapter 2 describes the development of a multilayer PDMS chip to simultaneously measure glycerol and NEFA release from on-chip perfused adipocytes. This integrated system made use of commercially available enzyme assay reagents to mix on-chip with the cell perfusate. The flow from the cell chamber was split into 2 chemical reaction channels, to conduct separate NEFA or glycerol enzyme assays. A fluorescent product was created through the enzyme assay and LIF detection was used for monitoring concentrations of the secreted metabolites. A reversibly-sealed chamber allowed re-use of the chip. On-chip valves allowed more automated delivery of chemical stimuli to the cells. This device is the first of its kind to demonstrate multiplexed analyte detection of secreted metabolites from cells on chip. Data and analysis of this research was published in *Analytical and Bioanalytical Chemistry* in 2014 and has been reproduced in this dissertation.[1.52]

In Chapter 3, a novel PDMS chip for coupling on-line adipocyte perfusion to MS detection is described. A multilayer, reversibly-sealed cell chamber was integrated with an injection loop on one device. The injection loop was operated with a series of microfabricated, pneumatically-actuated valves. The chip was directly connected to an off-chip capillary SPE bed and ESI spray tip. The SPE bed can generate backpressures, so the injection loop acts to fluidically isolate the SPE packing from the cell chamber; increased backpressures on the cells can be detrimental to inherent function. This set-up was positioned by the MS source and secreted NEFAs were identified under basal and stimulated conditions.

Chapter 4 outlines a series of biological experiments that were conducted on adipocytes in the chip developed in Chapter 2. Taking advantage of the ability to continuously monitor secreted metabolites from cells on chip, short stimulation experiments were performed to learn more about the kinetics of lipolysis. Additionally, cells of different age in culture were loaded on-chip to monitor the changes in lipolysis and NEFA re-esterification as a function of cell maturation. Finally, results from on-chip experiments were compared to traditional static culture analysis, to see how continuous perfusion of cells during analysis influences NEFA re-esterification.

Chapter 5 summarizes the findings from the aforementioned chapters. A series of follow-up and future experiments are proposed for continued understanding of adipocyte lipolysis and NEFA re-esterification, and as well as possible suggestions for improving the robustness and reproducibility of the chips detailed in Chapters 2 & 3.

References

1.1. Yang, W.; Woolley, A. T., *JALA* **2010,** *15*, 198-209.

1.2. Dittrich, P. S.; Manz, A., *Nat. Rev. Drug Discov.* **2006,** *5*, 210-218.

1.3. Vyawahare, S.; Griffiths, A. D.; Merten, C. A., *Chem. Biol.* **2010,** *17*, 1052-1065.

1.4. Culbertson, C. T.; Mickleburgh, T. G.; Stewart-James, S. A.; Sellens, K. A.; Pressnall, M., *Anal. Chem.* **2014,** *86*, 95-118.

1.5. Roman, G. T.; Hlaus, T.; Bass, K. J.; Seelhammer, T. G.; Culbertson, C. T., *Anal. Chem.* **2005,** *77*, 1414-1422.

1.6. McDonald, J. C.; Duffy, D. C.; Anderson, J. R.; Chiu, D. T.; Wu, H. K.; Schueller, O. J. A.; Whitesides, G. M., *Electrophoresis* **2000,** *21*, 27-40.

1.7. McDonald, J. C.; Whitesides, G. M., *Accounts Chem. Res.* **2002,** *35*, 491-499.

1.8. Sui, G. D.; Wang, J. Y.; Lee, C. C.; Lu, W. X.; Lee, S. P.; Leyton, J. V.; Wu, A. M.; Tseng, H. R., *Anal. Chem.* **2006,** *78*, 5543-5551.

1.9. Makamba, H.; Kim, J. H.; Lim, K.; Park, N.; Hahn, J. H., *Electrophoresis* **2003,** *24*, 3607-3619.

1.10. Zhou, J.; Khodakov, D. A.; Ellis, A. V.; Voelcker, N. H., *Electrophoresis* **2012,** *33*, 89-104.

1.11. Zhou, J. W.; Ellis, A. V.; Voelcker, N. H., *Electrophoresis* **2010,** *31*, 2-16.

1.12. Cellar, N. A.; Kennedy, R. T., *Lab Chip* **2006,** *6*, 1205-1212.

1.13. Roman, G. T.; McDaniel, K.; Culbertson, C. T., *Analyst* **2006,** *131*, 194-201.

1.14. Ocvirk, G.; Munroe, M.; Tang, T.; Oleschuk, R.; Westra, K.; Harrison, D. J., *Electrophoresis* **2000,** *21*, 107-115.

1.15. Bauer, W.-A. C.; Fischlechner, M.; Abell, C.; Huck, W. T. S., *Lab Chip* **2010,** *10*, 1814-1819.

1.16. Roman, G. T.; Culbertson, C. T., *Langmuir* **2006,** *22*, 4445-4451.

1.17. Byun, C. K.; Abi-Samra, K.; Cho, Y.-K.; Takayama, S., *Electrophoresis* **2014,** *35*, 245-257.

1.18. Cellar, N. A.; Burns, S. T.; Meiners, J.-C.; Chen, H.; Kennedy, R. T., *Anal. Chem.* **2005,** *77*, 7067-7073.

1.19. Gu, W.; Zhu, X.; Futai, N.; Cho, B. S.; Takayama, S., *P. Natl. Acad. Sci. USA* **2004,** *101*, 15861-15866.

1.20. Beebe, D. J.; Mensing, G. A.; Walker, G. M., *Annu. Rev. Biomed. Eng.* **2002,** *4*, 261-286.

1.21. deMello, A. J., *Nature* **2006,** *442*, 394-402.

1.22. Squires, T. M.; Quake, S. R., *Rev. Mod. Phys.* **2005,** *77*, 977-1026.

1.23. Song, H.; Tice, J. D.; Ismagilov, R. F., *Angew. Chem. Int. Ed.* **2003,** *42*, 768-772.

1.24. Seemann, R.; Brinkmann, M.; Pfohl, T.; Herminghaus, S., *Rep. Prog. Phys.* **2012,** *75*, 1-41.

1.25. Hung, P. J.; Lee, P. J.; Sabounchi, P.; Aghdam, N.; Lin, R.; Lee, L. P., *Lab Chip* **2005,** *5*, 44-48.

1.26. Kim, L.; Toh, Y. C.; Voldman, J.; Yu, H., *Lab Chip* **2007,** *7*, 681-694.

1.27. Hsu, Y.-H.; Moya, M. L.; Abiri, P.; Hughes, C. C. W.; George, S. C.; Lee, A. P., *Lab Chip* **2013,** *13*, 81-89.

1.28. Kovarik, M. L.; Gach, P. C.; Ornoff, D. M.; Wang, Y.; Balowski, J.; Farrag, L.; Allbritton, N. L., *Anal. Chem.* **2012,** *84*, 516-540.

1.29. Roman, G. T.; Kennedy, R. T., *J. Chromatogr. A* **2007,** *1168*, 170-188.

1.30. Pal, R.; Yang, M.; Lin, R.; Johnson, B. N.; Srivastava, N.; Razzacki, S. Z.; Chomistek, K. J.; Heldsinger, D. C.; Haque, R. M.; Ugaz, V. M.; Thwar, P. K.; Chen, Z.; Alfano, K.; Yim, M. B.; Krishnan, M.; Fuller, A. O.; Larson, R. G.; Burke, D. T.; Burns, M. A., *Lab Chip* **2005,** *5*, 1024-1032.

1.31. Unger, M. A.; Chou, H. P.; Thorsen, T.; Scherer, A.; Quake, S. R., *Science* **2000,** *288*, 113-116.

1.32. Livak-Dahl, E.; Sinn, I.; Burns, M., *Annu. Rev. Chem. Biomol. Eng.* **2011,** *2*, 325-353.

1.33. El-Ali, J.; Sorger, P. K.; Jensen, K. F., *Nature* **2006,** *442*, 403-411.

1.34. Zhang, C.; Zhao, Z. Q.; Rahim, N. A. A.; van Noort, D.; Yu, H., *Lab Chip* **2009,** *9*, 3185-3192.

1.35. Dhumpa, R.; Roper, M. G., *Anal. Chim. Acta* **2012,** *743*, 9-18.

1.36. Lai, N.; Sims, J. K.; Jeon, N. L.; Lee, K., *Tissue Eng. Part C-Methods* **2012,** *18*, 958-967.

1.37. Getty-Kaushik, L.; Richard, A. M. T.; Corkey, B. E., *Obes Res* **2005,** *13*, 2058-2065.

1.38. Allen, D. O.; Largis, E. E.; Miller, E. A.; Ashmore, J., *J. Appl. Physiol.* **1973,** *34*, 125-7.

1.39. Chen, C. S.; Jiang, X.; Whitesides, G. M., *MRS Bull.* **2005,** *30*, 194-201.

1.40. Clark, A. M.; Sousa, K. M.; Chisolm, C. N.; MacDougald, O. A.; Kennedy, R. T., *Anal. Bioanal. Chem.* **2010,** *397*, 2939-2947.

1.41. Clark, A. M.; Sousa, K. M.; Jennings, C.; MacDougald, O. A.; Kennedy, R. T., *Anal. Chem.* **2009,** *81*, 2350-2356.

1.42. Moraes, C.; Mehta, G.; Lesher-Perez, S. C.; Takayama, S., *Ann. Biomed. Eng.* **2011,** *40*, 1211-1227.

1.43. Korin, N.; Bransky, A.; Khoury, M.; Dinnar, U.; Levenberg, S., *Biotechnol. Bioeng.* **2009,** *102*, 1222-1230.

1.44. Walker, G. M.; Zeringue, H. C.; Beebe, D. J., *Lab Chip* **2004,** *4*, 91-97.

1.45. Salieb-Beugelaar, G. B.; Simone, G.; Arora, A.; Philippi, A.; Manz, A., *Anal. Chem.* **2010,** *82*, 4848-4864.

1.46. Primiceri, E.; Chiriaco, M. S.; Rinaldi, R.; Maruccio, G., *Lab Chip* **2013,** *13*, 3789-3802.

1.47. Martin, R. S.; Root, P. D.; Spence, D. M., *Analyst* **2006,** *131*, 1197-1206.

1.48. Goto, M.; Sato, K.; Murakami, A.; Tokeshi, M.; Kitamori, T., *Anal. Chem.* **2005,** *77*, 2125-2131.

1.49. Hathout, Y., *Expert Rev. Proteomic.* **2007,** *4*, 239-248.

1.50. Bowen, A. L.; Martin, R. S., *Electrophoresis* **2010,** *31*, 2534-2540.

1.51. Liu, Y.; Kwa, T.; Revzin, A., *Biomaterials* **2012,** *33*, 7347-7355.

1.52. Dugan, C. E.; Cawthorn, W. P.; MacDougald, O. A.; Kennedy, R. T., *Anal. Bioanal. Chem.* **2014,** *406*, 4851-4859.

1.53. Roper, M. G.; Shackman, J. G.; Dahlgren, G. M.; Kennedy, R. T., *Anal. Chem.* **2003,** *75*, 4711-4717.

1.54. Shackman, J. G.; Dahlgren, G. M.; Peters, J. L.; Kennedy, R. T., *Lab Chip* **2005,** *5*, 56-63.

1.55. Shackman, J. G.; Reid, K. R.; Dugan, C. E.; Kennedy, R. T., *Anal. Bioanal. Chem.* **2012,** *402*, 2797-2803.

1.56. Ges, I. A.; Brindley, R. L.; Currie, K. P. M.; Baudenbacher, F. J., *Lab Chip* **2013,** *13*, 4663-4673.

1.57. Wei, H.; Li, H.; Gao, D.; Lin, J.-M., *Analyst* **2010,** *135*, 2043-2050.

1.58. Price, A. K.; Fischer, D. J.; Martin, R. S.; Spence, D. M., *Anal. Chem.* **2004,** *76*, 4849-4855.

1.59. Dugan, C. E.; Kennedy, R. T.; Ormond, A. M., Chapter Eleven - Measurement of Lipolysis Products Secreted by 3T3-L1 Adipocytes Using Microfluidics. In *Methods in Enzymology*, Academic Press: 2014; Vol. Volume 538, pp 195-209.

1.60. Dishinger, J. F.; Reid, K. R.; Kennedy, R. T., *Anal. Chem.* **2009,** *81*, 3119-3127.

1.61. Wang, X.; Yi, L.; Mukhitov, N.; Schrell, A. M.; Dhumpa, R.; Roper, M. G., *J. Chromatogr. A* **2015,** *1382*, 98-116.

1.62. Mellors, J. S.; Jorabchi, K.; Smith, L. M.; Ramsey, J. M., *Anal. Chem.* **2010,** *82*, 967-973.

1.63. Jung, S.; Effelsberg, U.; Tallarek, U., *Anal. Chem.* **2011,** *83*, 9167-9173.

1.64. Koster, S.; Verpoorte, E., *Lab Chip* **2007,** *7*, 1394-1412.

1.65. Yang, Y.; Li, C.; Kameoka, J.; Lee, K. H.; Craighead, H. G., *Lab Chip* **2005,** *5*, 869-876.

1.66. Enders, J. R.; Marasco, C. C.; Wikswo, J. P.; McLean, J. A., *Anal. Chem.* **2012,** *84*, 8467-8474.

1.67. Furey, A.; Moriarty, M.; Bane, V.; Kinsella, B.; Lehane, M., *Talanta* **2013,** *115*, 104-122.

1.68. Arner, P., *Best Pract. Res. Clin. Endoc. Metab.* **2005,** *19*, 471-482.

1.69. Duncan, R. E.; Ahmadian, M.; Jaworski, K.; Sarkadi-Nagy, E.; Sul, H. S., *Annu. Rev. Nutr.* **2007,** *27*, 79-101.

1.70. Jelic, K.; Hallgreen, C. E.; Colding-Jørgensen, M., *Ann. Biomed. Eng.* **2009,** *37*, 1897-1909.

1.71. Bays, H.; Mandarino, L.; DeFronzo, R. A., *J. Clin. Endocrinol. Metab.* **2004,** *89*, 463-478.

1.72. Lafontan, M.; Langin, D., *Prog. Lipid Res.* **2009,** *48*, 275-297.

1.73. Reshef, L.; Olswang, Y.; Cassuto, H.; Blum, B.; Croniger, C. M.; Kalhan, S. C.; Tilghman, S. M.; Hanson, R. W., *J. Biol. Chem.* **2003,** *278*, 30413-30416.

1.74. Prentki, M.; Madiraju, S. R. M., *Mol. Cell. Endocrinol.* **2012,** *353*, 88-100.

1.75. Rosen, E. D.; Spiegelman, B. M., *Nature* **2006,** *444*, 847-853.

1.76. Beale, E. G.; Hammer, R. E.; Antoine, B.; Forest, C., **2004,** *15*, 129-135.

1.77. Frayn, K. N.; Humphreys, S. M., *Am. J. Physiol.-Endocrinol. Metab.* **2012,** *302*, E468-E475.

1.78. Altarejos, J. Y.; Montminy, M., *Nat. Rev. Mol. Cell Biol.* **2011,** *12*, 141-151.

1.79. Jensen, M. D., *Eur. Heart J. Suppl.* **2006,** *8*, B13-B19.

1.80. Forest, C.; Tordjman, J.; Glorian, M.; Duplus, E.; Chauvet, G.; Quette, J.; Beale, E. G.; Antoine, B., *Biochem. Soc. T.* **2003,** *31*, 1125-1129.

1.81. Beale, E. G.; Antoine, B.; Forest, C., *Trends Biochem. Sci.* **2003,** *28*, 402-403.

1.82. Niang, F.; Benelli, C.; Ribiere, C.; Collinet, M.; Mehebik-Mojaat, N.; Penot, G.; Forest, C.; Jaubert, A. M., *J. Nutr.* **2010,** *141*, 4-9.

1.83. Wan, Z.; Ritchie, I.; Beaudoin, M.-S.; Castellani, L.; Chan, C. B.; Wright, D. C., *PLoS ONE* **2012,** *7*, e41719.

1.84. Getty-Kaushik, L.; Richard, A. M. T.; Corkey, B. E., *Diabetes* **2005,** *54*, 629-637.

1.85. Asmar, M.; Simonsen, L.; Madsbad, S.; Stallknecht, B.; Holst, J. J.; Bulow, J., *Diabetes* **2010,** *59*, 2160-2163.

1.86. Vaillancourt, E.; Haman, F.; Weber, J.-M., *J. Physiol.* **2009,** *587*, 4349-4359.

1.87. Yuan, H.; Zhao, C., *Asian J. Anim. Vet. Adv.* **2011,** *6*, 482-487.

1.88. Gregoire, F. M.; Smas, C. M.; Sul, H. S., *Physiol. Rev.* **1998,** *78*, 783-809.

1.89. Rosen, E. D.; MacDougald, O. A., *Nat. Rev. Mol. Cell Biol.* **2006,** *7*, 885-896.

1.90. Gawronska-Kozak, B., Chapter One - Preparation and Differentiation of Mesenchymal Stem Cells from Ears of Adult Mice. In *Methods in Enzymology*, Ormond, A. M., Ed. Academic Press: 2014; Vol. Volume 538, pp 1-13.

1.91. Wang, S.; Soni, K. G.; Semache, M.; Casavant, S.; Fortier, M.; Pan, L.; Mitchell, G. A., *Mol. Gen. Metab.* **2008,** *95*, 117-126.

CHAPTER 2

MULTIPLEXED MICROFLUIDIC ENZYME ASSAYS FOR SIMULTANEOUS DETECTION OF LIPOLYSIS PRODUCTS FROM ADIPOCYTES

Reproduced with permission from Dugan, C. E.; Cawthorn, W. P.; MacDougald, O. A.; Kennedy, R. T., *Anal. Bioanal. Chem.* **2014**, *406*, 4851-4859.

Introduction

Microfluidic and lab-on-chip devices offer many benefits for analytical measurements over traditional techniques including reduced reagent and sample volumes, improved temporal resolution for monitoring, and increased automation. Such devices have also become powerful tools for cell biology.[2.1, 2] Specific cell lines or individual cells can be isolated in the reduced dimensions of a microfluidic device.[2.3, 4] Cells can be perfused in two or three dimensions with continual replenishment of media to more closely mimic the *in vivo* environment compared to traditional static incubation methods.[2.5, 6] Microfluidics also provides a way to miniaturize and provide higher throughput of cell culture-based experiments. Although growing cells in chips can be useful, in many cases it is also necessary to assess cell function. Visual inspection and fluorescence measurements of cells are straightforward on chips that are optically clear; however, chemical analysis of the cellular environment often requires other assays. Although chemical measurements can be performed off-chip[2.7], integrating analytical measurements with cells on microfluidic systems eliminates the need for sample collection and off-line analyte detection, and can provide real-time recording of cellular

dynamics.[2.8, 9] Several examples of this approach have been described including on-line immunoassays[2.10], sensors[2.11], and enzyme assays[2.12]. Most such systems perform a single assay on cells. In this chapter, we describe an advance on this capability in a system fabricated in polydimethylsiloxane (PDMS) that uses dual on-line enzyme assays to monitor metabolic activity in near real-time. We also demonstrate a method to avoid chemical loss to absorption by PDMS that improves sensitivity of measurements of hydrophobic compounds such as fatty acids.

Adipocytes were used as a model system for these experiments. Adipocytes are fat-storing cells that secrete glycerol and non-esterified fatty acids (NEFA) as a result of the catabolism of triglycerides through lipolysis. Flux of lipolytic products is regulated by a variety of signals. The adipocyte re-esterifies (recycles) a percentage of the NEFAs back into triglycerides, as a method of regulation for systemic NEFA supply.[2.13] Depending on the physiological energy state, different enzymes and glycerol-3-phosphate precursors dictate the pathway and amount of recycling.[2.14, 15] Increased adiposity, as in obese individuals, is often associated with a number of disorders including type 2 diabetes.[2.16-19] Thus, understanding the mechanisms of fatty acid recycling and the factors that lead to its dysfunction could be fundamental to providing improved treatment for obesity-related disorders.

Adipocytes have been previously mounted in microfluidic devices, mainly to monitor differentiation and culture of the cells on-chip.[2.20, 21] The influence of adipocyte secretions on other cell lines in a multi-chamber chip has also been monitored.[2.22] Despite these advances in using microfluidics to better understand adipocyte biology, automated and real-time quantification of adipocyte secretion is lacking.

Previous reports from our group have shown the ability to monitor either NEFA or glycerol secretion from 3T3-L1 adipocytes on glass microfluidic devices.[2.23, 24] These chips showed the potential to detect adipocyte secretion on-line, but individual measurements of NEFA or glycerol cannot provide information on fatty acid re-esterification. The concentration of glycerol secreted from adipocytes is a direct indication of the rate of lipolysis; glycerol is not directly recycled by the adipocyte because of the lack of sufficient glycerol kinase in the cell.[2.25-27] If NEFA secretion can be monitored at the same time as glycerol, from the same group of cells, the amount of fatty acid re-esterification can be inferred based on the rate of lipolysis and concentration of secreted NEFAs.

To accomplish dual analyte measurement, a microfluidic chip with two enzyme assay reaction networks was designed. Cultured murine 3T3-L1 adipocytes were perfused in a cell chamber, and the resulting perfusate was split into the two enzyme assay reaction channels. The chip design and reagent flow rates were chosen to provide good on-line assay sensitivity and response time. PDMS was chosen as the microfluidic substrate because of many convenient properties. PDMS is biocompatible and gas permeable, making it well suited for cell studies.[2.28] The inherently elastomeric PDMS permitted easier integration of a valve system, which was constructed upstream of the cell chamber to allow automated stream selection, reduce dead volume and prevent flow disruption when changing solutions. Despite the advantages of PDMS, it can absorb hydrophobic molecules. Since NEFAs are being detected on-chip, a surface modification was performed to prevent loss of the analyte. These improvements allow a rapid, automated

measurement method for monitoring adipocyte fatty acid re-esterification, and can be extended to other adipocyte secretion studies.

Experimental

Reagents

The fatty acid assay reagents and standard solution (oleic acid) were purchased in a kit, HR Series NEFA-HR(2), through Wako Chemicals USA, Inc. (Richmond, VA). Amplex UltraRed Reagent, Hank's buffered salt solution (HBSS, Cat. # 14175) and cell culture reagents were received from Life Technologies (Carlsbad, CA). Triton X-100 was purchased from Bio-Rad Laboratories (Hercules, CA). Free glycerol reagent, standard glycerol solution, fatty acid free bovine serum albumin (BSA), isoproterenol hydrochloride, sodium dodecyl sulfate (SDS), dimethyl sulfoxide (DMSO) and hexamethyldisilazane (HMDS) were obtained from Sigma-Aldrich (St. Louis, MO).

Microfluidic Chip Fabrication

The multilayer PDMS chips were fabricated with soft lithography techniques as previously described.[2.28-30] All of the PDMS used in the chip fabrication was RTV-615 (Curbell Plastics, Livonia, MI) and had a 10:1 base:curing agent ratio. The 4 PDMS layers are denoted 'control layer', 'mixing channel layer', 'lower cell chamber layer' and 'blank layer'. For the fabrication of the control layer, HMDS was spun on a 3-inch silicon wafer (University Wafer, Boston, MA) to facilitate photoresist adhesion. SU-8 2075 photoresist (MicroChem, Newton, MA) was spun onto the wafer to create a 60 μm layer and patterned using a dark-field photomask with the design shown as the black lines in Figure 2.1a. A thick layer (~1 cm) of PDMS was poured over the mold and heated to 80 °C for at least 30 min. The mold for the mixing channel layer was made the same as the

control layer, but with the pattern shown as the black lines in Figure 2.1b. After the SU-8 photoresist was developed, a 12 µm thick layer of AZ-9260 photoresist (Capitol Scientific, Austin, TX) was spun onto the wafer. The final pattern of the AZ photoresist is shown in Figure 2.1b as the red line. The wafer was heated at 125 °C for 5 min to round the AZ features. PDMS was spun on the wafer to create a 60 µm thick layer and heated to 80 °C for at least 30 min. The fabrication of the lower cell chamber layer was done with SU-8 2075 as described above, but to a thickness of 250 µm, with the pattern shown in Figure 2.1c. PDMS was poured over the mold and manually distributed across the wafer to create a ~1 mm thick layer. The PDMS was allowed to settle for 10 min before it was heated to 80 °C for at least 30 min. Finally, PDMS was spun on a blank wafer to a thickness of 170 µm and heated to 80 °C for at least 30 min, to create the blank layer.

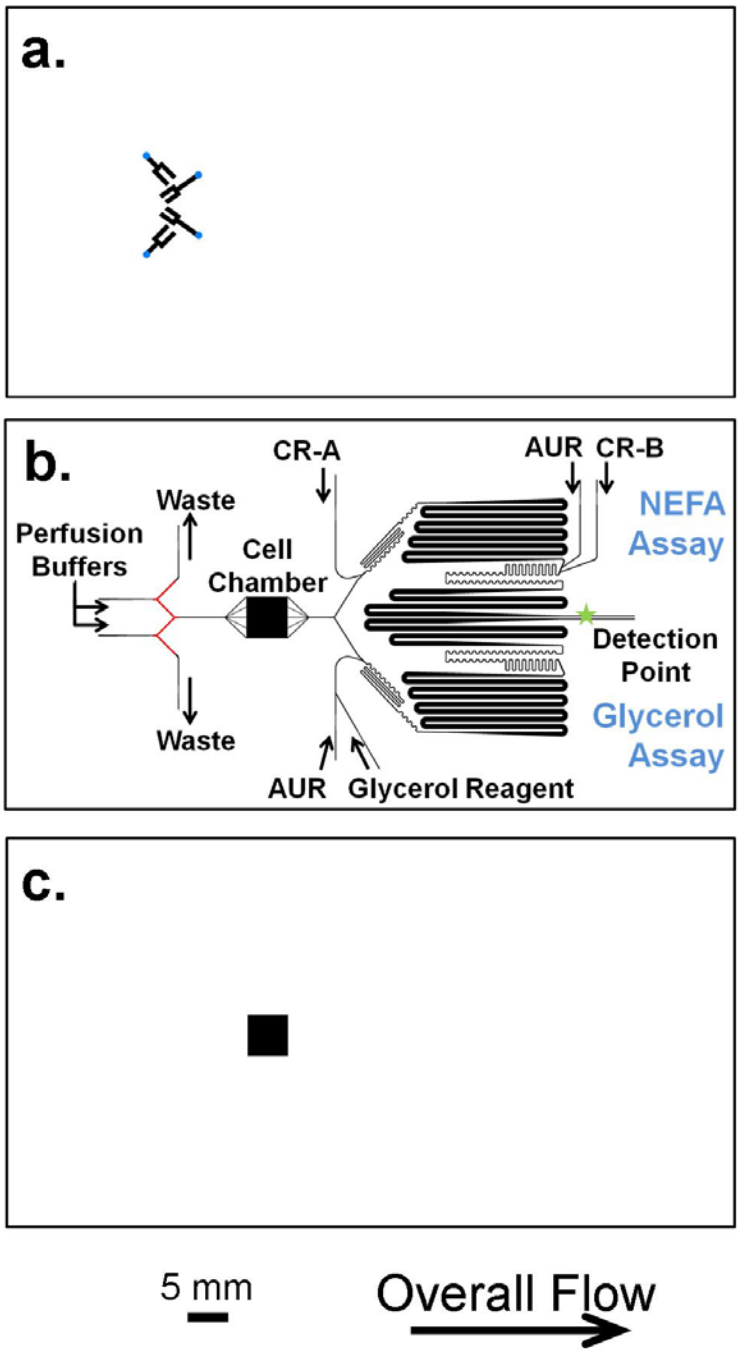

Figure 2.1: Design of the 3 different fabricated layers in the PDMS multi-layer chip. The control layer (a), the reaction channel layer (b), and the base chamber layer (c) fabrication patterns are shown. The fluorogenic dye, Amplex UlraRed, is abbreviated as AUR. The blue circles in (a) represent the points where access holes were punched through the PDMS, and the red line in (b) indicates the portion of the design that was fabricated with AZ photoresist.

The control layer PDMS was peeled away from the mold, and access holes were punched at the points indicated in blue in Figure 2.1a using a blunt 20 gauge needle (Small Parts, Logansport, IN). The control layer was bonded to the top of the mixing channel layer using corona discharge, and heated to 80 °C for 15 min. The two bonded layers were peeled from the mixing channel layer mold, bonded to the blank layer PDMS to enclose the channels, and heated to 80 °C for 15 min. The three bonded layers were peeled from the wafer and the blank layer PDMS was removed from inside the upper portion of the cell chamber using a scalpel blade. A 4.8 mm x 4.8 mm piece of cover glass (No. 1, Fisher Scientific, Waltham, MA) was bonded to the inside of the upper cell chamber. The lower cell chamber layer was peeled from the wafer mold and bonded to a glass slide (0.55 mm thick, Telic, Valencia, CA), feature side exposed, and heated to 80 °C for 15 min. The side view of the assembled chip is shown in Figure 2.2.

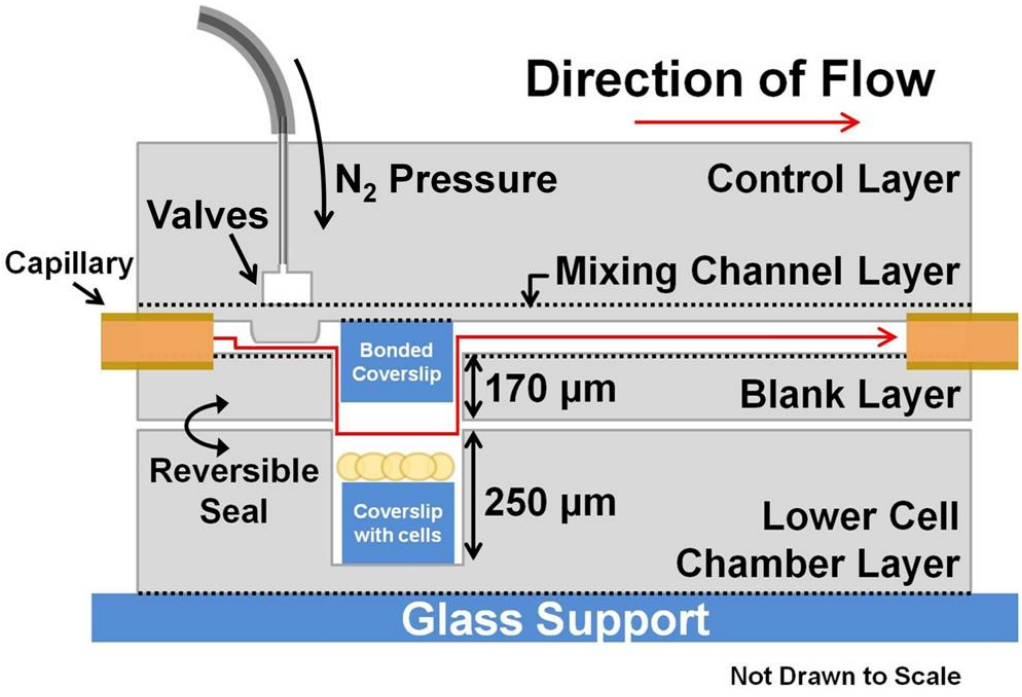

Figure 2.2: Side view of chip slice showing fabrication layers and direction of flow. The dotted lines represent the interfaces between layers that were irreversibly bonded.

Adipocyte Culture

Glass coverslips (No. 1, Fisher Scientific) were cut to 4.8 mm x 4.8 mm squares using a dicing saw. The coverslips were sterilized in 70% ethanol for at least 1 h, and were then dried in a sterile culture hood. Three to four coverslips were placed in each 35 mm petri dish using sterile tweezers prior to seeding preadipocytes. Murine 3T3-L1 preadipocytes were seeded into the 35 mm dishes (200,000 cells per dish), maintained in Dulbecco's modified Eagle's medium (Cat. #11965-092, Life Technologies) with 8% v/v bovine calf serum (Denville Scientific, South Plainfield, NJ), 100 units/mL penicillin, 100 µg/mL streptomycin, 2 mM L-glutamine, 1 mM sodium pyruvate, and stored in an incubator with 10% CO_2. Two days after the cells became confluent, differentiation (adipogenesis) was induced by adding 500 µM methylisobutylxanthine, 1 µM dexamethasone and 5 µg/mL insulin. Two days post-differentiation, medium was replaced with adipogenic medium that contained 5 µg/mL insulin. Adipogenic medium was the same as the preadipocyte medium except 10% fetal bovine serum replaced the bovine calf serum. Every two days following, culture medium was refreshed with adipogenic medium that did not contain insulin. Adipocytes were matured to at least 14 days post-induction before on-chip experiments.

Computational Modeling

The perfusion of the cell chamber and mixing channels were modeled using COMSOL Multiphysics 4.3b (COMSOL, Inc., Burlington, MA). The 'Laminar Flow' and 'Transport of Diluted Species' physics models were used to monitor the flow split and theoretical temporal resolution of the system. All simulations assumed water perfusing through the chip, with a density of 998 kg m^{-3} and viscosity of 1.002 x 10^{-3} Pa s

(20 °C). The cell chamber and mixing channel network were modeled separately in order to reduce computation times with finer meshes. The cell chamber was modeled in a 3D geometry and had dimensions of 5.0 mm x 5.0 mm x 0.33 mm with a 4.8 mm x 4.8 mm x 0.15 mm box removed from top to mimic the bonded coverslip in the actual chip. The inlet and outlet channels for the cell chamber were 60 µm tall. Based on initial cell experiments, the optimal flow rate to perfuse over the cells was 0.75 µL/min, so the cell chamber inlet was also set to that flow rate. The channels in the assay reaction channel network were modeled in 2D with the shallow channel approximation set to 60 µm.

Reversible Chip Assembly

The PDMS was cut so that the ends of the channels were exposed. Fluidic connections were made by inserting 50 µm ID/150 µm OD fused silica capillaries (Polymicro Technologies, Phoenix, AZ), ~13 cm long, with rounded tips into the exposed inlets (between the mixing channel layer and the blank layer). Sheath capillaries (180 µm ID/360 µm OD) were glued to the opposite ends of the 50/150 capillaries, to allow for easier connections to external pumps. An additional 17 cm of 100/360 capillary was connected to the valve waste capillaries during experiments to balance the back pressure.

The enzyme assay mixing channels were modified by pumping 20 mM SDS solution through both of the mixing channel outlets at 1.5 µL/min for 45 min. The channels were then flushed with water for an additional 20 min at the same flow rate. After every use of the chip, this process was repeated to refresh the treatment.

The control channels were operated by connection to an in-house built pneumatically-actuated system. A stainless steel tube (23 gauge, ~1 cm long) was inserted halfway into Tygon tubing (1/16” OD, 0.5 mm ID, IDEX, Lake Forest, IL). The

other half was inserted into the top of the chip where the access holes were punched in the control layer. The Tygon tubing was filled with water and 15 psi of nitrogen gas was applied to the desired channels with the aid of an in-house written LabView program.

Before the chip was used for an experiment, it was degassed in a vacuum chamber for ~1 h to reduce the presence of bubbles in the channels during perfusion. The channels were primed with water after the chip was degassed. The two parts of the PDMS chip were rinsed with 70% ethanol and dust was removed with Scotch tape. For cell experiments, a coverslip with ~48,000 attached 3T3-L1 adipocytes was removed from the culture dish with sterile tweezers and placed in the lower cell chamber. Cells per coverslip were roughly estimated by assuming an even distribution of cells on the culture plate so that the number of cells equaled the fraction of plate area occupied by the coverslip times the total number of cells. Total number of cells was estimated from the number of preadipocytes seeded onto the plate (measured by hemocytometer) and the replication rate during differentiation. About 10 μL of culture medium was added to prevent trapping bubbles during sealing. For calibration experiments, a blank coverslip was placed in the lower cell chamber. The upper cell chamber was aligned over the lower chamber and the two parts of the chip were pressed to make a conformal contact.

A compression frame to enclose the PDMS chip was built in-house from 2 sheets of acrylic plastic. Holes were drilled through both sheets along the outer edge to allow screws to pass through both sheets and tighten the compression frame. Additionally, four holes were drilled on the top for access to the control channel tubing, and a large chamfered hole was drilled on the bottom to allow the microscope objective to have closer access to the detection channels. The control tubing of the assembled chip was

threaded through the compression frame, and screws tightened the compression frame over the chip. Figure 2.3 shows the assembled chip in the compression frame.

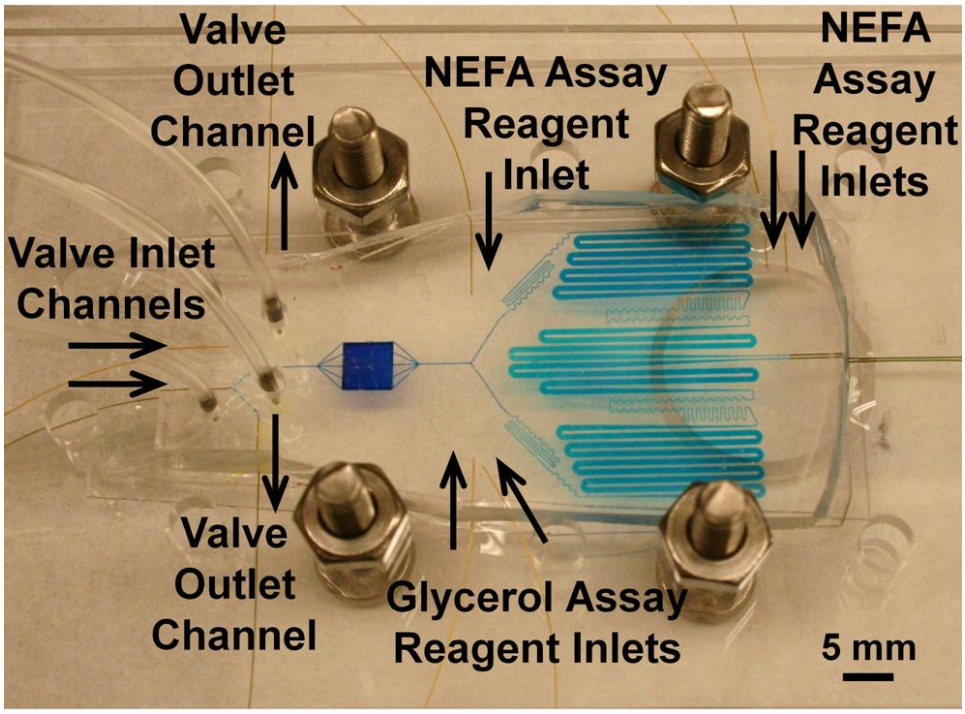

Figure 2.3: The assembled chip in compression frame. Blue food dye is being perfused through one of the valves for better visualization. The arrows highlight the capillary connections and the direction of fluid flow.

Perfusion

The fatty acid assay reagents were reconstituted as follows: Color Reagent A (CR-A) was reconstituted with 30 mL of solvent A (creating a solution 1.66x more concentrated than manufacturer specifications) and Color Reagent B (CR-B) was reconstituted with solvent B according to manufacturer instructions. CR-A was further modified by adding 200 µL 10% (v/v) Triton X-100 to every 800 µL CR-A. The free glycerol reagent was reconstituted with 40 mL 18.0 MΩ/cm distilled water. Amplex UltraRed was reconstituted with DMSO to make a 10 mM stock solution. The Amplex

UltraRed stock solution was further diluted to make a 1 mM solution in 35% DMSO, which was used for the on-line assays.

Prior to performing cell studies, calibrations were performed to characterize the actual delay and rise times of the two multiplexed assays. For these experiments, standards were diluted in HBSS containing 2% BSA (w/v) and pumped through the 2 valve inlets at 0.75 µL/min. When an additional standard was required (i.e., when creating a calibration curve with multiple standard concentrations), the solution that was being directed to waste through the valve was replaced, which prevented disruption in the flow. The glycerol assay was performed by adding the glycerol reagent and 1 mM Amplex UltraRed solution onto the chip at 0.29 µL/min (each) at the locations indicated in Figure 2.1b. The modified CR-A, CR-B and 1 mM Amplex UltraRed solutions were pumped at 0.30 µL/min (each) through the respective inlets shown in Figure 2.1b. All solution pumping was controlled by external syringe pumps. During cell experiments, one valve inlet was perfused with 2% BSA in HBSS (to monitor basal secretion) and the other valve inlet was perfused with 20 µM isoproterenol in HBSS with 2% BSA (to create lipolysis-stimulated conditions).

Detection

An Olympus IX71 inverted microscope was used to collect the signal from the fluorescent assay product. The light path was directed by a 10x, 0.40 numerical aperture objective (Olympus Part# 1-U2B823) and the appropriate mirrors/filters for resorufin detection. A Hamamatsu ImagEM X2 CCD camera allowed simultaneous detection of the 2 outlet channels at the point shown in Figure 1b. Data was collected at 2 Hz with an exposure time of 250 ms, and was analyzed with Microsoft Excel 2007.

Results & Discussion

Overview of Microfluidic Chip Design

In previous work we demonstrated different chips that could monitor NEFA and glycerol release from adipocytes.[2.23, 24] In these chips, cells were perfused, enzyme assay reagents were added on-line to mix with the perfusate, and reaction products were measured by fluorescence detection. The reagents for the NEFA assay contained coenzyme A (CoA), ATP, acyl-CoA synthetase, and acyl-CoA oxidase.[2.24] The glycerol assay reagent contained ATP, glycerol kinase, and glycerol phosphate oxidase.[2.23] Both assays create hydrogen peroxide from their respective reactions, which can then be reacted with peroxidase and Amplex UltraRed to create a fluorescent product. These chips demonstrated important principles such as loading pre-differentiated adipocytes on glass coverslips into reversibly sealed chips, prevention of shear stress on the fragile cells during perfusion, and continuous monitoring which were used in this work. To achieve simultaneous analysis capability we designed a chip (Figure 2.1) that split the perfusate and directed the flows to two separate, continuously operating enzyme assay streams. The detection points for the two assay channels were placed near each other so they could be imaged on a fluorescence microscope. Because the enzyme assays yielded the same fluorescent product, this arrangement allowed glycerol and NEFA to be monitored on-line simultaneously as they were secreted from the cells. Other improvements were also made including lowering the flow rate to cell ratio to reduce dilution of secreted chemicals by 11-fold. The new chip also integrates valves to automate physiologic experiments that require changing the perfusion conditions, e.g. adding drugs to the cells. Because valves are easily incorporated into PDMS by multi-layer lithography, we used

this material instead of glass. This change in material necessitated surface modification procedures that prevented adsorption of hydrophobic analytes to the chip.

Simultaneous Assay Chip Design and Flow Splitting

Stable and reliable split of the perfusate flow for each enzyme assay required careful consideration of the geometry and flow rates used. Although the assay reaction channels had approximately the same flow resistance, the different number and placement of reagent inlets required for each assay (see Supplementary Information section for pilot studies on individual assays), created differences in back-pressure. These differences made it difficult to predict how reagent flow would affect the perfusate flow into the two assay channels. To assist in determining the flow conditions, a COMSOL model was developed.

For simplicity, we operated the chip with a 50:50 split of perfusate to each assay channel. We also fixed the NEFA assay flow rates and adjusted glycerol reagent flow rates because the glycerol assay was more sensitive and adaptable to changes in analyte to reagent ratios than that of the NEFA assay. Based on data from the single channel chip for NEFA detection, the highest sensitivity response was achieved when the analyte to reagent ratio was set to 1.25:1:1:1 NEFA:CR-A:CR-B:Amplex UltraRed. Assuming an even flow split, and a flow rate of 0.75 µL/min through the cell chamber, this ratio required that the NEFA reagents be set to 0.3 µL/min. To determine the glycerol reagent flow rates that were needed, we used the COMSOL model to vary flow rates from 0.1 µL/min to 1 µL/min. The model showed that the 2 reagent inlets on the glycerol assay side of the chip should be set to 0.29 µL/min to achieve even flow split. The velocity map of the flow split using these flow rates is shown in Figure 2.4a. The map shows an even

split under these condition. It also shows a slight decrease in velocity before the split, which is due to a slight widening of the channel before the split. Additionally, it was determined that if the glycerol reagent flow rates were higher than 0.7 µL/min, 100% of the flow coming from the cell chamber would be directed to the NEFA assay channel showing the sensitivity of the system to changes in flow. Similarly, we found that that abrupt changes in pressure, such as from rapidly inserting capillaries or making connections, could result in unstable flows in the system.

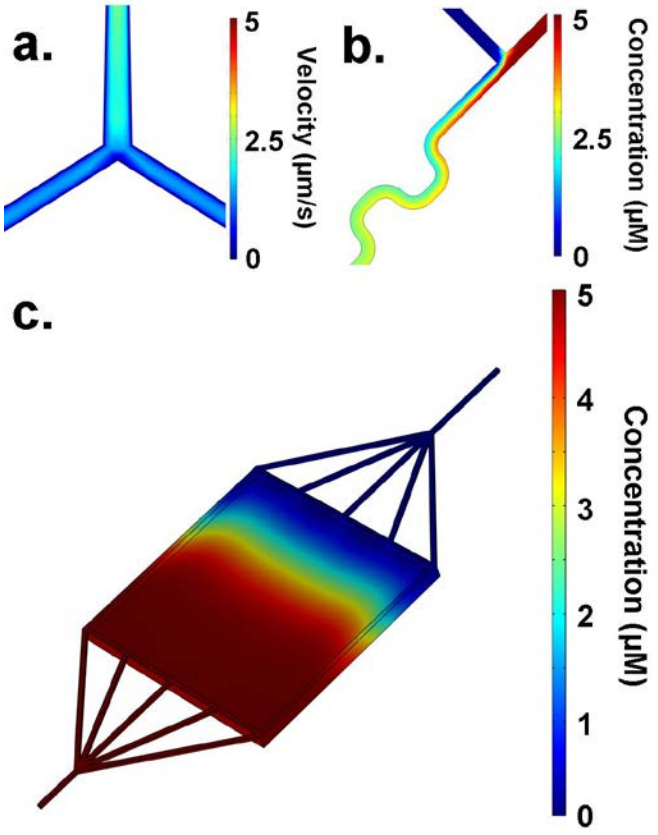

Figure 2.4: COMSOL modeling of the dual chip. (a) The velocity of laminar flow at the flow split allowed the ratio of cell perfusate that would be directed into each assay reaction channel to be determined. (b) The mixing efficiency could be measured at a reagent inlet by injecting a 5 µM chemical species at the flow split and a blank solution at the reagent inlet, and finding the point in which complete diffusion has occurred across the width of the channel. (c) A concentration gradient moving through the cell chamber when a 5 µM chemical species was injected was modeled to show the profile of flow across the width of the chamber.

To confirm that flow was symmetrical through both assay channels, we measured the flow rate through each channel separately. To do this, water was perfused through the chip and fractions were collected at the outlets every 2 min and weighed. The results were compared to theoretical values of 0.96 µL/min at the glycerol outlet and 1.28 µL/min at the NEFA outlet, assuming an even flow split of the cell chamber perfusate into the 2 reaction channel networks. (The NEFA channel should have a higher net flow out because of the extra reagent channel.) The flow rate exiting the chip was 1.0 ± 0.02 µL/min on the glycerol side and 1.3 ± 0.08 µL/min on the NEFA side (n = 4). The results show that the appropriate flow rates were exiting the chip and confirm an equal flow split.

We also used the model to confirm that complete mixing of reagents and sample would occur at the flow rates and channels used. As shown in Figure 2.4b, complete mixing was found after the fluid traveled 7 mm through the 100 µm wide serpentine channels. Another important issue for design is determining whether the cells are evenly perfused and if the chamber is well-swept. COMSOL modeling also assisted in establishing the appropriate flow profile through the cell chamber. Varying the number and angle of the channels leading to and from the chamber changed the profile and temporal response of the chip. It was desired to reduce the rise time of the system to detect cellular dynamics, therefore a flat even flow across the chamber was ideal. Figure 2.4c illustrates a simulation of a chemical species injection into the chamber to allow visualization of the flow profile of the cell chamber used in these experiments.

Chip Characterization

Figure 2.5a shows the detector response to a series step changes in analyte concentration performed on-chip. Figure 2.5b illustrates the resulting calibration curves for both assays. The limit of detection (LOD) was calculated as the concentration corresponding to a signal that was 3 times the standard deviation of the blank. The glycerol assay had a LOD of 5 µM and was linear through 110 µM. The NEFA assay had a LOD of 6 µM and had a linear calibration through 150 µM. The calibration curves were reproducible over multiple experiments using the same chip with RSD of slope and intercept below 6% (n = 4 chips, each used for at least 3 trials).

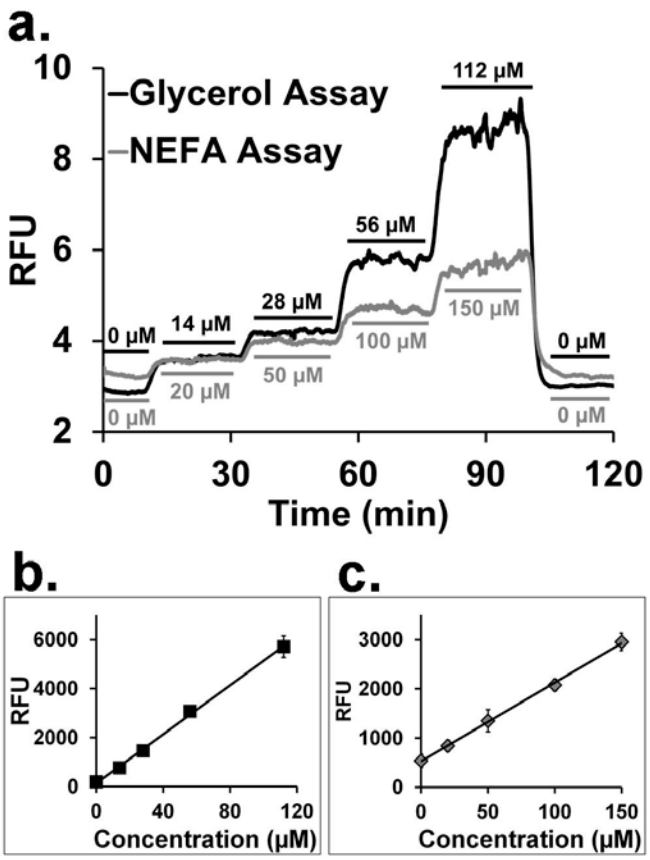

Figure 2.5: Dual chip calibration. (a) Detector trace (plotted as relative fluorescence units, RFU) from step changes of glycerol and NEFA standards in the dual chip, which are simultaneously detected. The resulting calibration curve for the glycerol assay (b) for 4 replicate experiments show a linear response through 112 µM, a LOD of 5 µM and R^2 of 0.998. The fatty acid assay (c) is linear through 150 µM, and has a LOD of 6 µM and R^2 of 0.999 for 4 replicate experiments.

These data also allow us to characterize the temporal response of the chip. The rise time was defined as the amount of time between a 10-90% change in signal when standard concentrations were switched. The delay time was calculated as the time between switching a solution and the initial 10% rise in signal. The rise times for the complete assembled chip were 2.3 ± 0.6 min for both the glycerol and NEFA assays. The delay times were 10.2 ± 0.3 min. The COMSOL model of the chip (including the same flow components such as valves, cell chamber, and mixing channels) predicts 4.6 min and 15.4 min for the rise and delay times of the glycerol assay, and 4.7 min and 17.8 min for the rise and delay times of the NEFA assay, respectively. The longer times predicted than observed suggest a difference in geometry that is not accounted for by the model. A likely source of the discrepancy is reduction of channel height caused by the compression frame closing off the channels of the compliant PDMS. Because the flow rates were through each channel as predicted (see above), the compression must have an equal effect on both sides of the chip. Experimental values were consistent across multiple chips and were used for subsequent calculations, such as accounting for delay times, related to cell experiments.

An important aspect of cell physiology experiments is manipulating the solutions flowing over cells. In prior work[2.23, 24], changing solutions was accomplished by switching connections to the chip. Making manual connections requires a stopping and starting flow and creates a change in pressure on-chip, which affects the detected signal. This effect is especially problematic in a dual channel chip with multiple flow paths. Figure 2.6a illustrates the effect on signal of such a switch. The use of fabricated valves on-chip significantly improved the stability of the flow through the chip when solutions

were switched, creating smooth step changes, as shown in Figure 2.6b. This addition also reduced dead volumes of the perfused solutions and increased automation of the device.

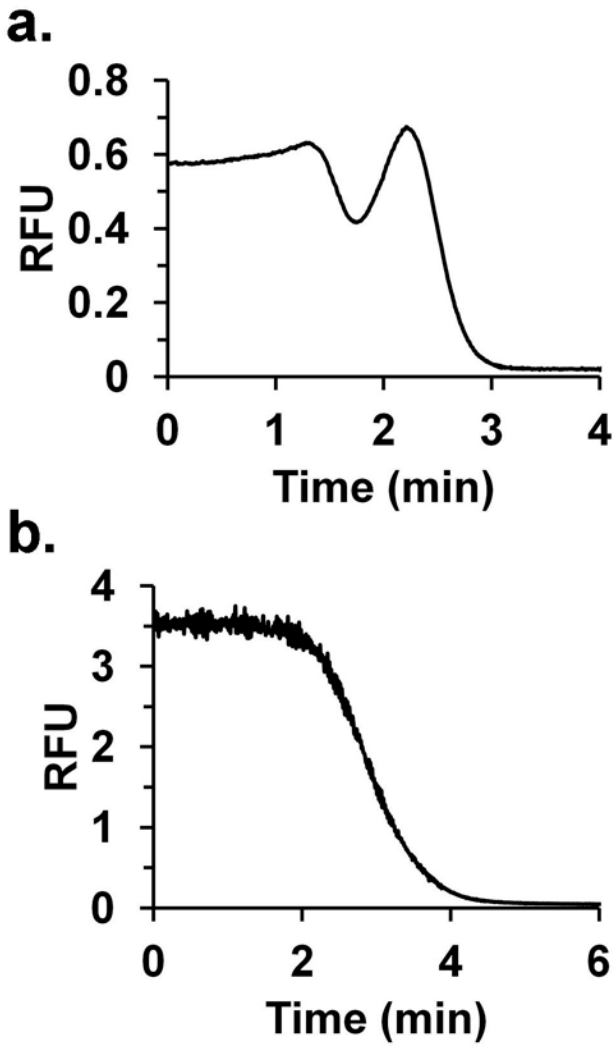

Figure 2.6: Step changes on glycerol assay independent chip from high to low concentration standards without (a) and with (b) fabricated valves.

Assay and PDMS Modifications

Preliminary experiments revealed low sensitivity and signal drift in the NEFA assay. Because this had not been observed with the glass devices, and it is well-known that PDMS can adsorb hydrophobic molecules[2.31, 32], the problems with signal were attributed to adsorption of the hydrophobic fatty acids by PDMS. A variety of PDMS

modifications that might prevent NEFA adsorption, including sol-gels, polyelectrolyte multilayers, and dynamic coating with SDS, polyethylene glycol, and Pluronic F-127, were tested for their effect on the NEFA signal.[2.33-37] The best results, as determined by NEFA assay sensitivity and stability, were obtained when the channels were dynamically coated with a 20 mM SDS solution.[2.38, 39]

For the SDS treatment, it was important that chips were modified a few days after fabrication. This ageing effect was attributed to corona discharge used for bonding. Corona discharge creates a hydrophilic surface, which slowly reverts back to its native hydrophobic state, that would be better able to bind SDS.[2.40, 41] The NEFA assay sensitivity increased from 7.6 ± 2.5 RFU·μM^{-1} (n = 3) to 11.1 ± 2.3 RFU·μM^{-1} (n = 3) with SDS modification (Figure 2.7). Day-to-day experiments on the same chip modified with SDS had reproducible calibration curve slopes with a RSD of 2.1% (n = 3). The coating was refreshed every day to maintain this performance.

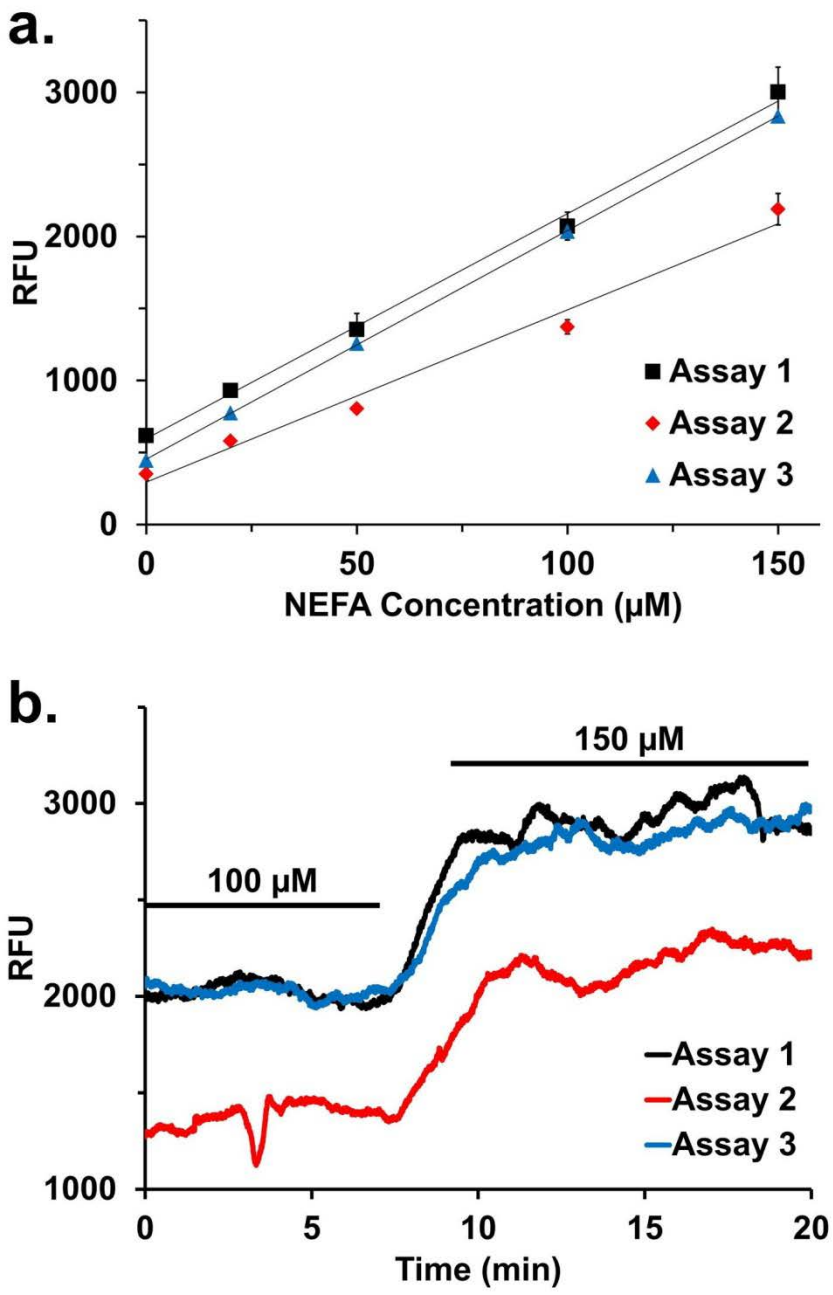

Figure 2.7: NEFA calibration curves illustrate the improved assay sensitivity with daily SDS modification (a). The real-time traces of on-line switching from low to high concentration are shown in (b). Assay 1 was performed immediately after SDS modification. Assay 2 was run a subsequent day without prior SDS modification, and a lower sensitivity is observed. The original sensitivity can be restored; SDS modification was done before assay 3 and improved signal is seen. All 3 assays were performed on the same chip.

To reduce the exposure of fatty acids to the PDMS, a glass coverslip was bonded to the top of the cell chamber. This lessened the surface area that the fatty acids could contact the PDMS while in the cell chamber, resulting in a further 44% improvement in assay sensitivity. The addition of the coverslip also had the benefit of directing flow towards the cells, allowing improved sampling of cell secretion.

Although these measures improved the sensitivity, we still observed drift in signal for the fatty acid assay over time. Addition of the non-ionic surfactant, Triton X-100, to CR-A reagent reduced drift of the signal at high standard concentrations so that the RSD improved from >12% to 1-5%. This effect may be due to both prevention of adsorption and improving enzyme solubility.

Adipocyte Perfusion

Representative simultaneous traces of adipocyte secretion of glycerol and NEFAs are shown in Figure 2.8a and b. Basal concentrations, i.e. secretion prior to drug treatment, were above the LOD of both assays for all cases. Upon addition with 20 μM isoproterenol, a drug that stimulates lipolysis, a simultaneous increase in concentration of both analytes was observed between 2 and 6-fold depending on the batch of cells used. Previous work with static culture systems have reported a 2 to 7-fold increase in lipolysis products with a similar stimulation.[2.42, 43] The simultaneous measurement of NEFA and glycerol allows an assessment of recycling. For example, for the case in Figure 2.8a, the NEFA:glycerol ratio was 1:1 implying some recycling that did not change after stimulation. In contrast, for the cells used in Figure 2.8b, we observed NEFA:glycerol of 1:3 that increased to 2:1 with isoproterenol suggesting high recycling that decreased with stimulation. Previous studies have reported a wide range of NEFA:glycerol ratios, e.g.

from 1:2[2.44] to 2:1[2.42] for 3T3-L1 adipocytes. In general values are less than the theoretical maximum of 3:1, similar to our results. Few results have been reported on NEFA:glycerol ratio for 3T3-L1 cells with isoproterenol treatment; however, studies of primary adipocytes have reported that isoproterenol generally evokes higher NEFA:glycerol ratios (less recycling) than basal as we observed for most of our trials. For example one report showed a 1.3-fold increase in NEFA:glycerol ratio.[2.45]

Interestingly, the NEFA:glycerol ratio showed a decreasing trend in adipocytes that were cultured for more extensive periods of time (Figure 2.8c). We also observed greater responsiveness of NEFA secretion to isoproterenol for longer times after induction (Figure 2.8d). The cause and significance of these trends is not known; however, the larger secretion of NEFA at longer times could relate to greater lipid content as the cells age in culture. Further studies with this method will be required to better understand the significance of such changes.

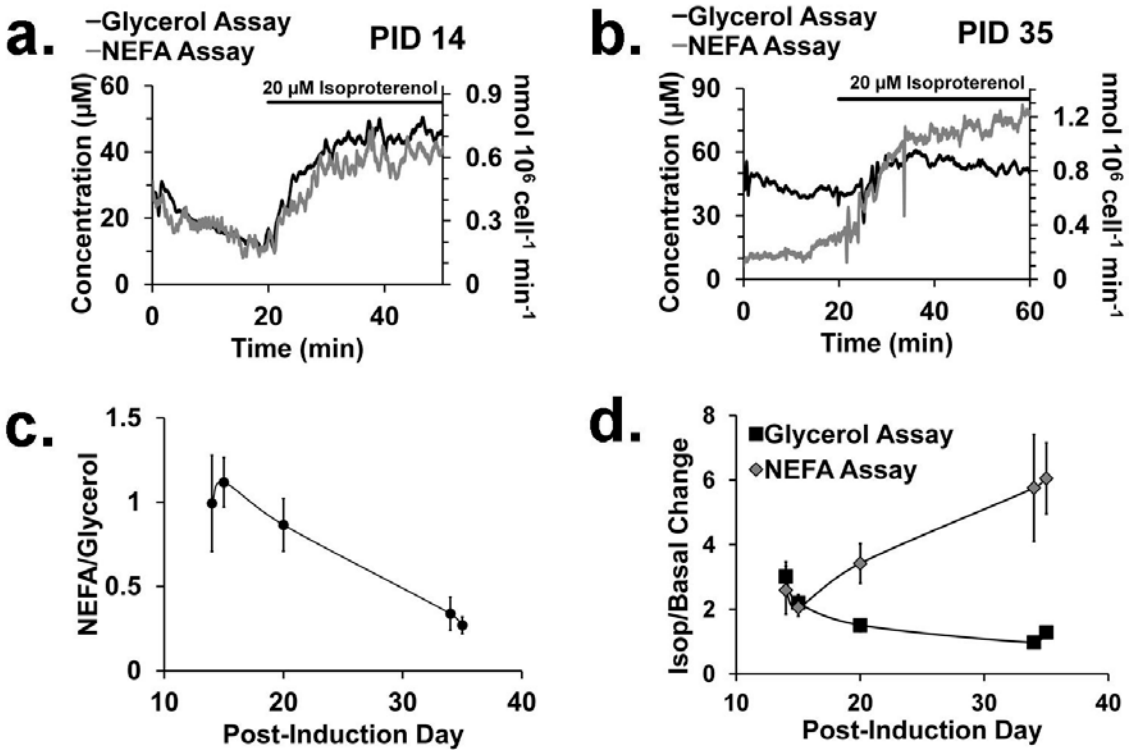

Figure 2.8: Representative traces of simultaneous detection of NEFA and glycerol secretion from adipocytes and trends in day-to-day experiments. Traces were collected during basal secretion and during lipolysis stimulation by the application of isoproterenol, represented by the black bar. (a) Cells day 14 post-induction (PID). (b) Cells day 35 post-induction. (c) The NEFA/glycerol ratio decreased for basal secretion the longer the adipocytes remained in culture. (d) As the cells matured, the ratio of average isoproterenol-stimulated cell response to the average basal response increased for the NEFA assay and decreased for the glycerol assay.

Conclusions

In this study, a multilayer PDMS chip was developed for the perfusion of adipocytes and analysis of their secreted metabolites. A multiplexed enzyme assay network allowed simultaneous detection of glycerol and NEFA concentrations released from cultured 3T3-L1 adipocytes. COMSOL modeling aided in the design and implementation of the dual, asymmetric assay system. PDMS proved to be a good substrate for these experiments following modification of the channels with SDS. Basal and stimulated lipolysis conditions were monitored from perfused adipocytes in real time.

Appropriate stimulation of analyte secretion was observed with the addition of isoproterenol. Initial trends imply that there are changes to the biology of 3T3-L1 adipocytes with time in culture, and could provide more detailed information about lipolysis and NEFA recycling. The continuous flow format allows changes in metabolism to be monitored within minutes of occurring. The novel microfluidic chip illustrated the potential of creating a complete, automated, and reusable analysis system for simultaneously monitoring multiple cellular functions. This tool could be extended to measure the lipolysis and fatty acid recycling in primary adipocytes and their response to different stimuli. Furthermore, principles learned from these experiments, such as split assays and SDS modifications for hydrophobic moieties, could be applied to monitoring other cell types in lab-on-chip systems.

Supplementary Information

To design a simultaneous chip, we first developed single assay chips for glycerol and NEFA, based largely on single channel devices reported previously.[2.23, 24] For on-line assays the following factors must be considered: 1) cell chamber volume should be low to allow use of small amounts of cells and reduced reagent costs; 2) flow rates should be high enough rapidly wash-out the cell chamber for good temporal resolution but not so high as to create excessive pressures that may cause leaks or excessive dilution of the chemicals to be measured; 3) reagent channels should allow both rapid mixing and enough incubation time for the assays.

As a starting point for chip design, we initially set the cell chamber volume to 8 μL, matching the dimensions previously reported.[2.24] We estimated that the perfusion flow rate should be no higher than 0.75 μL/min to avoid diluting the cell secretions below

the detection limit of the assays. Using this flow rate through the chamber, the downstream assay reagent inlet flow rates were optimized to provide the best sensitivity during calibration experiments. For the NEFA assay, it was determined that a flow of 0.6 µL/min for the assay reagents provided the optimum sensitivity. Likewise, with the glycerol assay, reagent flow rates of 0.75 µL/min were chosen. Because the assays require 5 min incubation time, we determined that the reaction channel volume should be 12.6 µL. A 600 µm wide by 60 µm deep by 350 mm long channel provides the volume necessary in a convenient size that does not create much back pressure at the flow rates used. In principle other channel dimensions could be used. To aid mixing, we created thinner (100 µm), serpentine channel regions after each reagent inlet.

Through off-line optimization experiments, it was discovered that the mixing order and duration was key to improving the NEFA assay sensitivity. The first reaction of the assay seems to be rate-limiting, and therefore needs sufficient time to incubate before addition of the second reagent and fluorogenic dye. Moreover, CR-B and AUR should be introduced in separate inlets, because pre-mixing the reagents increases the background of the assay. Therefore, the NEFA channel was altered to position the CR-B and AUR reagent inlets downstream after the CR-A reagent was added. Aside from the differences in reagent inlet number and location, the chip designs for the 2 independent assay devices were nearly identical. The linear calibration curves for both assays are shown in Figure 2.9. Using the independent chips as guides for developing a chip containing both assays, the resulting chip had 2 sets of mixing channels that were symmetrical aside from the number and location of reagent inlets.

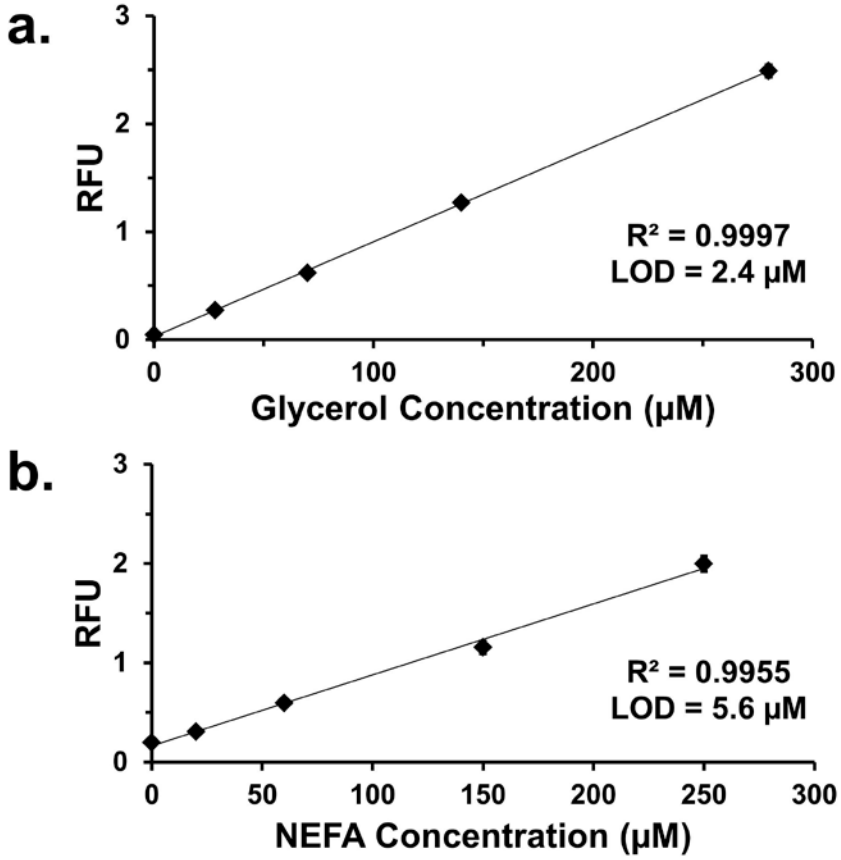

Figure 2.9: Calibration curves for the glycerol (a) and NEFA (b) assays, performed on the respective single assay chips. The error bars are the standard deviations of the averaged time points.

References

2.1. Salieb-Beugelaar, G. B.; Simone, G.; Arora, A.; Philippi, A.; Manz, A., *Anal. Chem.* **2010,** *82*, 4848-4864.

2.2. El-Ali, J.; Sorger, P. K.; Jensen, K. F., *Nature* **2006,** *442*, 403-411.

2.3. Walker, G. M.; Zeringue, H. C.; Beebe, D. J., *Lab Chip* **2004,** *4*, 91-97.

2.4. Cheng, W.; Klauke, N.; Smith, G.; Cooper, J. M., *Electrophoresis* **2010,** *31*, 1405-1413.

2.5. Kim, L.; Toh, Y. C.; Voldman, J.; Yu, H., *Lab Chip* **2007,** *7*, 681-694.

2.6. Young, E. W. K.; Beebe, D. J., *Chem. Soc. Rev.* **2010,** *39*, 1036-1048.

2.7. Godwin, L. A.; Pilkerton, M. E.; Deal, K. S.; Wanders, D.; Judd, R. L.; Easley, C. J., *Anal. Chem.* **2011,** *83*, 7166-7172.

2.8. Vyawahare, S.; Griffiths, A. D.; Merten, C. A., *Chem. Biol.* **2010,** *17*, 1052-1065.

2.9. Roper, M. G.; Shackman, J. G.; Dahlgren, G. M.; Kennedy, R. T., *Anal. Chem.* **2003,** *75*, 4711-4717.

2.10. Shackman, J. G.; Reid, K. R.; Dugan, C. E.; Kennedy, R. T., *Anal. Bioanal. Chem.* **2012,** *402*, 2797-2803.

2.11. Hiatt, L. A.; McKenzie, J. R.; Deravi, L. F.; Harry, R. S.; Wright, D. W.; Cliffel, D. E., *Biosens. Bioelectron.* **2012,** *33*, 128-133.

2.12. Goto, M.; Sato, K.; Murakami, A.; Tokeshi, M.; Kitamori, T., *Anal. Chem.* **2005,** *77*, 2125-2131.

2.13. Reshef, L.; Olswang, Y.; Cassuto, H.; Blum, B.; Croniger, C. M.; Kalhan, S. C.; Tilghman, S. M.; Hanson, R. W., *J. Biol. Chem.* **2003,** *278*, 30413-30416.

2.14. Beale, E. G.; Hammer, R. E.; Antoine, B.; Forest, C., *Trends Endocrin. Met.* **2004,** *15*, 129-135.

2.15. Nye, C.; Kim, J.; Kalhan, S. C.; Hanson, R. W., *Trends Endocrinol. Metab.* **2008,** *19*, 356-361.

2.16. Wyne, K. L., *Am. J. Med.* **2003,** *115*, 29-36.

2.17. Rosen, E. D.; Spiegelman, B. M., *Nature* **2006,** *444*, 847-853.

2.18. Kahn, S. E.; Hull, R. L.; Utzschneider, K. M., *Nature* **2006,** *444*, 840-846.

2.19. Guilherme, A.; Virbasius, J. V.; Puri, V.; Czech, M. P., *Nat. Rev. Mol. Cell Bio.* **2008,** *9*, 367-377.

2.20. Lai, N.; Sims, J. K.; Jeon, N. L.; Lee, K., *Tissue Eng. Part C-Methods* **2012,** *18*, 958-967.

2.21. Hemmingsen, M.; Vedel, S.; Skafte-Pedersen, P.; Sabourin, D.; Collas, P.; Bruus, H.; Dufva, M., *PLoS ONE* **2013,** *8*.

2.22. Zhang, C.; Zhao, Z. Q.; Rahim, N. A. A.; van Noort, D.; Yu, H., *Lab Chip* **2009,** *9*, 3185-3192.

2.23. Clark, A. M.; Sousa, K. M.; Jennings, C.; MacDougald, O. A.; Kennedy, R. T., *Anal. Chem.* **2009,** *81*, 2350-2356.

2.24. Clark, A. M.; Sousa, K. M.; Chisolm, C. N.; MacDougald, O. A.; Kennedy, R. T., *Anal. Bioanal. Chem.* **2010,** *397*, 2939-2947.

2.25. Guan, H. P.; Li, Y.; Jensen, M. V.; Newgard, C. B.; Steppan, C. M.; Lazar, M. A., *Nat. Med.* **2002,** *8*, 1122-1128.

2.26. Arner, P., *Best Pract. Res. Clin. Endoc. Metab.* **2005,** *19*, 471-482.

2.27. Lafontan, M.; Langin, D., *Prog. Lipid Res.* **2009,** *48*, 275-297.

2.28. Ng, J. M. K.; Gitlin, I.; Stroock, A. D.; Whitesides, G. M., *Electrophoresis* **2002,** *23*, 3461-3473.

2.29. McDonald, J. C.; Duffy, D. C.; Anderson, J. R.; Chiu, D. T.; Wu, H. K.; Schueller, O. J. A.; Whitesides, G. M., *Electrophoresis* **2000,** *21*, 27-40.

2.30. Unger, M. A.; Chou, H. P.; Thorsen, T.; Scherer, A.; Quake, S. R., *Science* **2000,** *288*, 113-116.

2.31. Wong, I.; Ho, C. M., *Microfluid. Nanofluid.* **2009,** *7*, 291-306.

2.32. Zhou, J. W.; Ellis, A. V.; Voelcker, N. H., *Electrophoresis* **2010,** *31*, 2-16.

2.33. Roman, G. T.; Hlaus, T.; Bass, K. J.; Seelhammer, T. G.; Culbertson, C. T., *Anal. Chem.* **2005,** *77*, 1414-1422.

2.34. Liu, Y.; Fanguy, J. C.; Bledsoe, J. M.; Henry, C. S., *Anal. Chem.* **2000,** *72*, 5939-5944.

2.35. Bauer, W.-A. C.; Fischlechner, M.; Abell, C.; Huck, W. T. S., *Lab Chip* **2010,** *10*, 1814-1819.

2.36. Lillehoj, P. B.; Ho, C. M., A Long-Term, Stable Hydrophilic Poly(dimethylsiloxane) Coating For Capillary-Based Pumping. In *Mems 2010: 23rd IEEE International Conference on Micro Electro Mechanical Systems, Technical Digest*, IEEE: New York, 2010; pp 1063-1066.

2.37. Zhou, J.; Khodakov, D. A.; Ellis, A. V.; Voelcker, N. H., *Electrophoresis* **2012,** *33*, 89-104.

2.38. Cellar, N. A.; Kennedy, R. T., *Lab Chip* **2006,** *6*, 1205-1212.

2.39. Roman, G. T.; Carroll, S.; McDaniel, K.; Culbertson, C. T., *Electrophoresis* **2006,** *27*, 2933-2939.

2.40. Maheshwari, N.; Kottantharayil, A.; Kumar, M.; Mukherji, S., *Appl. Surf. Sci.* **2010,** *257*, 451-457.

2.41. Lee, J. N.; Park, C.; Whitesides, G. M., *Anal. Chem.* **2003,** *75*, 6544-6554.

2.42. Zhou, D.; Samovski, D.; Okunade, A. L.; Stahl, P. D.; Abumrad, N. A.; Su, X., *FASEB J.* **2012,** *26*, 4733-4742.

2.43. Wang, Z. G.; Pini, M.; Yao, T.; Zhou, Z. X.; Sun, C. H.; Fantuzzi, G.; Song, Z. Y., *Am. J. Physiol. Endocrinol. Metab.* **2011,** *301*, E703-E712.

2.44. Hashimoto, T.; Segawa, H.; Okuno, M.; Kano, H.; Hamaguchi, H.-o.; Haraguchi, T.; Hiraoka, Y.; Hasui, S.; Yamaguchi, T.; Hirose, F.; Osumi, T., *J. Cell Sci.* **2012,** *125*, 6127-6136.

2.45. Getty-Kaushik, L.; Richard, A. M. T.; Corkey, B. E., *Diabetes* **2005,** *54*, 629-637.

CHAPTER 3

MONITORING CELL SECRETIONS ON MICROFLUIDIC CHIPS USING SOLID-PHASE EXTRACTION WITH MASS SPECTROMETRY

Introduction

Microfluidics has become an enabling technology for analytical chemistry by allowing miniaturization, integration, and automation, often with performance enhancements over larger scale instruments. Many examples of performing chemical assays or separations on microfluidic chips with impressive sensitivity and throughput have been reported.[3.1, 2] Microfluidics has also been enabling for cellular biology. Cells can be cultured on chips after loading into chambers by flow and other methods.[3.3, 4] The fluidic environment allows cell culture conditions to be exquisitely controlled and better match *in vivo* conditions.[3.4-6] Integrating chemical analysis with culture enables cell function to be assayed under different conditions.[3.7, 8] Such studies can be critical for studying cell physiology. In this work, we describe an approach to integrating living cell perfusion on-chips with electrospray ionization mass spectrometry (ESI-MS) to analyze secretions from the cells.

Culturing and monitoring cells on microfluidic chips has many advantages over conventional techniques. The inherent size of such devices reduces the number of cells required.[3.9, 10] Constant perfusion of culture media on chip allows replenishment of essential nutrients and removal of waste products, which creates a more physiologically relevant environment and provides the capability to change conditions for controlled experiments.[3.5, 11, 12] It is relatively straightforward to monitor cell function using

fluorescence microscopy on chips.[3.13-16] Perfusate can also be analyzed by other analytical techniques to measure cell secretions and other effects of the cells on chemical environment. Several examples of manually sampling perfusate from chips for detection of peptide or metabolite release from cells have been reported[3.17-20]; however, manual sampling of perfusate and off-line assay fails to fully to take advantage of the integration and automation possible on chips.

Several studies have reported integration of on-line analysis of perfusates to monitor cellular secretions on chips.[3.21, 22] Immunoassay[3.23-25] or enzyme assay[3.26-28] with fluorescent detection, capillary electrophoresis with electrochemical detection[3.29], and enzyme assay with chemiluminescent detection have all been used.[3.30] These methods give temporal resolution and selectivity in the measurement providing excellent insight into cell function. For example, rapid electrophoresis assays have been used to monitor insulin secretion in real time from single islets of Langerhans providing information on oscillations of secretion.[3.31] A commonality of these methods however, is that they are specific for a single (or small number) of compounds and new assays must be designed for each target analyte.

To develop a more versatile approach to chemical monitoring of cells on chips, we have investigated coupling MS to cell culture chips. MS is a powerful, sensitive, and widely available analytical technique. MS also provides high selectivity, the ability to detect multiple compounds in single scans, and direct detection of compounds without labels. ESI-MS is compatible with continuous flow systems and can be coupled to microfluidic chips.[3.32-36] All of these properties make ESI-MS well-suited as a general tool for analyzing cell perfusates. Combining the many advantages of on-chip cell

perfusion and MS detection suggests potential for a powerful approach to study cell secretion dynamics.

Although ESI-MS is well suited for this application, a significant impediment is that biological samples often contain high concentrations of salts and other species that can cause ion signal suppression in MS.[3.37] Sample "clean-up" methods like solid phase extraction (SPE) are often used to remove interfering species prior to ESI-MS. SPE can be implemented during off-line sample preparation prior to analysis (e.g., ZipTip)[3.18] or in an on-line format[3.33, 37, 38]. In SPE, samples are loaded onto a packed bed of sorbent. The bed is rinsed to remove poorly retained species, and then a solvent is passed through the bed to elute analytes. Hydrophobic sorbents are often used to retain analytes and allow removal of salts.

In previous work, microfluidic cell perfusion has been coupled to on-chip SPE and ESI-MS analysis.[3.39, 40] These devices were applied to monitor vitamin E metabolites secreted from lung epithelial cells[3.39] and glutamate release from neuronal cells[3.40]. This seminal work illustrated the potential for such approaches; however, in these reports, the components are on separate devices so that the steps of SPE required repeated and manual disconnection and reconnection of tubing to the chips. In addition, the cells are in direct fluidic connection to the SPE packing and therefore are exposed to higher backpressures generated by the bed. This higher (and changing) pressure is potentially detrimental to cell viability because high shear stress can cause changes in normal cell morphology and function.[3.10] Furthermore, increased shear can also cause detachment of adhered cells from the surface, which is especially undesirable for buoyant adipocytes.

To create an automated, on-line microfluidic cell perfusion system with ESI-MS analysis, we have developed a PDMS chip that integrates a cell chamber with an injection loop that functions like a conventional 6-port valve. The injection loop allows automated collection of perfusate and then injection onto an in-line SPE-ESI-MS system. The injection system fluidically isolates cells from the SPE packing to prevent exposing cells to changing pressure. The pneumatically-actuated valves were integrated on the PDMS chip through multilayer assembly.[3.41] In such devices, a 'control' channel is overlaid across a shallow fluidic channel. When gas pressure is applied through the control channel, the fluid channel is constricted via deformation of the elastomeric PDMS to block flow.

Cultured adipocytes are used as a model cell system in this study. Adipose tissue is integral to maintaining systemic energy balance by storing and releasing lipids based on physiological requirements. Adipocytes secrete non-esterified fatty acids (NEFAs) through regulated lipolysis.[3.42, 43] Adipocytes represent a particularly challenging cell type because they are fragile and buoyant, making them susceptible to changes in pressure or shear. In previous reports, NEFAs secreted from perfused adipocytes have been measured on PDMS chips with enzyme assays and laser-induced fluorescence.[3.26, 28] These enzyme assays only allow total NEFA measurement; MS is a more versatile detection technique, allowing detection of specific NEFAs. With this chip-MS method, the change in specific NEFAs released during lipolysis stimulation could be determined, better indicating the composition of circulating NEFAs due to lipolysis than with previous methods.

Experimental

Reagents

LC-grade acetonitrile (ACN) and water, isoproterenol hydrochloride, forskolin, palmitoleic acid standard and fatty acid free bovine serum albumin (BSA) were purchased from Sigma-Aldrich (St. Louis, MO). Ammonium hydroxide was obtained from Fisher Scientific (Pittsburgh, PA). Cell culture reagents and Hank's buffered salt solution (HBSS, Cat. No. 14175) were received from Life Technologies (Carlsbad, CA).

PDMS Chip Fabrication

Chip fabrication used procedures similar to those described before[3.28]. The injection loop chip was composed of two separate pieces and all layers were formed from 10:1 base:curing agent PDMS (RTV 615, Curbell Plastics, Livonia, MI). Three Si wafers with raised features were made using SU-8 2075 photoresist (MicroChem, Newton, MA). Wafer A contained the lower cell chamber and was 250 μm thick (mask shown in Figure 3.1a). Wafer B consisted of the fluidic channels with SU-8 features 60 μm thick and AZ 9260 (Capitol Scientific, Austin, TX) features 12 μm thick (Figure 3.1b). Wafer C contained the SU-8 control channel features that were 60 μm thick (Figure 3.1c). PDMS was poured over wafer A and manually spread to create a layer ~1 mm thick. PDMS was spun on wafer B to a height of 70 μm. A thick layer (~1 cm) of PDMS was poured over wafer C. Additionally, PDMS was spun on a blank wafer to a height of 170 μm. All wafers were baked at 80 °C for 1 hr. The PDMS molded from wafer C was peeled off the wafer and holes were punched through the PDMS at the green points indicated on Figure 3.1c. This layer was irreversibly bonded to the PDMS spun on wafer B, feature side down, using corona discharge. The bonded layers were peeled away from wafer B and

were then bonded, feature side down, to the PDMS spun on the blank wafer. The 3 layers (forming the top part of the chip) were peeled away and the bottom layer of PDMS was cut away around the cell chamber dimensions. A glass coverslip (No. 1, Fisher Scientific) was bonded to the top of the cell chamber. Capillary tubing was used to move fluid in and out of the chip. One side of 50 μm inner diameter (ID)/150 μm outer diameter (OD) capillaries (Polymicro Technologies, Phoenix, AZ) were rounded with fine sand paper and inserted into the sides of the chip. The other end of the capillary was sheathed with 180/360 capillary and the two capillaries were then permanently secured using cyanoacrylate glue. Stainless steel tubing, (23 G, 1 cm long) sheathed halfway with Tygon Tubing (1/16 in. OD, 0.5 mm ID, IDEX, Lake Forest, IL), was inserted into the aforementioned holes made in the PDMS layer taken from wafer C. The PDMS from wafer A was peeled away and bonded to a glass slide, feature side up, forming the bottom part of the chip.

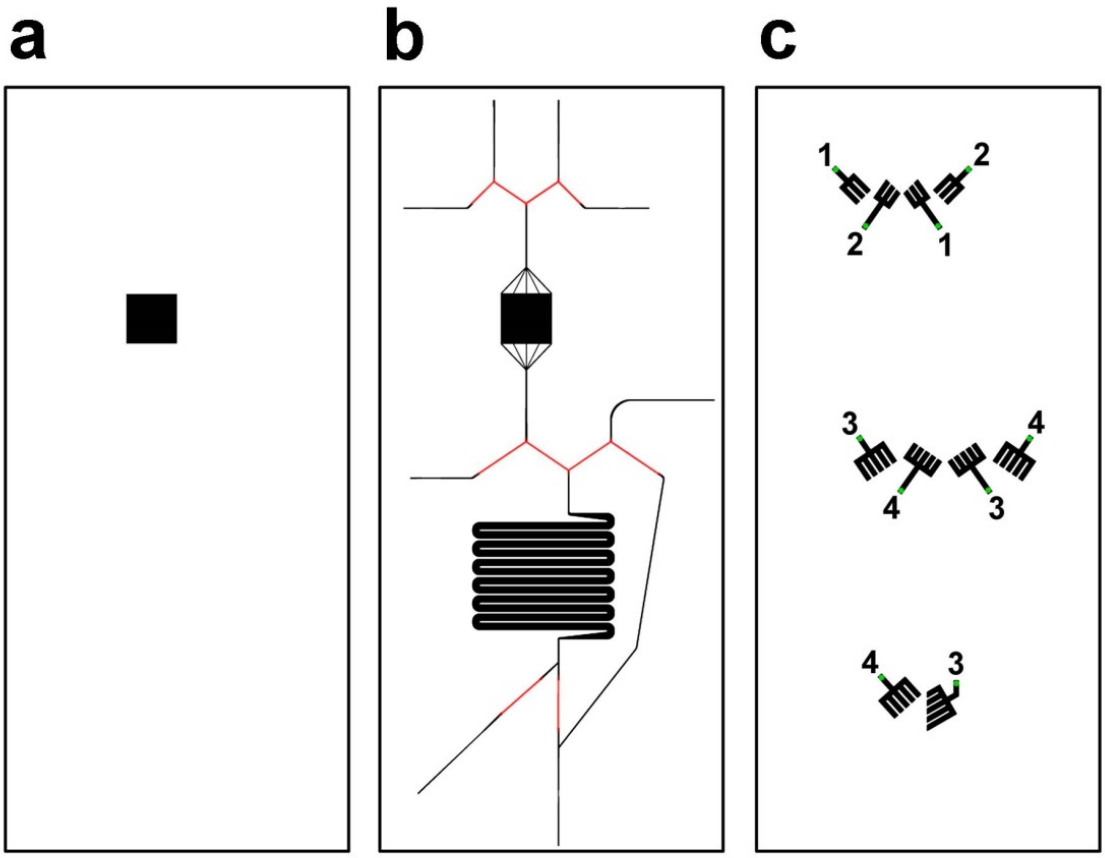

Figure 3.1: PDMS mold layers. Each box indicates a different fabricated layer; (a) lower cell chamber, (b) fluidic layer, and (c) valve control layer. The numbers in (c) indicate the valves that are operated together on the same solenoid valve.

Adipocyte Culture

Murine 3T3-L1 adipocytes were cultured to day 11-13 post-induction as previously described.[3.28] Briefly, glass coverslips (No. 1, Fisher Scientific) were cut to 4.8 mm x 4.8 mm and placed in the bottom of 6-well plates. Preadipocytes were plated over the coverslips at a density of 100,000 cells/mL. Two days after the cells reached confluence, adipogenesis was induced with 500 µM isobutylmethylxanthine, 1 µM dexamethasone, and 1 µg/mL insulin in adipogenic media. Adipogenic media consisted of 10% fetal bovine serum (FBS), 1 mM sodium pyruvate, 2 mM L-glutamine, 100

units/mL penicillin, and 100 µg/mL streptomycin in Dulbecco's eagle medium (Cat. No. 11965, Life Technologies). 2-3 days after induction treatment, the media was replaced with adipogenic media containing 1 µg/mL insulin. Every 2-3 days following, fresh adipogenic media was added.

Chip Assembly and Operation

Prior to each use, the top portion of the PDMS chip was degassed for 30 min and the channels and Tygon tubing were primed with water. A coverslip with adhered adipocytes was removed from culture, rinsed with basal perfusion buffer (0.1% BSA and 25 mM glucose in HBSS) and transferred to the lower cell chamber. An additional 10 µL basal perfusion buffer was added to the top of the cells and the 2 chip pieces were sealed together, using the outline of the cell chamber in both portions for alignment. During calibration experiments, the same assembly procedure was used, but with a blank coverslip placed in the lower cell chamber. All air and excess liquid was removed between the layers. To ensure a leak-free operation, the assembled chip was compressed in plastic frame. One side of the compression frame had holes drilled at the same spacing as where the PDMS control channel layer was punched. Both pieces had holes drilled around the chip dimensions for adding bolts to compress the plastic. The valve Tygon tubing was threaded through the compression frame and the chip was lightly tightened in the frame. A LabView 12.0 (National Instruments, Austin, TX) script was written to operate a series of solenoid valves (LHDA1211111H, The Lee Co., Westbrook, CT), which controlled flow from an N_2 tank to the Tygon tubing in the chip, similar to that described previously.[3.44]

Chip-to-MS Connection

A suspension of 20 µm fully porous C18 particles (Alltima, Grace Davison, Deerfield, IL) was made in methanol (~2 mg/mL). Polished ends of 150/360 and 40/360 capillary were connected with a PicoClear union (New Objective, Woburn, MA). The particle slurry was pushed into the 150/360 capillary using a syringe until the bed length was ~1 mm long. The outlet of the injection loop chip was connected to the 150/360 capillary with a Teflon union as shown in Figure 3.2. The other end of the 40/360 capillary was inserted into a metal tee which was used to apply voltage for electrospray. A spray tip (75/360 capillary with a 15 µm tip, New Objective) was inserted in the opposite end of the metal tee (the third port was plugged with an optical fiber). The entire assembly was mounted on a platform, built on an x-y-z stage for easier alignment with the MS source.

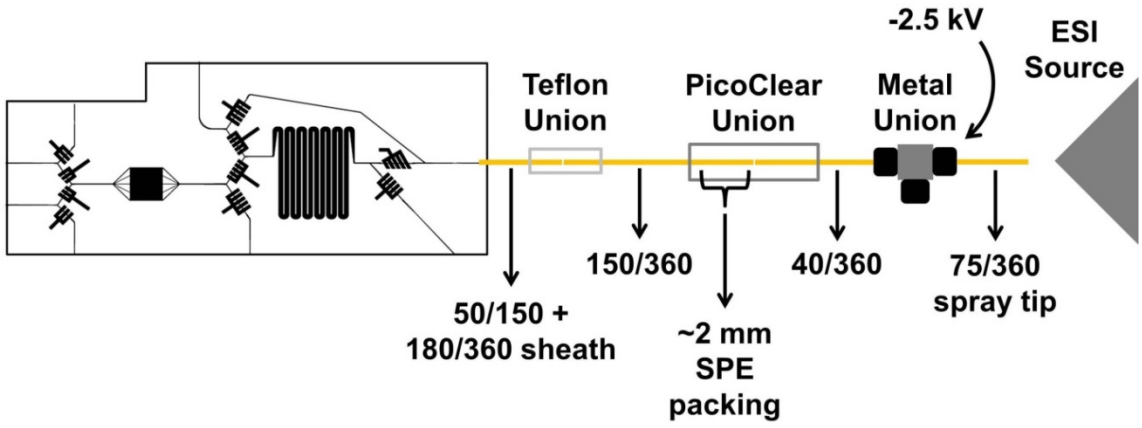

Figure 3.2: Schematic of chip connection to SPE column and ESI components.

Mass Spectrometry Detection and Analysis

A triple quadrupole (QQQ) mass spectrometer (TSQ Quantum Ultra, Thermo-Scientific, Waltham, MA) was used for detection of the NEFA species. The platform supporting the chip and connections was inserted through the door of the ion source and

the spray tip was positioned ~8 mm from the ion funnel. The spray voltage was kept off during the SPE loading phase, but was set at -2.5 kV during the wash and elution steps. The ion source capillary was maintained at a temperature of 250 °C and full scan mode ranging 200-320 m/z with a scan rate of 2 Hz was used for recording. Peak areas of the detected NEFAs were measured with a range of ± 0.5 Da of the $[M-H]^-$. In some cases, high resolution time-of-flight MS was used for analysis (see Supporting Information).

Results and Discussion

Chip Design & Operation

This work builds upon a previous chip that was reported to measure NEFA secretion from on-chip adipocyte perfusion.[3.28] In that work, cell perfusate was mixed on-chip with enzyme assay reagents in a continuous flow system to allow real-time monitoring of NEFA release; however, this method did not allow identification of individual NEFAs. With this new PDMS chip (Figure 3.2), it is possible to perfuse cells and directly monitor secretion of NEFAs via SPE-ESI-MS. The integration of an injection loop on chip enables automated fraction collection and coupling to a SPE-ESI capillary without exposing cells to changes in pressure due to flow through the packed bed. A square cell chamber design is used on this chip like previously described[3.28]. Chamber inlets were positioned so that buffer flows as a flat front (as opposed to parabolic profile) down the length of the chamber which improved the temporal response of the system. Approximately 25,000 3T3-L1 adipocytes are loaded into the cell chamber. This cell requirement is an ~80-fold reduction compared to conventional cell analysis in a 6-well plate, illustrating the potential for miniaturization.

Four valves were constructed upstream of the cell chamber to automate selection of cell perfusate solution (Figure 3.3). One inlet upstream of the cell chamber was infused with basal buffer and the other with 20 μM isoproterenol/10 μM forskolin with 0.1% DMSO in basal buffer. (During calibration, different concentrations of standards were infused through the inlets). The valves operated so that as one solution flowed to the cell chamber, the other flowed to waste. Actuating the valves changed the solution flowing over the cells. These solutions had a flow rate of 0.75 μL/min, which was therefore the flow rate perfused over the cells. There were a number of tradeoffs when selecting the flow rate. A high flow rate would be advantageous for temporal response by decreasing the time for each round of injections; however, excessively high flow rate may damage or dislodge cells, overly dilute analytes, and cause valves to fail.

Downstream of the cells, the direction of flow was controlled through the switching of 6 multilayer valves (see Figure 3.3), which operated independently of the 4 valves upstream of the cell chamber. These valves controlled sample collection and SPE. In the first step of chip operation, cell perfusate from the cell chamber was directed into a serpentine loop, while a wash solvent (10% ACN/90% H_2O with 15 mM NH_4OH) was infused through a side inlet. During loop filling mode, the cell perfusate (sample) was directed through the loop to waste at the loop exit, while the wash solvent bypassed the loop and flowed directly into the SPE column as illustrated in Figure 3.3a. Once the loop was filled, the valves were switched and the sample was pumped onto the SPE bed while cell perfusate was directed to waste as shown in Figure 3.3b. The valve was set in this position for 12 min to fully load sample and allow rinse of the SPE column with wash solvent. Once the sample was fully loaded onto the SPE bed, the valves were switched

back to their original position. The wash solvent bypassed the loop and was pumped onto the SPE bed for an additional 5 minutes to ensure all the salts were removed from the SPE packing. The wash solvent was replaced with the high organic elution solvent (75% ACN/25% H_2O with 15 mM NH_4OH) via an external 4-port valve to elute the NEFAs for detection (Figure 3.3c). During the third step, the sample loop was filled with cell perfusate in preparation for the next fraction analysis. Using this procedure, 3 assays were performed with cells under basal conditions, and another 3 with cells stimulated with the isoproterenol/forskolin mixture (each iteration taking a total of 30 min). With this isocratic method, the NEFAs were all eluted to the MS at the same time. Implementing a gradient elution protocol could allow chromatographic separation of the NEFAs and improve their detection.

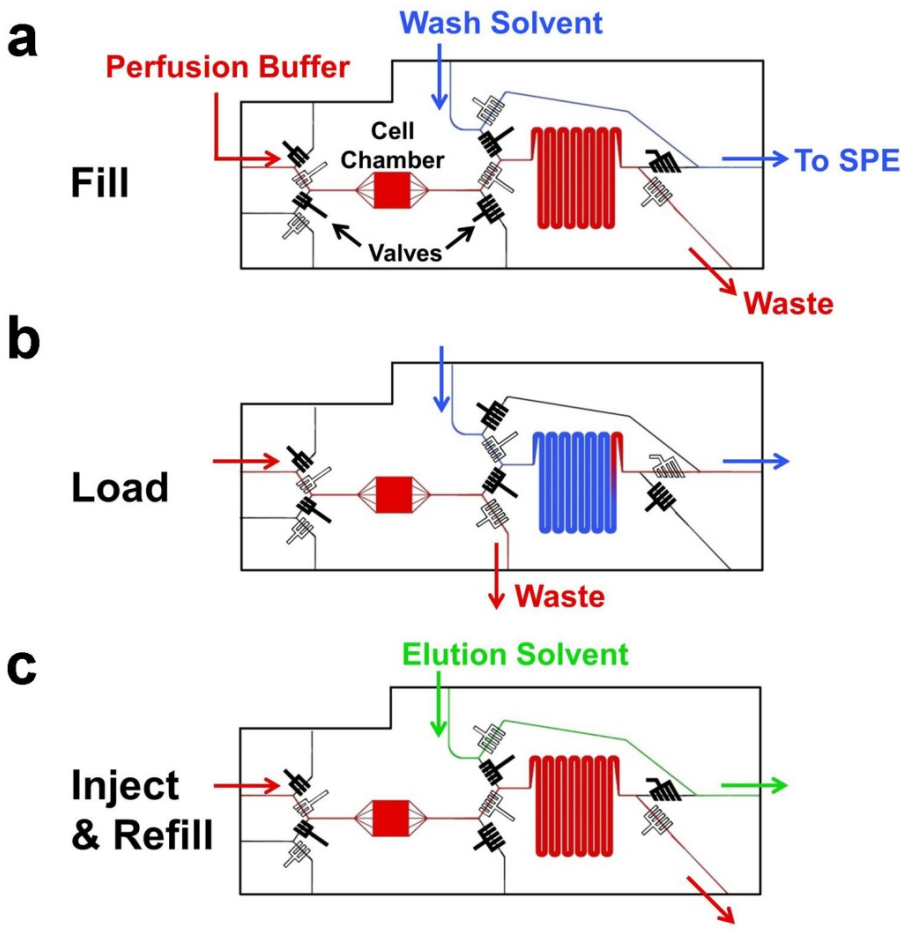

Figure 3.3: Operation modes for the injection loop chip. Closed valves are black and open valves are white. (a) Loop fills with perfusate from cell chamber (red) and flows to a waste outlet, while the wash solvent (blue) bypasses the loop and is directed towards the SPE bed. (b) The cell perfusate is flushed out of the loop and onto the SPE bed by the wash solvent. Flow from the cell chamber is directed towards a waste outlet upstream of the loop. (c) Valves are in the same mode as (a), but wash solvent is replaced with elution solvent (green). Elution solvent bypasses the loop and is flowed onto the SPE bed, while the loop fills with cell perfusate again.

Overall, this system operated like a conventional HPLC injection valve coupled with a short SPE bed. Integration of the loop allowed fluidic isolation of the cells from the downstream elements that could generate back pressures (SPE packing, spray tip). The serpentine pattern reduced the footprint of the chip, while providing enough channel length to collect adequate sample for MS injection. The injection loop was designed to

hold 7.5 µL of sample, so with the flow rate used, it took 10 min to fill/empty the loop. The size of this channel could be reduced in future generations of the chip, improving temporal response.

Initial experiments revealed that back pressure of the SPE bed caused control channels fail. To prevent this, the 6 valves that operated the injection loop were modified so that control channels for each valve were branched to five channels. This branching allowed complete channel closure under conditions with downstream backpressure. Using inlet flow rates of 0.75 µL/min, the valves remain functional (i.e., completely sealed the lower fluid channels) up to back pressures of ~7 psi at the chip outlet. A video showing the operation of the multilayer valves is available in the supplementary information. This pressure limit, while sufficient for SPE as demonstrated here, constitutes a limit of this system for using longer columns or smaller particles.

The SPE bed was made with 20 µm particles packed into a large bore capillary (150 µm ID) to minimize flow resistance. A 40 µm ID capillary at the exit of the SPE bed served to hold the particles in the capillary because particles will not flow through this capillary once packed due to the keystone effect.[3.45] A ~1 mm long SPE bed packed in this manner creates about 2.5 psi backpressure at a flow rate of 0.75 µL/min. We also explored using glass fiber frits to hold the particles in place[3.46]; however, we found that the back pressure was too high to operate at effective flow rates.

The spray tip size was another consideration taken into account for this system. Smaller tips create more efficient spray, but they were prone to clogs. A capillary that had a 75 µm ID, pulled to 15 µm at the tip, provided sufficient spray (with low back pressure) and was able to be used for routine experiments without clogging.

Chip Characterization

To determine the reproducibility of injections using the chip, a 50 µM standard of palmitoleic acid (16:1, $[M-H]^-$ = 253.2 Da) was perfused through the cell chamber, filled the loop, loaded onto the SPE bed and eluted to the MS repeatedly. It was found that the average peak area of 5 replicate injections was $5.8 \pm 0.41 \times 10^{10}$ (8% RSD). The average peak width was 50 s, indicating 12x sample concentration on the SPE bed (10 min load time). Similarly, to demonstrate the potential for quantification of NEFAs by chip-MS, a calibration curve of palmitoleic acid standards was created, shown in Figure 3.4. With standards measured in duplicate, the calibration curve had a R^2 of 0.98. The limit of detection for palmitoleic acid was 1.4 µM, as determined by the concentration of the signal that was 3 times the standard deviation of the two blank injections. This performance is not as good as might be expected for on-line SPE using a conventional HPLC valve and SPE bed, but such an instrument would be less integrated than the design described here. Furthermore, the analytical figures of merit for this chip are adequate for many physiological studies.

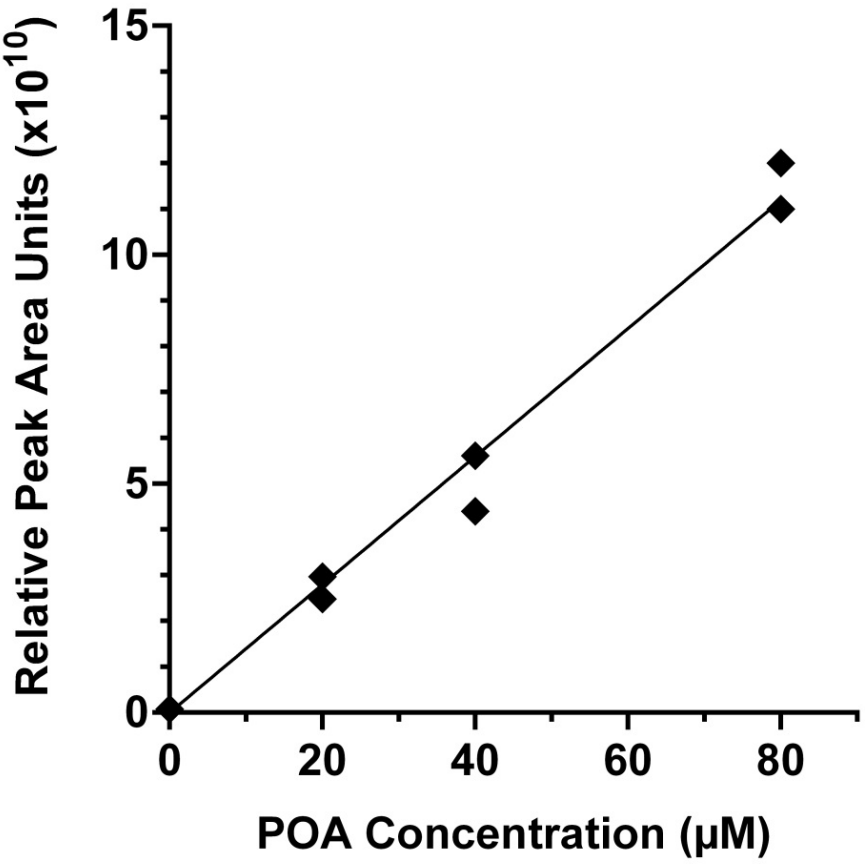

Figure 3.4: Calibration curve of palmitoleic acid (POA) standard, performed in duplicate. POA was dissolved in basal buffer and perfused through the chip at the inlet upstream of the cell chamber. Standard filled the loop, was loaded onto the SPE bed, washed and eluted to the MS in an on-line format.

NEFA Detection

Using the injection loop chip, select NEFAs secreted by adipocytes were analyzed by coupling on-chip cell perfusion to ESI-MS. Negative ion mode ESI was used for NEFA detection as the preferred ionization mechanism for NEFAs is the removal of a proton from the acidic carboxyl group.[3.47] All experiments were performed with adipocytes under basal conditions, followed by the perfusion of solutions containing isoproterenol and forskolin to stimulate lipolysis.

Initial experiments were aimed at evaluating what compounds were detected. Figure 3.5 shows a mass spectrum collected from the cells on chip compared to background. For this data, the mass spectrometer was scanned from 200 to 320 m/z comprising the range of the most common NEFAs. To determine the source of the signals, we matched the signal to m/z values for NEFAs known to be present in 3T3-L1 adipocytes. Previous work using GC-MS has shown that NEFAs from C8 to C20, both saturated and monounsaturated, are present in adipocytes with C14-C18 being the most prevalent. In agreement with those findings, we found peaks matching the nominal mass of C14:0, C15:1, C15:0, C16:1, C16:0, C17:1, C17:0, C18:1, C18:0, and C20:4. Small peaks for C16:0 and C18:0 were also found in background signals and therefore not further investigated. (Previous studies have also reported background signal from 16:0 and 18:0 in fresh LC solvents).[3.48] To better verify the identity of the signals, we also analyzed cell conditioned media by HPLC-TOF-MS (see supplemental). We found matching peaks for all of the NEFAs detected from the chip system but at the higher mass accuracy (as low as 1 ppm) of the TOF-MS. These results and matching what was found in the prior GC-MS studies, provide better confidence in the identifications shown in Figure 3.5. Collision-induced dissociation (CID), a fragmentation method used to more accurately identify compounds, was attempted but did not prove successful with the native NEFAs of interest in our study or in other reports.[3.49]

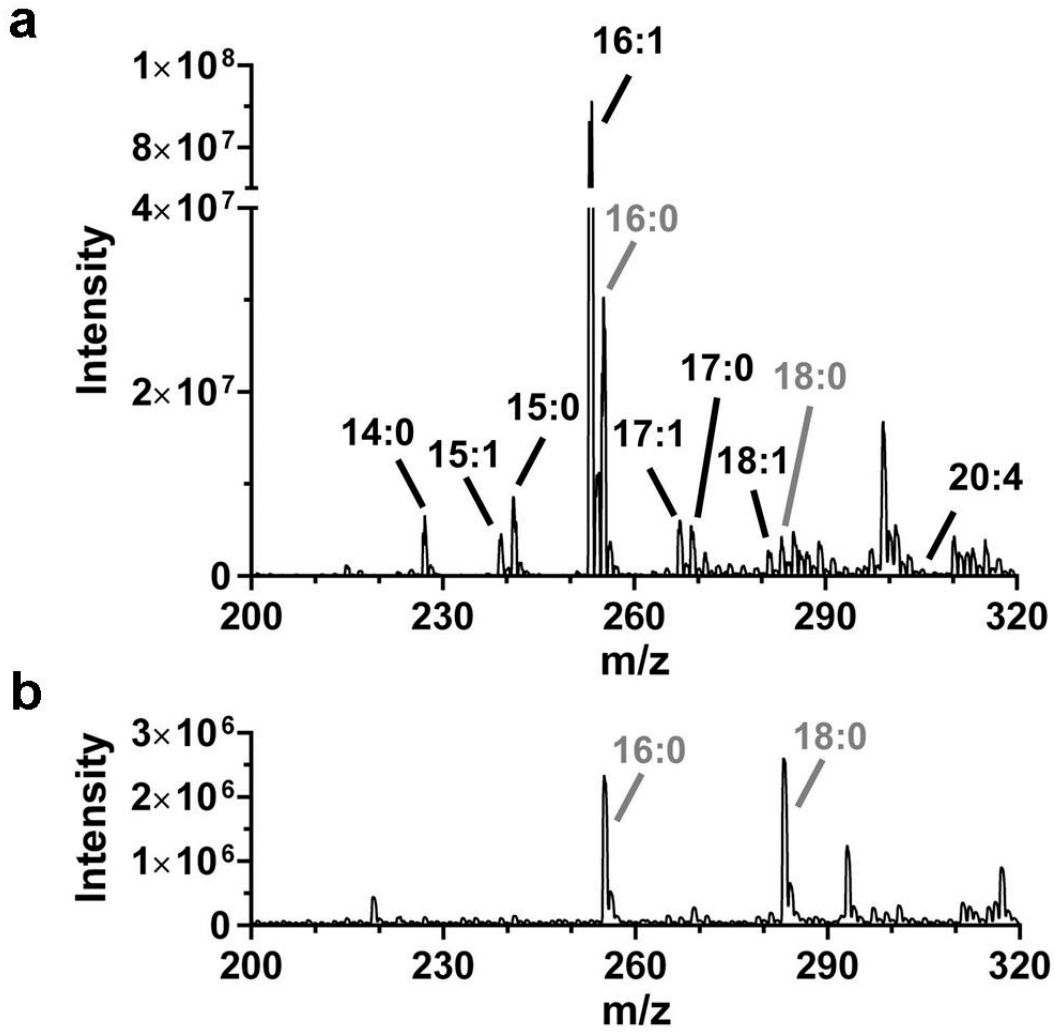

Figure 3.5: Full scan analysis of m/z ranging from 200-320 was performed for all experiments on a QQQ-MS. (a) Mass spectrum of on-line elution profile from 3T3-L1 adipocytes. Adipocytes were loaded in the cell chamber and stimulated with isoproterenol/forskolin in this example spectrum. Perfusate was loaded onto the on-line SPE bed. The SPE bed was subsequently washed and sample was eluted to the MS. Peaks are labeled with the NEFAs that associate with the appropriate m/z. (b) Mass spectrum of direct injection of elution buffer, showing background signal of 16:0 and 18:0.

We then used the chip to monitor the effect of treatment with forskolin/isoproterenol on NEFA secretion (Figure 3.6). These agents are known to stimulate lipolysis and evoke release of NEFA from adipocytes. To measure the various NEFAs, the peak areas of the extracted ion chromatograms (EICs) were calculated at the

expected m/z of the NEFAs. This is the first MS study for measurement of secreted NEFAs from living, perfused adipocytes. Stimulation of lipolysis with forskolin or isoproterenol generally results in a 2- to 10-fold increase in NEFA secretion over basal conditions as measured by enzyme assay in static culture or on-chip perfusion.[3.26, 28, 50-52] As shown in Figure 3.6, a statistically significant increase in 7 NEFAs was found with the application of lipolysis stimulating agents. The increase measured with the MS detection method was 1.2- to 1.9-fold over basal levels. This increase in less than what has been detected using enzyme assays for all NEFAs.[3.28] The smaller magnitude of stimulation detected with this technique could be accounted for by the fact that the enzyme assays measure every NEFA released from the adipocytes, while with the current method, two of the most abundant NEFAs were not able to be accurately detected. Furthermore, the relative abundance of secreted NEFAs could vary depending on culture conditions (i.e. the types of NEFAs present in a FBS aliquot, which is the source of lipid accumulation in cultured 3T3-L1 adipocytes).

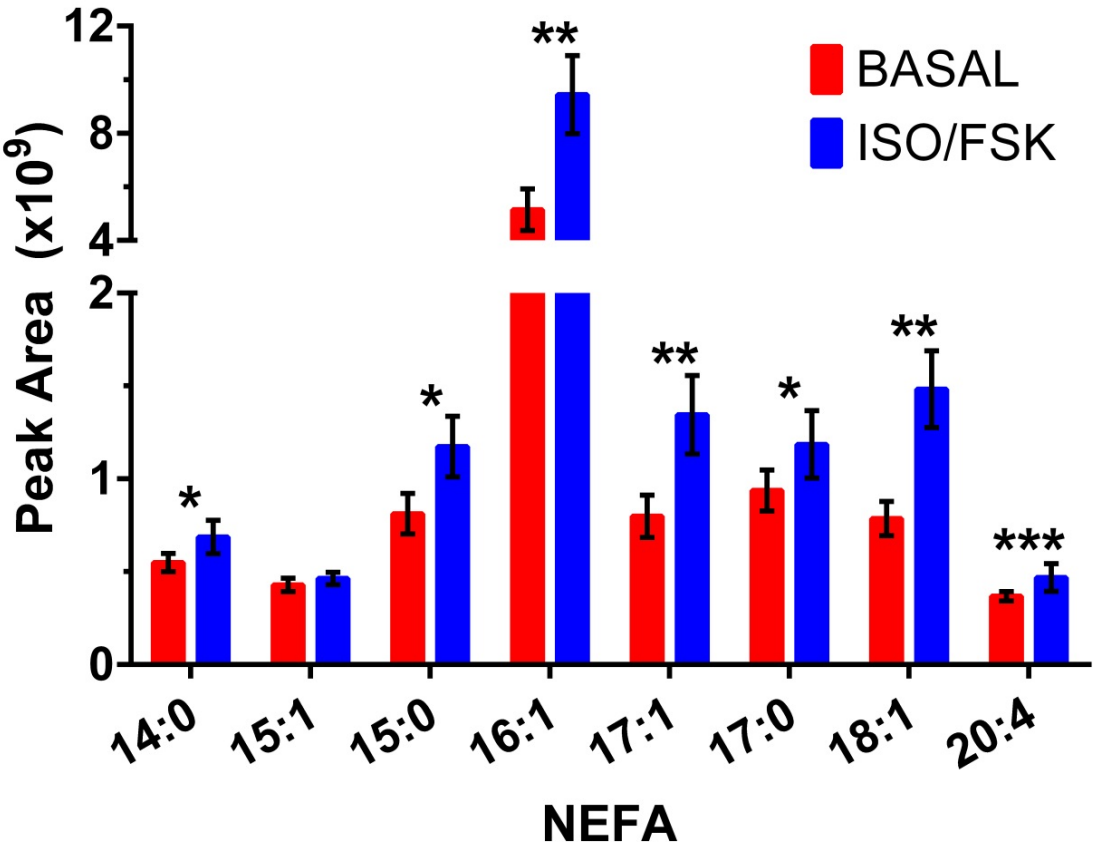

Figure 3.6: Averaged peak area of various NEFAs detected by MS from on-chip adipocyte secretion under basal and isoproterenol/forskolin (iso/fsk) stimulation. Data is average of 3 cell experimental replicates ± standard deviation, statistical significance determined by paired, 2-tailed Student's t-test, * P < 0.1, ** P < 0.05, *** P < 0.01.

Conclusions

An integrated microfluidic chip has been developed that is capable of perfusing cultured cells and monitoring secreted metabolites with MS detection. This continuous flow device allows cells to be cultured under physiologically-relevant conditions while coupling to MS enables potential detection of a wide variety of secreted metabolites. PDMS as the microfluidic substrate enable multilayer valve construction, similar to conventional 4- or 6-port valves, increasing the automation of analysis. The injection

loop valve system allowed discrete volumes of sample to be loaded onto an SPE bed, while isolating the cells from the backpressure generated by downstream clean-up or separation techniques. Using adipocytes as a model cell system, a variety of NEFAs were detected with this on-line perfusion format. NEFA secretion was measured under basal and stimulated conditions, demonstrating the capability of performing a range of biologically significant experiments on cultured cell lines on one miniaturized platform.

Although NEFA secretion was measured from adipocytes, this basic system could, in principle, be used for measuring release of other secretions from other cell types. The advantage of the MS system, compared to enzyme and immunoassay previously used for monitoring cell secretion on chips, is the versatility to detect a wide variety of compounds. Further, the ability to detect multiple compounds with a rapid scan enables multi-analyte monitoring. In the current system, a perfusate was collected in a loop and then extracted by SPE. The integration of SPE enables removal of ion suppressing components and concentrates the analytes 12x for greatly improved sensitivity of ESI-MS. Indeed, the NEFAs would not be detectable at the flow rates used without SPE. A weakness of the system as described here is the low temporal resolution for monitoring (30 min to fill loop and elute one sample). Chips with other materials may allow higher pressures to be used to increase flow rate over the SPE bed. Alternatively, other on-line extraction methods might prove useful.

Supplementary Information

Pilot NEFA-MS Studies

Initial studies of NEFA secretion from 3T3-L1 adipocytes were analyzed by HPLC-TOF-MS. Media from wells of incubated adipocytes was collected and samples

were injected onto a reversed-phase column (with a SPE guard column). Samples underwent a gradient elution to the MS, from water with 0.1% formic acid to ACN with 0.1% formic acid. The extracted ion chromatogram (with the mass spectra of select NEFAs) using the TOF is shown in Figure 3.7. The measured masses of the various detected NEFAs are shown in Table 2, and are compared to those measured with the QQQ interfaced to the chip. TOF mass analyzers have greater mass accuracy than QQQ, allowing more conclusive identification.[3.53] With the QQQ instrument, extracted ion chromatograms with mass ranges of ± 0.5 Da of the exact $[M-H]^-$ were generated to account for the decreased mass accuracy of the instrument.

Table 2: Comparison of measured NEFA mass accuracy on TOF and QQQ.

NEFA	Exact $(M-H)^-$	TOF		QQQ	
		Measured	Error (ppm)	Measured	Error (ppm)
14:0	227.200	227.197	13.2	227.02	792.3
15:1	239.202	239.205	12.5	238.92	1178.9
15:0	241.218	241.210	33.2	241.02	820.8
16:1	253.217	253.218	3.9	252.93	1133.4
17:1	267.233	267.234	3.7	266.93	1133.8
17:0	269.246	269.212	126.3	269.03	802.2
18:1	281.249	281.250	3.6	281.07	636.4
20:4	303.232	303.228	13.2	303.05	600.2

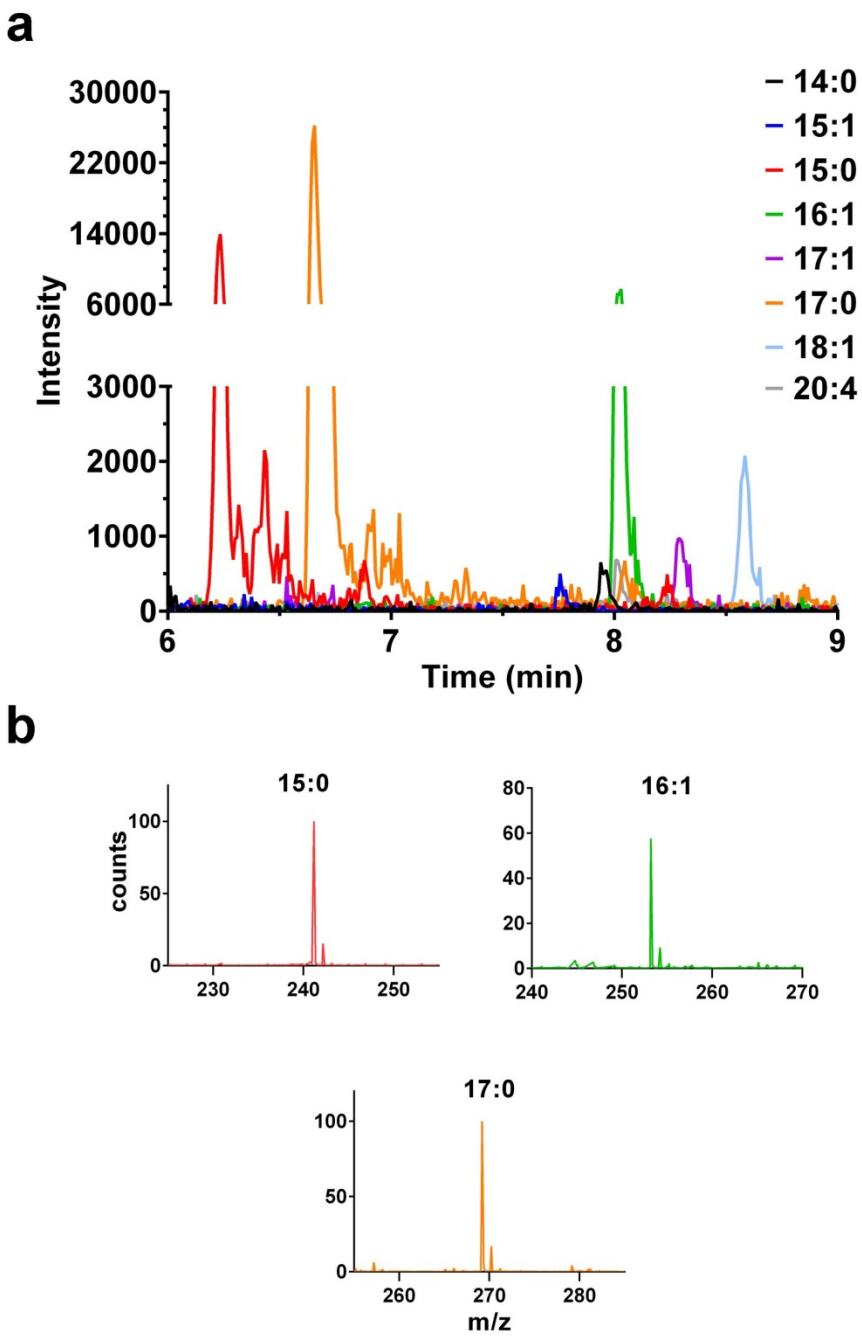

Figure 3.7: Extracted ion chromatogram of 8 NEFAs in adipocyte conditioned buffer, measured with HPLC-TOF-MS (a) along with the associated mass spectra of the most abundant NEFAs (b).

References

3.1. Nge, P. N.; Rogers, C. I.; Woolley, A. T., *Chem. Rev.* **2013,** *113*, 2550-2583.

3.2. Roman, G. T.; Kennedy, R. T., *J. Chromatogr. A* **2007,** *1168*, 170-188.

3.3. Hung, P. J.; Lee, P. J.; Sabounchi, P.; Aghdam, N.; Lin, R.; Lee, L. P., *Lab Chip* **2005,** *5*, 44-48.

3.4. Kim, L.; Toh, Y. C.; Voldman, J.; Yu, H., *Lab Chip* **2007,** *7*, 681-694.

3.5. El-Ali, J.; Sorger, P. K.; Jensen, K. F., *Nature* **2006,** *442*, 403-411.

3.6. Vyawahare, S.; Griffiths, A. D.; Merten, C. A., *Chem. Biol.* **2010,** *17*, 1052-1065.

3.7. Salieb-Beugelaar, G. B.; Simone, G.; Arora, A.; Philippi, A.; Manz, A., *Anal. Chem.* **2010,** *82*, 4848-4864.

3.8. Primiceri, E.; Chiriaco, M. S.; Rinaldi, R.; Maruccio, G., *Lab Chip* **2013,** *13*, 3789-3802.

3.9. Culbertson, C. T.; Mickleburgh, T. G.; Stewart-James, S. A.; Sellens, K. A.; Pressnall, M., *Anal. Chem.* **2014,** *86*, 95-118.

3.10. Walker, G. M.; Zeringue, H. C.; Beebe, D. J., *Lab Chip* **2004,** *4*, 91-97.

3.11. Dhumpa, R.; Roper, M. G., *Anal. Chim. Acta* **2012,** *743*, 9-18.

3.12. Kovarik, M. L.; Gach, P. C.; Ornoff, D. M.; Wang, Y.; Balowski, J.; Farrag, L.; Allbritton, N. L., *Anal. Chem.* **2012,** *84*, 516-540.

3.13. Sankar, K. S.; Green, B. J.; Crocker, A. R.; Verity, J. E.; Altamentova, S. M.; Rocheleau, J. V., *PLoS ONE* **2011,** *6*.

3.14. Nagrath, S.; Sequist, L. V.; Maheswaran, S.; Bell, D. W.; Irimia, D.; Ulkus, L.; Smith, M. R.; Kwak, E. L.; Digumarthy, S.; Muzikansky, A.; Ryan, P.; Balis, U. J.; Tompkins, R. G.; Haber, D. A.; Toner, M., *Nature* **2007,** *450*, 1235-U10.

3.15. Hung, P. J.; Lee, P. J.; Sabounchi, P.; Lin, R.; Lee, L. P., *Biotechnol. Bioeng.* **2005,** *89*, 1-8.

3.16. Huh, D.; Fujioka, H.; Tung, Y.-C.; Futai, N.; Paine, R.; Grotberg, J. B.; Takayama, S., *P. Natl. Acad. Sci. USA* **2007,** *104*, 18886-18891.

3.17. Godwin, L. A.; Pilkerton, M. E.; Deal, K. S.; Wanders, D.; Judd, R. L.; Easley, C. J., *Anal. Chem.* **2011,** *83*, 7166-7172.

3.18. Croushore, C. A.; Supharoek, S.-a.; Lee, C. Y.; Jakmunee, J.; Sweedler, J. V., *Anal. Chem.* **2012,** *84*, 9446-9452.

3.19. Kane, B. J.; Zinner, M. J.; Yarmush, M. L.; Toner, M., *Anal. Chem.* **2006,** *78*, 4291-4298.

3.20. Godwin, L. A.; Brooks, J. C.; Hoepfner, L. D.; Wanders, D.; Judd, R. L.; Easley, C. J., *Analyst* **2015,** *140*, 1019-1025.

3.21. Ong, T. H.; Tillmaand, E. G.; Makurath, M.; Rubakhin, S. S.; Sweedler, J. V., *BBA-Proteins Proteomics* **2015,** *1854*, 732-740.

3.22. Goto, M.; Sato, K.; Murakami, A.; Tokeshi, M.; Kitamori, T., *Anal. Chem.* **2005,** *77*, 2125-2131.

3.23. Shackman, J. G.; Dahlgren, G. M.; Peters, J. L.; Kennedy, R. T., *Lab Chip* **2005,** *5*, 56-63.

3.24. Shackman, J. G.; Reid, K. R.; Dugan, C. E.; Kennedy, R. T., *Anal. Bioanal. Chem.* **2012,** *402*, 2797-2803.

3.25. Dishinger, J. F.; Reid, K. R.; Kennedy, R. T., *Anal. Chem.* **2009,** *81*, 3119-3127.

3.26. Clark, A. M.; Sousa, K. M.; Chisolm, C. N.; MacDougald, O. A.; Kennedy, R. T., *Anal. Bioanal. Chem.* **2010,** *397*, 2939-2947.

3.27. Clark, A. M.; Sousa, K. M.; Jennings, C.; MacDougald, O. A.; Kennedy, R. T., *Anal. Chem.* **2009,** *81*, 2350-2356.

3.28. Dugan, C. E.; Cawthorn, W. P.; MacDougald, O. A.; Kennedy, R. T., *Anal. Bioanal. Chem.* **2014,** *406*, 4851-4859.

3.29. Bowen, A. L.; Martin, R. S., *Electrophoresis* **2010,** *31*, 2534-2540.

3.30. Price, A. K.; Fischer, D. J.; Martin, R. S.; Spence, D. M., *Anal. Chem.* **2004,** *76*, 4849-4855.

3.31. Nunemaker, C. S.; Dishinger, J. F.; Dula, S. B.; Wu, R.; Merrins, M. J.; Reid, K. R.; Sherman, A.; Kennedy, R. T.; Satin, L. S., *PLoS ONE* **2009,** *4*, e8428.

3.32. Wang, X.; Yi, L.; Mukhitov, N.; Schrell, A. M.; Dhumpa, R.; Roper, M. G., *J. Chromatogr. A* **2015,** *1382*, 98-116.

3.33. Nge, P. N.; Pagaduan, J. V.; Yu, M.; Woolley, A. T., *J. Chromatogr. A* **2012,** *1261*, 129-135.

3.34. Mellors, J. S.; Gorbounov, V.; Ramsey, R. S.; Ramsey, J. M., *Anal. Chem.* **2008,** *80*, 6881-6887.

3.35. Lazar, I. M.; Trisiripisal, P.; Sarvaiya, H. A., *Anal. Chem.* **2006,** *78*, 5513-5524.

3.36. Liuni, P.; Rob, T.; Wilson, D. J., *Rapid Commun. Mass Spec.* **2010,** *24*, 315-320.

3.37. Enders, J. R.; Marasco, C. C.; Wikswo, J. P.; McLean, J. A., *Anal. Chem.* **2012,** *84*, 8467-8474.

3.38. Gasilova, N.; Qiao, L.; Momotenko, D.; Pourhaghighi, M. R.; Girault, H. H., *Anal. Chem.* **2013,** *85*, 6254-6263.

3.39. Gao, D.; Wei, H.; Guo, G.-S.; Lin, J.-M., *Anal. Chem.* **2010,** *82*, 5679-5685.

3.40. Wei, H.; Li, H.; Gao, D.; Lin, J.-M., *Analyst* **2010,** *135*, 2043-2050.

3.41. Unger, M. A.; Chou, H. P.; Thorsen, T.; Scherer, A.; Quake, S. R., *Science* **2000,** *288*, 113-116.

3.42. Arner, P., *Best Pract. Res. Clin. Endoc. Metab.* **2005,** *19*, 471-482.

3.43. Lafontan, M.; Langin, D., *Prog. Lipid Res.* **2009,** *48*, 275-297.

3.44. Cellar, N. A.; Burns, S. T.; Meiners, J.-C.; Chen, H.; Kennedy, R. T., *Anal. Chem.* **2005,** *77*, 7067-7073.

3.45. Ceriotti, L.; de Rooij, N. F.; Verpoorte, E., *Anal. Chem.* **2002,** *74*, 639-647.

3.46. Maiolica, A.; Borsotti, D.; Rappsilber, J., *Proteomics* **2005,** *5*, 3847-3850.

3.47. Banerjee, S.; Mazumdar, S., *Int. J. Anal. Chem.* **2012**, 40.

3.48. Bollinger, J. G.; Rohan, G.; Sadilek, M.; Gelb, M. H., *J. Lipid Res.* **2013,** *54*, 3523-3530.

3.49. Murphy, R. C., Fatty Acids. In *Tandem Mass Spectrometry of Lipids: Molecular Analysis of Complex Lipids*, The Royal Society of Chemistry: 2015; pp 1-39.

3.50. Rosenstock, M.; Greenberg, A. S.; Rudich, A., *Diabetologia* **2001,** *44*, 55-62.

3.51. Zhou, D.; Samovski, D.; Okunade, A. L.; Stahl, P. D.; Abumrad, N. A.; Su, X., *FASEB J.* **2012,** *26*, 4733-4742.

3.52. Wang, Z. G.; Pini, M.; Yao, T.; Zhou, Z. X.; Sun, C. H.; Fantuzzi, G.; Song, Z. Y., *Am. J. Physiol. Endocrinol. Metab.* **2011,** *301*, E703-E712.

3.53. Rousu, T.; Herttuainen, J.; Tolonen, A., *Rapid Commun. Mass Spec.* **2010**, *24*, 939-957.

CHAPTER 4

MICROFLUIDIC DUAL ASSAY CHIP FOR MONITORING ADIPOCYTE LIPOLYSIS PRODUCTS

Introduction

Microfluidics has become a valuable tool for culturing cells and analyzing their biological processes. The miniaturized microenvironment of microfluidic devices is ideal for the scale of cells, with chambers on the order of microliters in volume.[4.1, 2] Therefore, fewer cells and reagents are necessary for experiments, reducing consumption compared to traditional techniques and potentially enabling studies with rare cells. Constant perfusion of cells on-chip creates a setting more closely resembling that of the *in vivo* framework.[4.3] Continual flow allows replenishment of nutrients and removal of secreted products. Harnessing this inherent aspect of flow, analysis of released metabolites from living cells can be performed in a real time.[4.4-6] Methods have demonstrated fraction collection from perfusion chambers that provide more temporal information than static sampling.[4.7, 8] Integration of an analysis system on the same microfluidic platform is possible and can greatly improve the automation capacity and the understanding of cellular dynamics.[4.9, 10]

For many cell types it is critical to be able to supply the appropriate stimuli to maintain their inherent physiology. These stimuli can range from nutrient content to mechanical expansion, but often need to be applied in a repetitive, recurring fashion. This was initially demonstrated on large volume perfusion columns. In one example, glucose

production from rat hepatocytes was greater when repeated glucagon injections were administered in comparison to constant perfusion of glucagon.[4.11] It is more difficult to automate and precisely control stimuli dispensing on discrete timescales in the macroscale, therefore microfluidic devices have been employed to administer delivery of a chemical stimulus. This was exemplified with yeast cells; glucose was applied to the cells in pulses of varying frequency to monitor gene expression.[4.12] Beyond being able to maintain proper cell function, it is also of great interest to enable temporally-controlled delivery of hormones or drugs to gain further understanding of cellular pathways or to develop new disease treatments.[4.10]

Discrete delivery of chemical treatments on microfluidic devices can be accomplished through valving of perfused solutions, either on external tubing[4.13] or integrated on-chip[4.14, 15]. Polydimethyl siloxane (PDMS) is a commonly used substrate for cell-on-chip experiments because it is biocompatible and gas permeable. It also is inherently elastomeric, allowing pressure driven valves to be constructed in multilayer PDMS devices. Pressure application to a channel will cause it to expand and if properly aligned over a fluidic channel in a lower layer, the flow in the fluidic layer can be regulated.[4.16] Similarly, Braille networks have been implemented on PDMS channels; mechanical pressure from plastic pins can constrict a channel.[4.17]

Due to the increased population with obesity-related disorders like type 2 diabetes, it has become increasingly important to understand the inherent pathways and mechanisms of adipose tissue.[4.18, 19] Adipocytes play a key role in maintaining overall homeostasis through the regulation of energy distribution.[4.20] A central metabolic process in adipocytes is lipolysis; the breakdown of triglyceride molecules into glycerol and non-

esterified fatty acids (NEFAs). While this process results in a 3:1 breakdown of NEFA:glycerol from the original lipid, a percentage of the NEFAs are immediately re-esterified back into triglyceride molecules.[4.21-23] These processes are highly regulated by a wide variety of naturally occurring hormones and signaling molecules, and pharmaceutical drugs that either promote or inhibit lipolysis and NEFA recycling (eg. insulin, glucagon, leptin, catecholamines, glucocorticoids, thiazolidinediones, etc.).[4.24-26] Understanding time dependent roles that these agents play on adipocytes could be crucial to extending our knowledge of the regulation of lipolysis.

Adipocyte secretions have been examined *in vitro* under different chemical stimuli in static culture. Most reports involve cell incubation with chemical agents on the order of hours, which is beneficial for monitoring long term response to a drug.[4.27] One report measured protein phosphorylation in adipocytes under different durations (as short as 5 min) of insulin stimulation by LC-MS.[4.28] Microfluidic applications have the potential to explore adipocyte response to different stimuli on even shorter time scales and with the direct integration of analysis techniques to allow real time monitoring. At present however, little is known about the rapid, dynamic responses of adipocytes.

We previously described a novel microfluidic device that integrated on-chip perfusion of 3T3-L1 adipocytes with enzyme assay reaction channels for directly monitoring the secretion of glycerol and NEFAs.[4.29] The PDMS microfluidic chip was designed with a multilayer construction to allow fabrication of pneumatically-actuated valves upstream of the cell chamber. These valves can be used to administer different chemical stimuli to the adipocytes. The report monitored glycerol and NEFA secretion under basal conditions; then the valves were switched to supply an isoproterenol (β-

adrenergic agonist) solution for the duration of the experiment (30-60 min). This continuous application of isoproterenol resulted in a rapid increase in secretion of both analytes followed by a sustained elevated release over basal levels. These experiments were replicated, and results from this on-chip adipocyte perfusion were compared to static incubation of cells (and off-line assay/detection) to monitor variations in NEFA recycling between the two techniques. Additionally, to demonstrate a novel utility of this chip, short injections of isoproterenol were applied to test the adipocyte lipolytic response and determine whether there is a temporal threshold for glycerol and NEFA stimulation, something not possible to accomplish with static culture.

Experimental

Reagents

Hanks buffered salt solution (HBSS, Cat. No. 14175), Amplex UltraRed and cell culture reagents were purchased from Life Technologies (Carlsbad, CA). Isoproterenol hydrochloride, sodium dodecyl sulfate (SDS), fatty acid-free bovine serum albumin (BSA), dimethylsulfoxide (DMSO) and glycerol assay reagents were received from Sigma-Aldrich (St. Louis, MO). NEFA assay reagents were purchased from Wako Chemicals USA, Inc. (Richmond, VA). Triton X-100 was received from Bio-Rad Laboratories (Hercules, CA). PDMS was obtained from Curbell Plastics, Inc. (Livonia, MI). 18.0 MΩ/cm distilled water was used for making aqueous solutions and flushing the chip.

Adipocyte Culture

Coverslips (No. 1, Fisher Scientific, Waltham, MA) were cut to 4.8 mm x 4.8 mm with a dicing saw and sterilized with 70% ethanol. The dried coverslips were placed in

the bottom of 6-well plates (3-4 per well). Murine 3T3-L1 preadipocytes were seeded in the plate at a density of 200,000 cells/well. Cells were cultured in preadipocyte media until 2 days post confluence, when they were induced for adipogenesis. Preadipocyte media was made of DMEM (Cat. No. 11965-092, Life Technologies) with 8% bovine calf serum, 100 units/mL penicillin, 100 µg/mL streptomycin, 2 mM L-glutamine, and 1 mM sodium pyruvate. Induction was done by adding 500 µM isobutylmethylxanthine, 1 µM dexamethasone, and 5 µg/mL insulin to adipocyte media. Adipocyte media was the same as preadipocyte media, but the bovine calf serum was replaced with 10% fetal bovine serum. 2 days after induction, media on the cells was replaced with adipocyte media with 5 µg/mL insulin. Media was replaced with fresh adipocyte media every 2-3 days thereafter. Adipocytes were maintained in an incubator with 10% CO_2 until 9 days after induction; they were then moved to an incubator supplying 5% CO_2.

PDMS Chip Fabrication

The fabrication procedures and chip operation were similar to that described in Chapter 2. Three PDMS casting molds were made on silicon wafers (University Wafer, Boston, MA). The features shown in black in Figure 2.1a-c were made using SU-8 2075 (MicroChem, Newton, MA), each on a separate wafer. The features in Figure 2.1a & b were 60 µm tall (the control and fluidic channels, respectively), and 250 µm tall for the design shown in Figure 2.1c (the lower cell chamber). Additionally, the red features shown in Figure 2.1b were made 12 µm tall on the respective wafer using AZ-9260 (Capitol Scientific, Austin, TX) photoresist over the SU-8 mold. The AZ channels were rounded by heating to 125 °C for 5 minutes. PDMS pre-polymer was made in a 10:1 ratio of base polymer to curing agent, and degassed in a vacuum chamber. The PDMS was

poured over the wafer containing the control channels to a height of ~1 cm, spun onto the wafer containing the fluidic channels to a height of ~60 μm, and poured over the lower cell chamber wafer to a height of ~1 mm. PDMS was also spun onto a blank Si wafer to a height of ~170 μm. All PDMS was cured at 80 °C, 5-60 min, with the thicker layers requiring longer times.

The PDMS from the control channel layer was peeled from the wafer and holes were punched through at the points shown in blue in Figure 2.1a using a 20-gauge blunt needle (Small Parts, Logansport, IN). The side containing the features was exposed to corona discharge, as was the top of the PDMS of the fluidic channels (side without features). After heating for 10 minutes at 80 °C, the bonded layers were peeled off the wafer. Likewise, the bonded piece of PDMS was exposed to corona discharge on the side with the fluidic channel features, along with the non-feature side of the PDMS spun on the blank wafer. These 3 bonded layers were heated for 10 minutes at 80 °C, and then peeled away from the wafer. Using a sharp scalpel, the lower layer of PDMS (originally spun on the blank wafer) was removed from the square, upper cell chamber region. A 4.8 mm x 4.8 mm glass coverslip (No. 1, Fisher Scientific) was bonded in the area where the PDMS was just removed. These 3 bonded layers of PDMS made the top portion of the reversibly-sealed chip. To form the lower portion of the chip, a glass slide (0.55 mm thick; Telic, Valencia, CA) was irreversibly bonded to the feature-less side of the lower cell chamber PDMS (making feature exposed) using corona discharge.

Chip-to-world connections were made using fused silica capillary (Polymicro Technologies, Phoenix, AZ) which were inserted into the sided of the top PDMS chip, between the fluidic channel and the blank layer. About 15 cm of 50 μm inner

diameter/150 µm outer diameter capillary was sheathed at one end with ~2.5 cm 180/360 capillary, using cyanoacrylate glue to seal together. The opposite end of the 50/150 capillary was rounded using fine sand paper. This was repeated, making capillaries for all 7 inlets and 4 outlets. Additionally, tubing connects were necessary to operate the valves. Stainless steel pins, cut to ~1.5 cm from 23-gauge tubing, were inserted halfway into Tygon tubing (1/16 in. OD, 0.5 mm ID; IDEX, Lake Forest, IL). The other end of the pin was inserted into the top PDMS chip, where holes were punched into the control channel layer before assembly. The Tygon tubing ultimately connected to a N_2 gas tank; the 15 psi of gas pressure it supplied was operated using a series of solenoid valves (LHDA1211111H, The Lee Co., Westbrook, CT), controlled with an in-house designed LabView program (National Instruments, Austin, TX).

Chip Assembly and Perfusion

Prior to chip assembly, 20 mM SDS was pumped through the 2 chip outlets for 45 min at 1.5 µL/min. The channels were then flushed with water at the same flow rate for 20 min. The chip was degassed in a vacuum chamber for ~1 hr. All capillaries, tubing and channels were then primed with water. To calibrate the chip (done between every 2 experiments), a blank 4.8 mm x 4.8 mm coverslip was placed in the lower cell chamber and was covered with ~10 µL perfusion buffer (HBSS + 2% (w/v) BSA). The 2 parts of the chip were sealed together, aligning using the square dimensions of the top and bottom cell chamber, and all air and liquid was squeezed out from between the layers. To ensure a leak proof seal, the chip was enclosed with an in-house built plastic compression frame. The compression frame consisted of 2 pieces of acrylic plastic, with holes drilled in them for screws to tighten the pieces around the chip. Additionally, there were holes drilled in

the top piece of the compression frame for valve tubing access, and in the bottom to allow closer contact of the fluorescent microscope optics.

Once assembled, the chip was placed on the stage of the inverted microscope. All solutions were made in the aforementioned perfusion buffer. The blank and the lowest concentration standard solution were connected to the valve inlets 1 and 2, respectively, as shown in Figure 1, and perfused at 0.75 µL/min. The valves were engaged, with the blank solution flowed through the cell chamber and the standard solution flowed to waste 2. Additional 17 cm of 100/360 capillary was added to the valve waste outlets to stabilize the flow switching, as described in Chapter 2. Assay reagents were connected to the respective inlets shown in Figure 4.1. Reagents on the glycerol and NEFA sides were set to flow rates of 0.29 and 0.30 µL/min, respectively. The 1 mM Amplex UltraRed was made in 35% DMSO. The glycerol and NEFA reagent B solutions were made per manufacturer's directions. The NEFA reagent A was make 1.66x more concentrated than manufacturer's directions, and the final solution perfused onto the chip was a 4:1 mix of concentrated NEFA reagent A to 10% Triton X-100. After the blank assay signal was detected, the valves were switched to the first standard solution flowing through the chip. The blank solution, flowed towards waste 1, was replaced with the next standard solution. Increasing concentration standard solutions were added to the chip in this manner to make a complete calibration curve. During cell experiments, only a few changes were made: a coverslip with ~25,000 adhered 3T3-L1 adipocytes was placed in the lower cell chamber before assembly, and instead of a standard solution flowing through valve inlet 2, a solution of 20 µM isoproterenol was perfused.

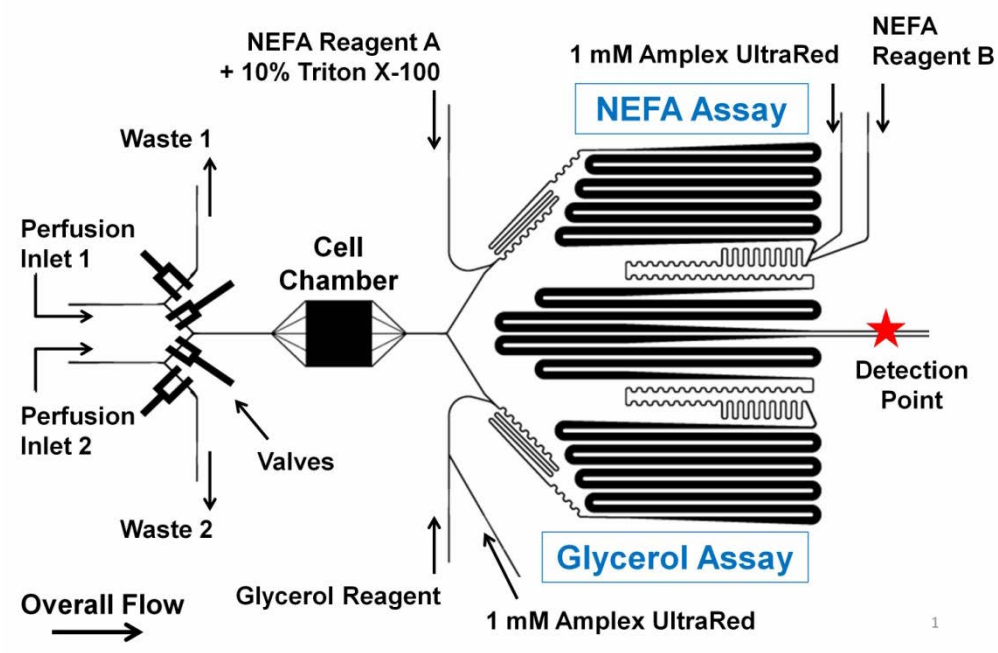

Figure 4.1: Overview of microfluidic chip design. Arrows indicate inlet and outlet channels, with the respective reagents flowing through each.

LIF Detection

An Olympus IX71 inverted fluorescence microscope was used for detection. A 10x, 0.40 numerical aperture was used along with the appropriate filters for resorufin detection. To image both outlets simultaneously, a Hamamatsu ImagEM X2 CCD camera was used. The lamp provided 250 ms light exposure intervals, and data was recorded at 2 Hz. Data was processed with ImageJ and Microsoft Excel.

Off-line Adipocyte Incubation, Enzyme Assay & Detection

Wells in a 96-well plate (Corning Life Sciences, Corning, NY) were filled with 70 µL basal perfusion buffer with or without 20 µM isoproterenol. Coverslips with adherent 3T3-L1 adipocytes were washed with basal buffer, placed in wells and incubated for 40 min. Triplicate sampling from each well was performed to run off-line assays for NEFA and glycerol concentration. For the glycerol assay, 10 µL standard (in basal buffer) or

sample was mixed with 6.5 µL 10 mM Amplex UltraRed (stock made in DMSO) and 90 µL glycerol reagent. Assay solutions were vortexed and incubated for 5 minutes at room temperature. To measure NEFA concentration, 10 µL standard or sample was mixed with 50 µL 1.66x concentrated NEFA reagent A, vortexed and incubated for 5 minutes at room temperature. To the solution was added 7.5 µL 10 mM Amplex UltraRed and 25 µL NEFA reagent B, which was then vortexed and incubated for 5 minutes at room temperature. Solutions from both assays were plated in low volume 384-well plates (20 µL/well in triplicate). Fluorescence detection was performed in a Perkin Elmer Fusion (Waltham, MA) plate reader, with excitation and emission filters used for resorufin detection.

Results & Discussion

Comparison of Off-line to On-line Analysis

In addition to differences in automation and scale between conventional culture/sampling and microfluidic techniques, there is a difference in the type of environment that the cells are exposed to in static and perfused conditions. Perfusion systems continually replenish the media cells are exposed to, both providing a constant supply of nutrients and removing secreted products. In static culture, cells gradually consume the nutrients in the media, resulting in a varying concentration of available nutrients over time. Furthermore, secreted cellular products can act as signaling molecules on the surrounding cells, potentially changing their response. This effect can be observed in adipose tissue. Excess NEFAs in the surrounding environment acts to inhibit lipolysis and increase NEFA recycling[4.22], whereas circulation can elicit NEFA release[4.30].

The off-line incubation of cells was performed on adipocytes grown on coverslips and in smaller wells in an effort to be more consistent with microfluidic observations. As described in Chapter 2, a multilayer PDMS chip allowed on-line simultaneous monitoring of NEFA and glycerol release from perfused adipocytes. Using averaged NEFA re-esterification as a comparison between on-line and off-line analysis methods, the basal and isoproterenol-stimulated NEFA/glycerol ratios are lower in the off-line analysis, as shown in Figure 4.2. The lower ratio indicates that there is more NEFA recycling in comparison to the on-line, microfluidic method. This result seems to follow the hypothesis that with continuous flow, more NEFAs will be detected, as they are less available to be re-esterified immediately by the adipocytes and act as a negative feedback signaler.

As expected, the NEFA/glycerol ratio increases with the application of isoproterenol (over basal).[4.7] Reports of NEFA recycling of 3T3-L1 adipocytes in control static culture experiments demonstrate basal ratios of 0.5:1[4.31] to 2:1[4.32] and isoproterenol ratios of 1.3:1[4.33] to 2.5:1[4.32]. As plotted in Figure 4.2, a NEFA/glycerol ratio of 0.5:1 was observed with basal buffer and 1:1 with isoproterenol application from off-line sampling. While there might be slight variation in sampling techniques between reports, there is still a wide range in NEFA recycling values reported. Using a large volume perfusion column, Getty-Kaushik et al. reported NEFA/glycerol ratios of 1.39:1 with basal media and 1.80:1 with 1 μM isoproterenol stimulation from primary rat adipocytes.[4.7] The differences between adipocyte microenvironment during lipolysis sampling will have to be investigated further to reliably understand the changes that occur with the continuous flow, microfluidic method.

Interestingly, the NEFA/glycerol ratio increases about the same fold change for both on-line and off-line methods (1.6- vs. 1.7-fold, respectively) with the application of isoproterenol, indicating a similar NEFA recycling response with lipolysis stimulation, regardless of circulating conditions. This suggests that the concentration of isoproterenol (20 µM) supplied in static culture over the incubation period studied is sufficient to elicit a response similar to constant application of isoproterenol, as accomplished with microfluidics.

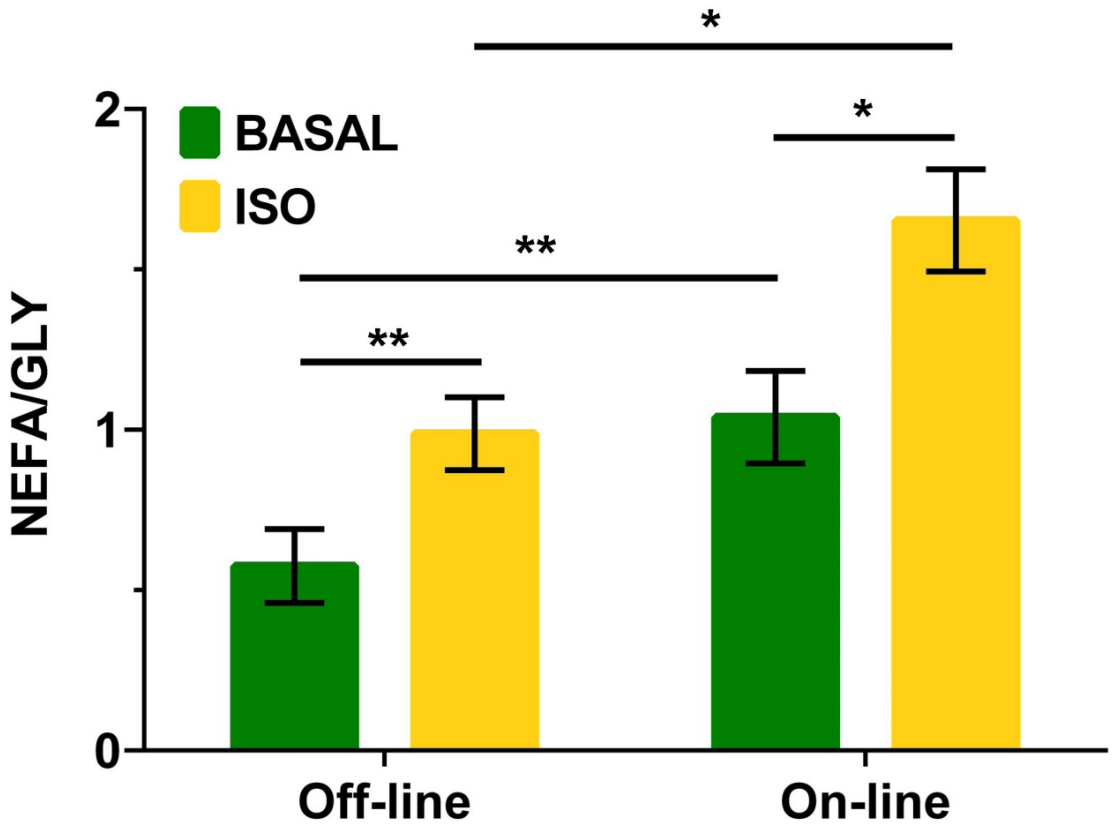

Figure 4.2: Basal and isoproterenol-stimulated (ISO) measurements plotted as a function of NEFA/GLY release from 3T3-L1 adipocytes. Statistical significance determined by paired (between BASAL and ISO for each technique) or unpaired (between bars of the same color) Student's t-test. * P < 0.01, ** P < 0.0001, n = 10.

Short Lipolysis Stimulation

With the integration of the multilayer valves upstream of the cell chamber, it was possible to have automated switching of perfused solutions that were directed to the chamber. In Chapter 2, it was observed that with sustained application of isoproterenol resulted in an immediate and continuously elevated concentration of release over basal levels. In an initial experiment, cells were stimulated for 30+ min as done in Chapter 2, and the valves were switched back to apply blank buffer to the adipocytes. The lipolysis products remained elevated over another 30 min period indicating that lipolysis continues even in the absence of the stimulus. The isoproterenol stimulation period was then decreased to 6 min. The NEFA and glycerol secretion increased, but as opposed to the 30 min stimulation, it then began to decline when switched back to basal buffer. However, analyte concentrations remained elevated over basal concentrations for an additional 60 min as illustrated in Figure 4.3a.

In an effort to determine if there was an isoproterenol stimulation time that would result in a reversible NEFA and glycerol secretion response, the adipocyte stimulation time was decreased to 50 s. As shown in Figure 4.3b, after the initial, rapid increase in concentration for both NEFA and glycerol, the concentrations of both analytes return to the initial basal levels. Furthermore, it was investigated whether this response could be duplicated within the same run (i.e. continuing to perfuse the same group of adipocytes). Figure 4.3b shows that a second stimulation of 60 s resulted in a similar effect; the second stimulated NEFA concentration was slightly lower than during the first stimulation, but the concentrations of NEFAs and glycerol return to basal concentrations. Moreover, the relative ratios of NEFA to glycerol remained consistent between the 2

stimulations, implying identical changes in NEFA recycling. A basal ratio of 1:1 and stimulated ratio of ~2:1 NEFA:glycerol was observed in both runs.

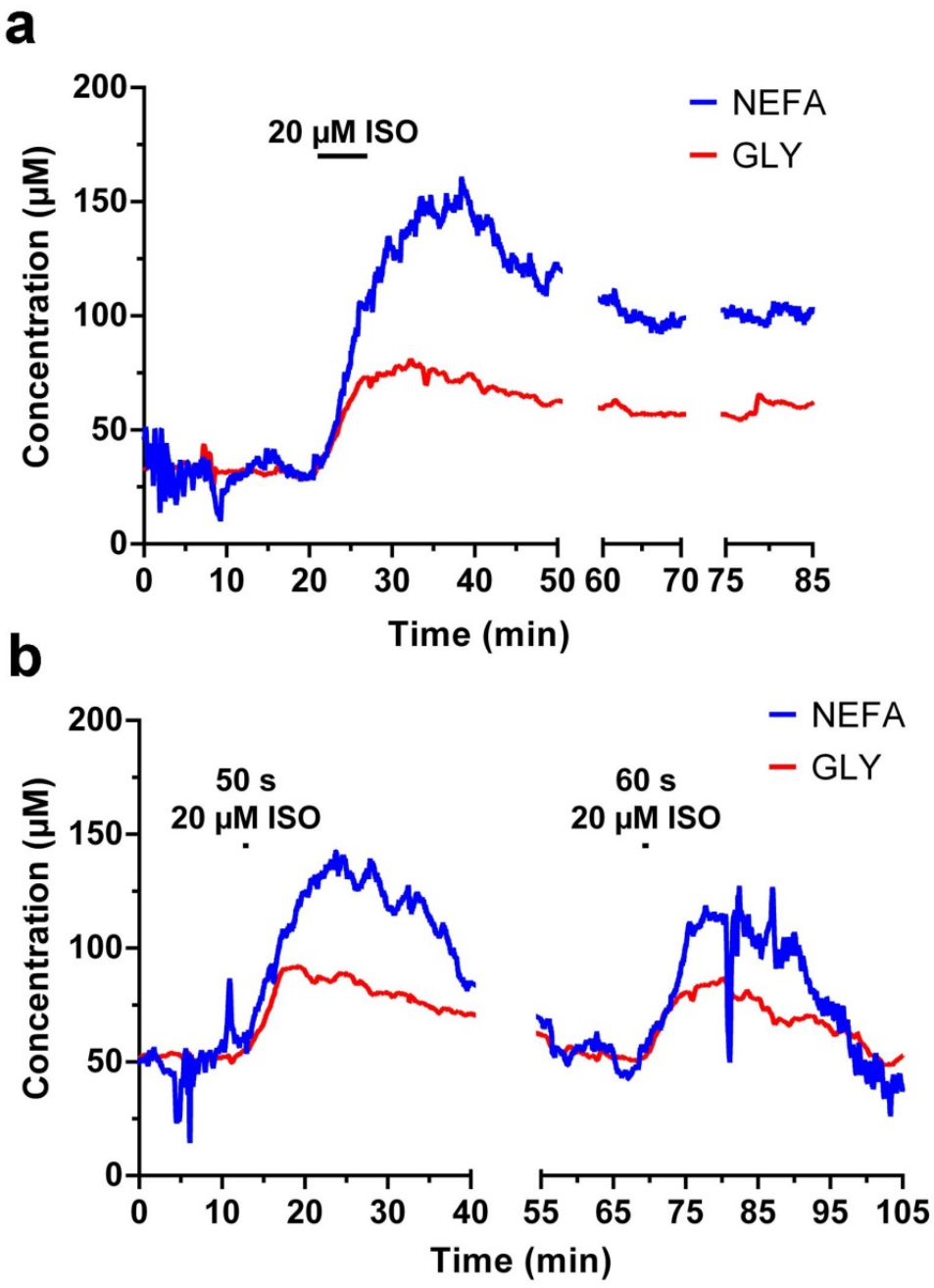

Figure 4.3: Simultaneous detection of NEFA and glycerol (GLY) release from 3T3-L1 adipocytes. Cells are perfused with basal buffer and then stimulated with 20 µM isoproterenol as indicated by the black bar. (a) Isoproterenol stimulation of 6 min. (b) Isoproterenol stimulation of 50 s and 60 s in the same experiment.

The pathway of isoproterenol stimulation has been thoroughly investigated in literature; however, these experiments could offer more insight into the kinetics of isoproterenol (or other chemical) stimulation on adipocytes. It is well understood that β-adrenergic agonist exposure initiates the lipolytic cascade by 1) activating adenylyl cyclase which 2) increases cellular AMP levels and 3) activates protein kinase A, that then 4) phosphorylates lipid droplet-bound protein, perilipin (PLIN), and hormone sensitive lipase (HSL), shown in Figure 4.4a.[4.24, 34] Additionally, that phosphorylation allows another protein, CGI-58 to activate adipose triglyceride lipase (ATGL). From our initial findings it is interesting that there would be differences in lipolytic response with acute and prolonged isoproterenol exposure. It would appear that there is a threshold for duration of β-adrenergic agonist application before the stimulation is irreversible. It is possible that acute isoproterenol exposure only allows a certain percentage of the PLIN or HSL to be phosphorylated, whereas more are during prolonged exposure. As illustrated in Figure 4.4b, it has also been suggested that a protein, G0S2, acts to modulate ATGL activation under acute adrenergic agonist exposure, however degrades upon chronic exposure, allowing continually elevated lipolysis to occur.[4.24] Degradation of a lipolysis inhibitor like G0S2 could be the reason that it is observed that NEFA and glycerol concentrations cannot revert back to basal levels after prolonged stimulation. Further investigations of this type of lipolysis stimulation kinetics will help elucidate adipocyte metabolism.

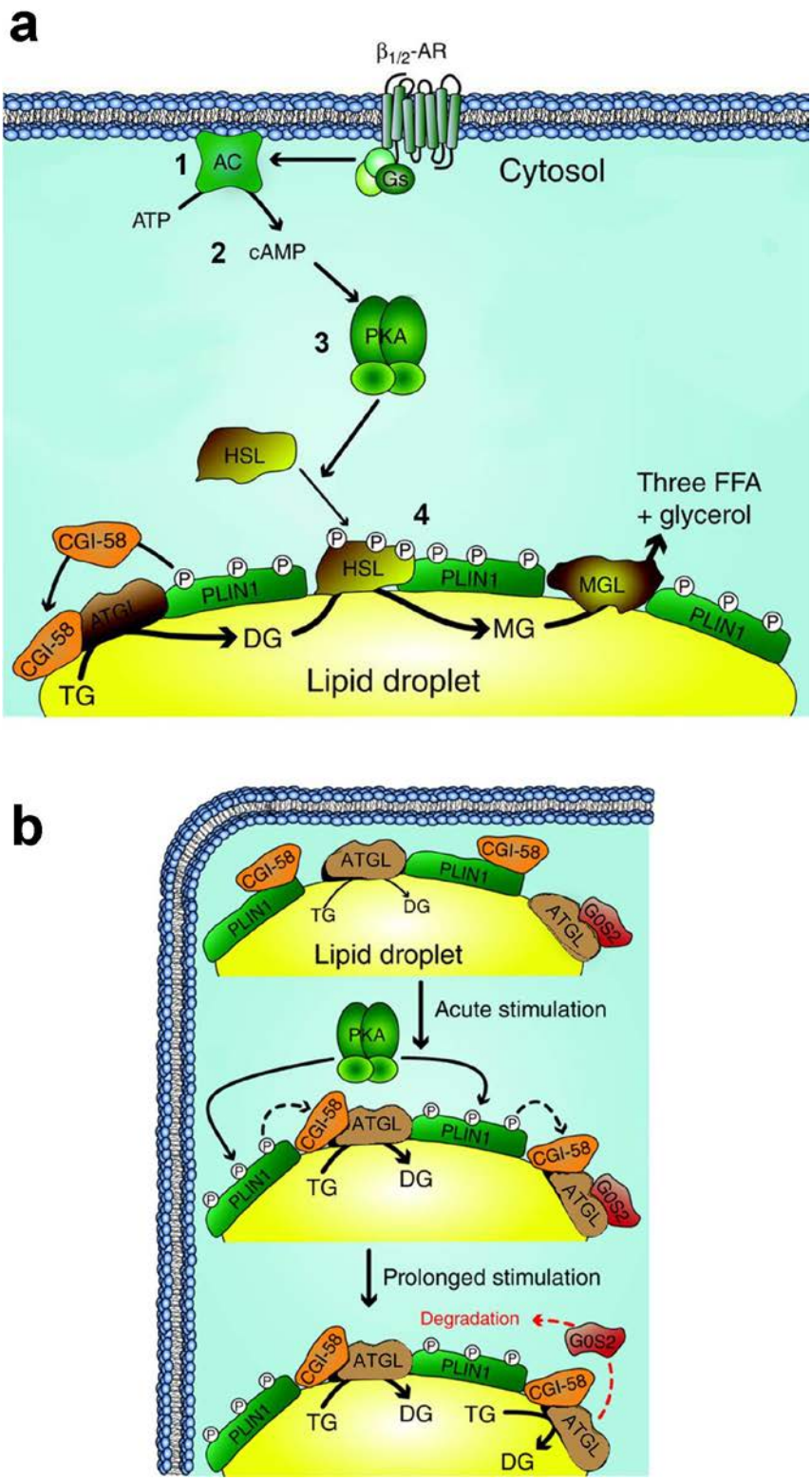

Figure 4.4: Mechanisms of adipocyte lipolysis: pathway of stimulated lipolysis by an adrenergic agonist (a) and possible variations in protein action with acute or prolonged stimulation (b). Adapted with permission from BioScientifica Ltd.[4.24]

Conclusions

This multilayer PDMS chip allows a unique demonstration of microfluidic devices having the potential to both deliver very short chemical stimuli and ability to record response in near real time, without any manual involvement. Comparisons in adipocyte secretion of glycerol and NEFAs between conventional static culture and microfluidic perfusion platforms were demonstrated. While more experiments are needed, this is further evidence that culturing and perfusing cells in microfluidic devices could create an environment more closely resembling *in vivo* dynamics. Further, it was found that 50-60 s of lipolysis stimulation with isoproterenol causes the appropriate increase in NEFA and glycerol secretion, but then slowly returns to basal concentrations over the following 50 min.

Isoproterenol is often used as a positive control for static adipocyte experiments, to ensure proper lipolytic response. Therefore, it was of interest to determine if it could be used for the same purpose on-chip within the same experiment. If the concentration of NEFAs and glycerol could return back to basal levels after initial stimulation with isoproterenol, a subsequent stimulus of interest could be applied to monitor changes in lipolysis. Additionally, the kinetics of subsequent stimuli could be tested with this integrated PDMS chip to learn more about factors affecting adipocyte function. The integrated valves on the PDMS chip allowed automated and rapid switching of cell perfusion buffer, making these short stimulation experiments possible. Similar studies could also be performed on other cell lines, adjusting the downstream flow network the desired chemical assay, allowing valuable insight into the physiology of many different tissues.

References

4.1. Kim, L.; Toh, Y. C.; Voldman, J.; Yu, H., *Lab Chip* **2007,** *7*, 681-694.

4.2. Moraes, C.; Mehta, G.; Lesher-Perez, S. C.; Takayama, S., *Ann. Biomed. Eng.* **2011,** *40*, 1211-1227.

4.3. El-Ali, J.; Sorger, P. K.; Jensen, K. F., *Nature* **2006,** *442*, 403-411.

4.4. Shackman, J. G.; Reid, K. R.; Dugan, C. E.; Kennedy, R. T., *Anal. Bioanal. Chem.* **2012,** *402*, 2797-2803.

4.5. Roper, M. G.; Shackman, J. G.; Dahlgren, G. M.; Kennedy, R. T., *Anal. Chem.* **2003,** *75*, 4711-4717.

4.6. Shackman, J. G.; Dahlgren, G. M.; Peters, J. L.; Kennedy, R. T., *Lab Chip* **2005,** *5*, 56-63.

4.7. Getty-Kaushik, L.; Richard, A. M. T.; Corkey, B. E., *Diabetes* **2005,** *54*, 629-637.

4.8. Getty-Kaushik, L.; Richard, A. M. T.; Corkey, B. E., *Obes Res* **2005,** *13*, 2058-2065.

4.9. Salieb-Beugelaar, G. B.; Simone, G.; Arora, A.; Philippi, A.; Manz, A., *Anal. Chem.* **2010,** *82*, 4848-4864.

4.10. Dittrich, P. S.; Manz, A., *Nat. Rev. Drug Discov.* **2006,** *5*, 210-218.

4.11. Weigle, D. S.; Koerker, D. J.; Goodner, C. J., *Am. J. Physiol.* **1984,** *247*, E564-E568.

4.12. Bennett, M. R.; Pang, W. L.; Ostroff, N. A.; Baumgartner, B. L.; Nayak, S.; Tsimring, L. S.; Hasty, J., *Nature* **2008,** *454*, 1119-1122.

4.13. Hersen, P.; McClean, M. N.; Mahadevan, L.; Ramanathan, S., *P. Natl. Acad. Sci. USA* **2008,** *105*, 7165-7170.

4.14. Mosadegh, B.; Kuo, C.-H.; Tung, Y.-C.; Torisawa, Y.-s.; Bersano-Begey, T.; Tavana, H.; Takayama, S., *Nat. Phys.* **2010,** *6*, 433-437.

4.15. Wang, C. J.; Li, X.; Lin, B.; Shim, S.; Ming, G.-l.; Levchenko, A., *Lab Chip* **2008,** *8*, 227-237.

4.16. Unger, M. A.; Chou, H. P.; Thorsen, T.; Scherer, A.; Quake, S. R., *Science* **2000,** *288*, 113-116.

4.17. Gu, W.; Zhu, X.; Futai, N.; Cho, B. S.; Takayama, S., *P. Natl. Acad. Sci. USA* **2004,** *101*, 15861-15866.

4.18. Duncan, R. E.; Ahmadian, M.; Jaworski, K.; Sarkadi-Nagy, E.; Sul, H. S., *Annu. Rev. Nutr.* **2007,** *27*, 79-101.

4.19. Bays, H.; Mandarino, L.; DeFronzo, R. A., *J. Clin. Endocrinol. Metab.* **2004,** *89*, 463-478.

4.20. Rosen, E. D.; Spiegelman, B. M., *Nature* **2006,** *444*, 847-853.

4.21. Reshef, L.; Olswang, Y.; Cassuto, H.; Blum, B.; Croniger, C. M.; Kalhan, S. C.; Tilghman, S. M.; Hanson, R. W., *J. Biol. Chem.* **2003,** *278*, 30413-30416.

4.22. Nye, C.; Kim, J.; Kalhan, S. C.; Hanson, R. W., *Trends Endocrinol. Metab.* **2008,** *19*, 356-361.

4.23. Prentki, M.; Madiraju, S. R. M., *Mol. Cell. Endocrinol.* **2012,** *353*, 88-100.

4.24. Nielsen, T. S.; Jessen, N.; Jørgensen, J. O. L.; Møller, N.; Lund, S., *J. Mol. Endocrinol.* **2014,** *52*, R199-R222.

4.25. Frayn, K. N.; Karpe, F.; Fielding, B. A.; Macdonald, I. A.; Coppack, S. W., *Int. J. Obesity* **2003,** *27*, 875-888.

4.26. Granneman, J. G.; Kimler, V. A.; Moore, H. P. H., *J. Anim. Sci.* **2011,** *89*, 701-10.

4.27. Louis, C.; Van den Daelen, C.; Tinant, G.; Bourez, S.; Thomé, J.-P.; Donnay, I.; Larondelle, Y.; Debier, C., *In Vitro Cell Dev.-An.* **2014,** *50*, 507-518.

4.28. Schmelzle, K.; Kane, S.; Gridley, S.; Lienhard, G. E.; White, F. M., *Diabetes* **2006,** *55*, 2171-2179.

4.29. Dugan, C. E.; Cawthorn, W. P.; MacDougald, O. A.; Kennedy, R. T., *Anal. Bioanal. Chem.* **2014,** *406*, 4851-4859.

4.30. Wang, S.; Soni, K. G.; Semache, M.; Casavant, S.; Fortier, M.; Pan, L.; Mitchell, G. A., *Mol. Gen. Metab.* **2008,** *95*, 117-126.

4.31. Hashimoto, T.; Segawa, H.; Okuno, M.; Kano, H.; Hamaguchi, H.-o.; Haraguchi, T.; Hiraoka, Y.; Hasui, S.; Yamaguchi, T.; Hirose, F.; Osumi, T., *J. Cell Sci.* **2012,** *125*, 6127-6136.

4.32. Lei, T.; Xie, W.; Han, J.; Corkey, B. E.; Hamilton, J. A.; Guo, W., *Obes. Res.* **2004,** *12*, 599-611.

4.33. Gauthier, M.-S.; Miyoshi, H.; Souza, S. C.; Cacicedo, J. M.; Saha, A. K.; Greenberg, A. S.; Ruderman, N. B., *J. Biol. Chem.* **2008,** *283*, 16514-16524.

4.34. Czech, M. P.; Tencerova, M.; Pedersen, D. J.; Aouadi, M., *Diabetologia* **2013,** *56*, 949-964.

CHAPTER 5

DISSERTATION SUMMARY

In this thesis, fabrication and operation procedures of 2 novel PDMS chips have been detailed along with their preliminary applications to understanding secretion dynamics of lipolysis products from adipocytes. Microfluidic devices have the capability to miniaturize, automate and integrate many analysis techniques. With the addition of cell perfusion on chip, conditions mimicking the *in vivo* environment can be achieved. On-line detection of secreted metabolites from cells can be accomplished through integration on microfluidic chips, reducing sample handling and allowing more temporal information to be gathered.

The chip described in Chapter 2 was developed for multiplexed detection of 2 secreted products from a continuously perfused group of cells.[5.1] This was the first demonstration of a chip with this capability. By simultaneously monitoring both NEFAs and glycerol secreted from 3T3-L1 adipocytes, more information about cellular metabolism and lipolysis can be determined than if the analytes are measured separately. The measured quantities of glycerol signify the rate of lipolysis, whereas the concentration of secreted NEFAs can imply the amount of NEFA re-esterification occurring under particular conditions. Simultaneous measurement was accomplished on chip by integrating a flow split after the adipocyte perfusion chamber; media from the same temporal domain could be sampled for different analytes. The channels from the flow split were directed towards either a NEFA or glycerol fluorescently-modified

enzyme assay network where reactions with reagents added downstream occurred. The outlets of the 2 channel networks were closely spaced, so the fluorescent product in both channels could be imaged together. This chip greatly reduced cell requirements and increased automation of sampling and analysis compared to conventional static sampling techniques. Furthermore, this PDMS chip enabled reversible sealing, allowing its re-use, and the integration of multilayer valves to automate selection of the perfusion buffer flowing over the cells.

This chip design was optimized using computer modelling to reduce temporal resolution and ensure sufficient mixing of assay reagents. On-chip enzyme assay reactions were also optimized by altering reagent flow rates and modifying the PDMS surface to prevent analyte (NEFA) adsorption/loss. The multiplexed assay chip had linear calibration curves when perfused with standards, and had limits of detection of 6 µM for the NEFA assay and 5 µM for the glycerol assay. Adipocytes were perfused with basal buffer followed by an isoproterenol solution (to stimulate lipolysis). This stimulation resulted in a 1.5- to 6-fold increase in NEFA and glycerol concentration over basal levels. In addition, it was also observed that NEFA:glycerol ratios varied as the cells aged, implying different capacity for NEFA recycling with cellular maturation.

Using this dual assay chip, comparisons in NEFA re-esterification were also drawn between on-chip perfusion/detection and static incubation/off-line analysis. It was found that the fold increase of ~1.6 with isoproterenol application over basal levels was consistent between both techniques. However, cell adipocyte perfusion resulted in less NEFA recycling for both the basal and isoproterenol conditions than static incubation. It would follow that since the NEFAs are secreted into a flowing solution, they are less

available to be re-esterified, which could imply something about the kinetics of cellular uptake. Stimulation dynamics were also investigated by supplying short pulses of isoproterenol to the cells. It was found that application of 60 s or less resulted in a brief elevation in lipolysis that then reverted to basal levels in ~50 min. These findings could also imply kinetics of adipocyte stimulation pathways, which is useful to further mechanistic understanding of adipocytes.

The second chip developed and described in Chapter 3 allowed on-line MS analysis of microfluidic adipocyte perfusate. While the multiplexed assay chip allowed detection of NEFAs, it could only quantify total NEFA concentration. A variety of different NEFAs are secreted from adipocytes, so it was of interest to have a detection method that could identify the NEFAs released into circulation. Cells were perfused in a similar manner to the other chip design, but instead of an enzyme assay reaction channel, an injection loop was constructed downstream of the cell chamber. Prior to MS detection, a SPE bed was used to remove buffered media salts to improve ESI efficiency. However, this SPE bed created back pressure that was unfavorable to the cells. To fluidically isolate the cells from the packed bed, multilayer, pneumatically-actuated valves were integrated into the PDMS chip. With this chip, 8 NEFAs were successfully identified with MS detection under basal and lipolysis-stimulated conditions. All but one of the detected NEFAs had statistically significant increases in release with the application of isoproterenol/forskolin, ranging from 1.2- to 1.9 fold elevation over basal concentrations.

While these chips were designed for adipocyte secretion studies of lipolysis products, the general layout is versatile and could be applied to a variety of secreted metabolites or cell types, leading to greater understanding of cellular systems.

Future Directions

In regards to the chips developed in this dissertation, there are many directions that could be pursued for their further improvement and application. These potential biological uses and analytical enhancements are detailed in the following section.

Alternate Detection Schemes for Dual Enzyme Assay Chip

The PDMS chip described in Chapter 2 was developed to monitor 2 metabolites secreted from adipocytes in parallel. This was accomplished through the integration of reaction channels that enabled on-line use of a fluorescently-modified commercially available enzyme assay. Transparent chips (i.e. PDMS) can be placed on a microscope stage or homemade optics set-up, and excitation and emission light can be easily transmitted. The inverted microscope used for LIF detection of the dual assay chip was equipped with a CCD camera for fluorescence emission collection and data recording, allowing both outlet channels to be imaged simultaneously. While this technique was straightforward and robust, it somewhat negates the miniaturized footprint of the microfluidic device. Furthermore, if this general chip design were used with other cell lines on chip, fluorescent enzyme assays for the analytes of interest may not be available and could require another detection mode.

Electrochemical Detection

Both the NEFA and glycerol enzyme assay reaction schemes create one equivalent of hydrogen peroxide. This product is electroactive and could be readily detected with electrochemical detection on chip.[5.2] Many groups have demonstrated deposition of various types of electrodes for detection of a range of analytes.[5.3-7] Electrodes could be placed in the 2 assay outlet channels of the PDMS chip. Additionally,

with electrochemical detection, the fluorogenic dye, Amplex UltraRed, wouldn't be necessary, reducing reagent cost for the system.

Fiber Optics

Our group has developed a fiber optic detection platform for fluorescent product sensing (currently in preparation for publication). These probes are 1.1 mm x 0.5 mm, and include a series of air gaps enclosed in PDMS to act as light filters and mirrors, illustrated in Figure 5.1a. The probes are portable, and can simply be placed on microfluidic channels for detection, like that used for the on-chip glycerol enzyme assay. As shown in Figure 5.1b, step changes between different glycerol standards were readily detected, with a R^2 of 0.988 and LOD of 0.7 μM. Two of these probes could be positioned over the outlet channels on the dual assay chip, with the potential of expansion beyond just 2 channels if more parallel assays were integrated onto a similar chip design.

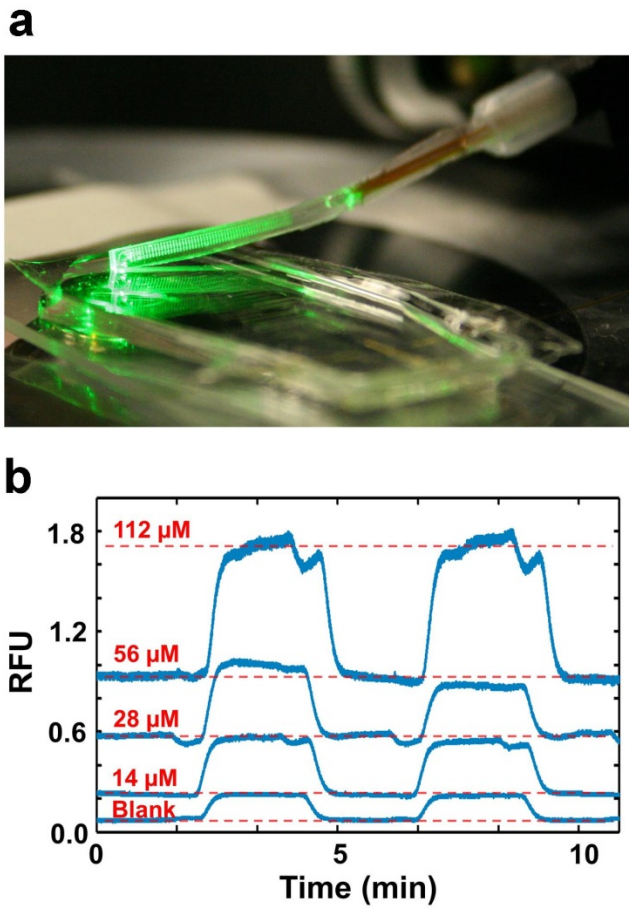

Figure 5.1: Microfabricated fluorescence fiber optic probe (a) and calibration step plots of on-chip glycerol enzyme assay, measured with the probe (b).

Low-cost Absorbance Detector

Another product developed in our lab, an absorbance detector, could be implemented with the dual assay chip. This detector was created with 3D printing; a 2 cm x 2 cm black polymer cube was constructed with a channel through the center and an enclosure for a light source. Transparent tubing (i.e. fused silica capillary with a burned window) is fed through the center channel, wherein the dye of interest can be flowed. Various wavelength LED lights can be integrated into the detector depending on the necessary excitation source needed for the dye. The read-out of the system is operated with Arduino electronics and can be connected to a computer via USB-port. Capillary

from the outlet channels of the dual assay could be connected to 2 of these detectors. As with electrochemical detection, the fluorogenic dye would not need to be added to the on-chip assays, as the commercially available enzyme assays are designed to be used with colorimetric detection. Besides the significant size reduction compared to a fluorescent microscope, this detector can be multiplexed and transported.

Injection Loop Chip Improvements

To create a more automated, on-line injection loop for MS detection of cell secretion, a few of the current off-chip components could be integrated onto the chip described in Chapter 3. While the initial study used an off-chip SPE bed coupled to the device, this bed could also be packed on chip, downstream of the injection loop. This can be accomplished by creating a 'moat' at the outlet; the channel height could be decreased to 12 µm for ~100 µm using the same fabrication procedure as that used for the valve regions. The 20 µm particle slurry could be pumped into the chip through the outlet and packed against the moat. To prevent the particles from flowing back through the outlet during normal operation, a short length of 40/150 could act as a frit. This capillary could be directly connected to a metal-coated capillary spray tip for ESI-MS. This on-chip packing method was constructed (as shown in Figure 5.2), but has not yet been tested.

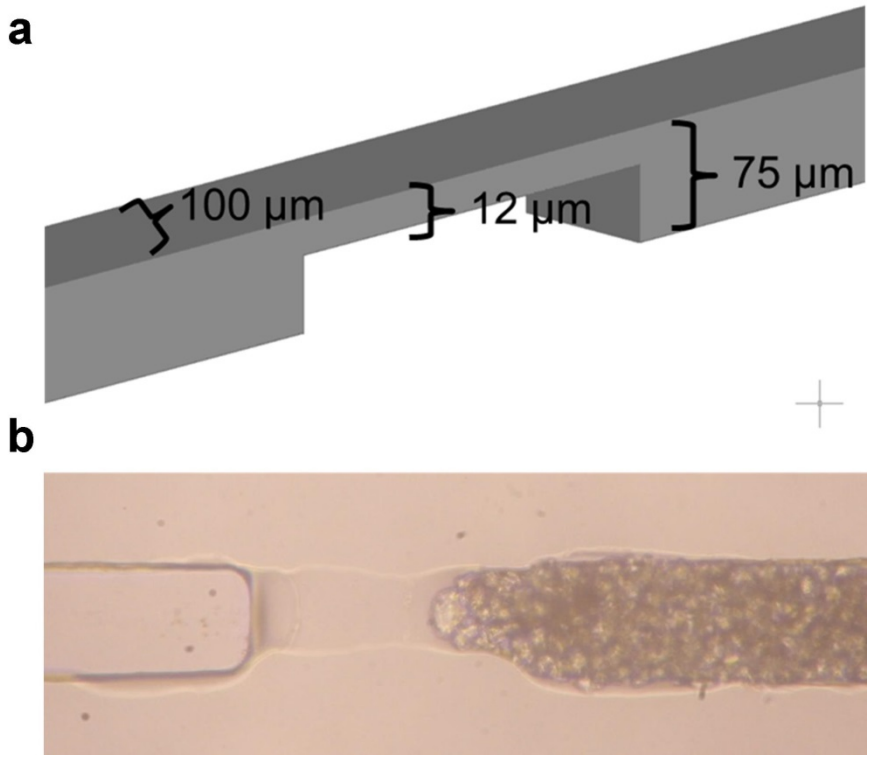

Figure 5.2: Moat design for on-chip SPE packing. (a) Schematic of channel dimensions and (b) 20 µm particles packed in a PDMS channel.

Another on-chip addition that could be implemented is a set of valves at the wash/elution solvent inlet as highlighted in red in Figure 5.3. This would eliminate the need for an off-chip 4-port valve to switch between solutions introduced on chip, further integrating solvent delivery. Finally, the volume of the injection loop could be decreased, improving the throughput of the method by shortening the time required for each injection. The current 7.5 µL design was implemented to ensure enough analyte was loaded onto the SPE bed for injection, but could be decreased to ~5 µL and still be able to detect NEFA levels above the LOD of the assay.

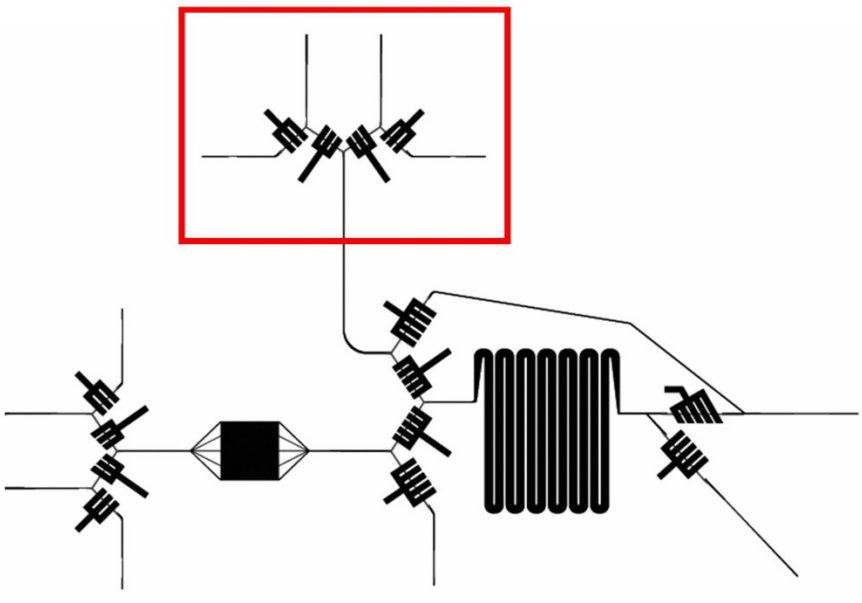

Figure 5.3: Proposed injection loop chip design with added valve at the wash/elution solvent inlet.

Droplet Reagent Addition

While the dual assay chip developed in Chapter 2 improves automation and temporal resolution of cell secretion sampling compared to traditional off-line methods, the assays still have a temporal response of 2 minutes. To understand more rapid changes that are occurring in regards to cell secretion, it would be advantageous to reduce the temporal response of the system. The flow through the chamber has been optimized to reduce temporal resolution with computer modeling, but the enzyme assay reaction channels are relatively long (to allow adequate mixing and assay incubation times) and are subject to the effects of Taylor dispersion. Segmenting flow after the cell chamber could circumvent this problem. Droplets are created by the addition of immiscible oil phase to an aqueous stream, forming discrete sample plugs. Droplets allow rapid, efficient mixing of reagents and also maintain temporal information within the discrete plugs.[5.8]

For implementation with the dual assay chip, an oil inlet channel would have to be constructed downstream of the cell chamber, before the flow split. Alternately, 2 oil inlets could be integrated after the flow split. Once the droplets have been formed, additional inlets for the enzyme assay reagents could add the appropriate amounts of the enzyme to the droplets, controlled by relative flow rates of the fluid streams. Optimization of the assay reactions would have to be performed to get maximum readout signal, but with the more efficient mixing and smaller reaction 'vessels', it's possible that the incubation times would be lower. This would allow shorter channels, and the use of droplets would remove the necessity of having 2 different channel widths in the enzyme reaction portion of the chip. Detection of the reaction products could be accomplished with LIF or the 3D-printed absorbance detector.

A few potential challenges are envisioned with the formation of droplets on chip, but different options are available to remedy these problems if they occur. The first is that the addition of an oil stream to an aqueous stream can cause some back pressure, which if great enough, would not be suitable for coupling to a chip containing cells (for reasons mentioned in previous chapters). Flow rates may have to be optimized if this effect is great enough to damage the cells. The other potential challenge would be the affinity of NEFAs to the oil phase, resulting in a loss of detectable analyte. This may not be a problem if the NEFAs are bound to BSA or react readily with the assay reagents; however various surfactants could also be added to the oil phase to potentially prevent the loss of NEFAs.

Monitor Lipolysis from eMSCs and Primary Adipocytes

Experiments with the 2 chip designs presented in this dissertation were conducted with 3T3-L1 adipocytes. For initial experiments, these are the ideal cell types to work with because they are relatively easy to obtain and culture, and adhere well to surfaces without any modifications. As previously discussed, 3T3-L1 are not the best genetic models for understanding *in vivo* adipocyte physiology, containing multilocular lipid droplets and missing chromosomes. Ear mesenchymal stem cells (eMSCs) would be of interest to load into the cell chamber of the dual assay chip. These cells are taken directly from a tissue punch of a mouse ear, making them a primary cell model and more physiologically relevant. According to studies, eMSCs differentiate more robustly into adipocytes than preadipocytes isolated from stromal-vascular tissue.[5.9, 10] These cells can also be grown on coverslips as the 3T3-L1 adipocytes were; if loaded into the PDMS cell chamber, lipolysis and NEFA recycling could be investigated under perfusion conditions (with dual assay or MS detection), not previously investigated. Additionally, if the mice were bred with a genetic knockout, the eMSCs will also contain that same genetic makeup which will enable the study of how various genes regulate lipolysis mechanisms.

While primary adipocytes (mature adipocytes collected from dissected fat pads) are more difficult to handle, they would be the most ideal adipocyte to study. Primary adipocytes are unilocular, have been differentiated with endogenous regulation, and were exposed to the circulating signaling molecules and conditions of the *in vivo* environment. Primary adipocytes have been loaded in perfusion columns for analysis of lipolysis regulation, but required large cell and reagent volumes as well as off-line fraction collection and analysis. More automated analysis of primary adipocytes could be

accomplished using microfluidic devices. Additionally, one advantage of using primary adipocytes is that they can be collected from different fat depots for analysis; it has been shown that fat depots (subcutaneous, visceral, marrow, etc.) exhibit various morphologies and functions[5.11-13], and further understanding of regulation in the different depots could provide a better picture of systemic white adipose tissue physiology.

A new cell chamber construction would have to be developed to load primary adipocytes onto a microfluidic chip. After digestion of the tissue, isolated primary adipocytes float in a suspension of media. An inverted cell chamber (from that developed in previous chapters) could be fabricated, with the bulk of the chamber area above the fluid path instead of below. Another option would be to load an aliquot of cells into the chamber of the existing dual assay chip, cover with a thin, permeable membrane and seal the chip. This would keep the cells sequestered in the lower portion of the chamber, while still being able to sample secreted metabolites. This was briefly tested on-chip; the chip was able to be reversibly sealed without leaking from the added membrane, but further optimization of the flow parameters need to be conducted to acquire adequate signal due to the slower diffusion rates of metabolites through the membrane (compared to direct fluid flow). A third method would be to modify the surface of the coverslips with a cell adhesion agent like poly-l-lysine or Cell-Tak; the coverslips could then be loaded into the previously developed cell chamber, but control studies would have to be performed to ensure the adhesion agent doesn't interfere with the inherent function of the cell. Once implemented on chip, studies investigating the lipolysis and NEFA recycling rates of primary cells from different depots could be performed by enzyme assay or MS detection, and compared to cultured lines and previous reports.

Widening scope of on-chip adipocyte stimuli

In all of the experiments conducted in this dissertation with adipocytes on-chip, the cells were perfused with basal buffer and a positive control to increase lipolysis (isoproterenol or forskolin). While great proof-of-concept studies, it would be interesting to see the lipolytic response of adipocytes under a variety of stimuli. Adipocytes are responsive to subtle changes in their surroundings (chemical or mechanical); these could be elucidated with microfluidic assays and online detection. A myriad of chemical stimuli and pharmaceutical drugs have been tested on adipocytes in static culture, but as observed in Chapter 4, there are differences in the secretion of lipolysis products with continuous cell perfusion. For example, physiological concentrations of insulin act to inhibit lipolysis, whereas glucagon, TNFα and glucocorticoids increase lipolysis as illustrated in Figure 5.4.[5.14] These chemical stimuli could be perfused over the cells acutely or for long periods of time to monitor temporal changes with cell secretion. As demonstrated in Chapter 4, if cells are stimulated for 60 s or less with isoproterenol before adding these other stimuli, the isoproterenol will act as a positive control for lipolysis within the same experiment/group of cells. Furthermore, these chemical stimuli could be used with knock-out eMSC models or primary adipocytes from different depots, proposed in the previous section, to gain more knowledge about cellular conditions that effect lipolysis, and thereby our understanding of this dynamic tissue.

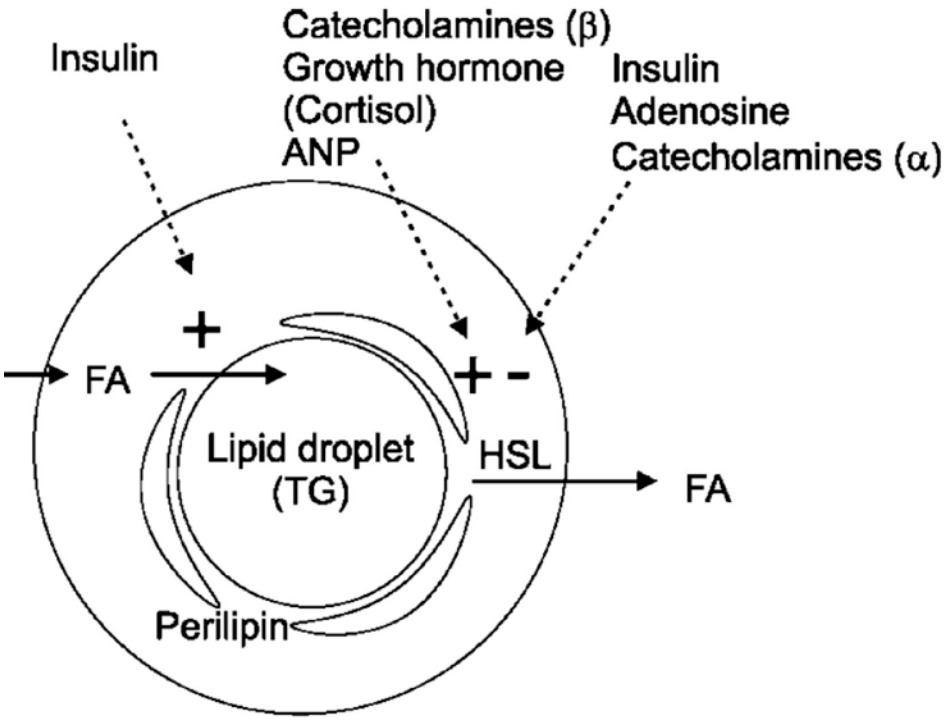

Figure 5.4: Schematic of adipocyte with different chemical stimuli regulatory action on fatty acid (FA) storage/lipolysis. Insulin promotes FA re-esterification into the lipid droplet, and inhibits lipolysis. Adenosine and a-catecholamines also inhibit lipolysis, whereas b-catecholamines, growth hormones promote lipolysis. Adapted by permission from Macmillan Publishers Ltd: International Journal of Obesity, copyright 2003.[5.14]

References

5.1. Dugan, C. E.; Cawthorn, W. P.; MacDougald, O. A.; Kennedy, R. T., *Anal. Bioanal. Chem.* **2014,** *406*, 4851-4859.

5.2. Yan, J.; Pedrosa, V. A.; Enomoto, J.; Simonian, A. L.; Revzin, A., *Biomicrofluidics* **2011,** *5*.

5.3. Bowen, A. L.; Martin, R. S., *Electrophoresis* **2010,** *31*, 2534-2540.

5.4. Amatore, C.; Arbault, S.; Chen, Y.; Crozatier, C.; Tapsoba, I., *Lab Chip* **2007,** *7*, 233-238.

5.5. Gunasekara, D. B.; Siegel, J. M.; Caruso, G.; Hulvey, M. K.; Lunte, S. M., *Analyst* **2014,** *139*, 3265-3273.

5.6. Ges, I. A.; Brindley, R. L.; Currie, K. P. M.; Baudenbacher, F. J., *Lab Chip* **2013,** *13*, 4663-4673.

5.7. Zor, K.; Heiskanen, A.; Caviglia, C.; Vergani, M.; Landini, E.; Shah, F.; Carminati, M.; Martinez-Serrano, A.; Moreno, T. R.; Kokaia, M.; Benayahu, D.; Keresztes, Z.; Papkovsky, D.; Wollenberger, U.; Svendsen, W. E.; Dimaki, M.; Ferrari, G.; Raiteri, R.; Sampietro, M.; Dufva, M.; Emneus, J., *RSC Adv.* **2014,** *4*, 63761-63771.

5.8. Song, H.; Tice, J. D.; Ismagilov, R. F., *Angew. Chem. Int. Ed.* **2003,** *42*, 768-772.

5.9. Rim, J.-S.; Mynatt, R. L.; Gawronska-Kozak, B., *FASEB J.* **2005**.

5.10. Gawronska-Kozak, B., Chapter One - Preparation and Differentiation of Mesenchymal Stem Cells from Ears of Adult Mice. In *Methods in Enzymology*, Ormond, A. M., Ed. Academic Press: 2014; Vol. Volume 538, pp 1-13.

5.11. Gesta, S.; Tseng, Y. H.; Kahn, C. R., *Cell* **2007,** *131*, 242-256.

5.12. Jensen, M. D., *J. Clin. Endocrinol. Metab.* **2008,** *93*, s57-s63.

5.13. Lee, M.-J.; Wu, Y.; Fried, S. K., *Mol. Aspects Med.* **2013,** *34*, 1-11.

5.14. Frayn, K. N.; Karpe, F.; Fielding, B. A.; Macdonald, I. A.; Coppack, S. W., *Int. J. Obesity* **2003,** *27*, 875-888.

APPENDIX A

FABRICATION AND OPERATION TIPS

PDMS Microfluidic Chip Fabrication

60 µm SU-8 channels:

1. If necessary, clean Si wafer with IPA.
2. Spin coat on ~1 mL HDMS (1000 rpm for 15 s)
3. Spin coat SU-8 2075 photoresist (pre-spin 500 rpm for 10 s, 4000 rpm for 60 s)
4. Pre Bake: 3 min at 65 °C, 8 min at 95 °C
5. Align photomask (dark-field) on wafer and expose to UV for 13.3 s
6. Post Bake: 2 min at 65 °C, 6 min at 95 °C
7. Develop in SU-8 developer (~5 min, until rinsed clean with IPA)

12 µm AZ 9260 channels:

1. Spin coat AZ 9260 photoresist (pre-spin 500 rpm for 10 s, 4000 rpm for 60 s)
2. Heat for 2 min at 95 °C
3. Align mask (clear-field) on wafer and expose to UV for 60 s
4. Develop in 20 mL AZ 400K developer and 50 mL water (rinse with water)
5. Heat at ~125 °C for 5 min to round features

PDMS:

1. Mix 10:1 (base:curing agent) PDMS prepolymer
2. Degas until all bubbles are removed (let sit or in vacuum chamber)

3. Pour over wafer master for thick layer (in Petri dish or make containment area with aluminum foil) or spin for thin layer (~170 µm, pre-spin 500 rpm for 8 s, 1500 rpm for 40 s)
4. Bake at 80 °C until firm (20-30 min for thick layer, 5-10 min for thin layer)
5. Cut out PDMS and peel away from wafer (thick layer) (Tip: if using Petri dish containment, cut just inside wafer edge with razor blade; if you run off the edge of the wafer with the blade it will likely shatter)
6. Use corona discharge and oxidize the surface
7. Bond to another oxidized surface and press to remove all bubbles between layers
8. Bake at 80 °C for 5-10 min to irreversibly bond layers

Dual Assay Chip Set-Up

Calibration:

1. Perfuse outlet channels with 20 mM SDS at 1.5 µL/min for ~ 1 hr, followed by water for ~10 min
2. Degas chip in vacuum chamber for at least 1 hr
3. While degassing:
    a. Rinse syringes, remove all bubbles
    b. Flush unions and capillary connections with water
    c. Set up syringe pumps and valve system by microscope
    d. Prepare standards/reagents as necessary
    e. Fill syringes with solutions and put on pumps
    f. Start flow and make sure no bubbles in Teflon connections
    g. Pause flow until chip on microscope

4. Take chip out of vacuum chamber and perfuse outlet with water, flush all capillaries with water
5. If valve channels are empty, fill with water and connect to nitrogen to force water into control channels (will leach air into solutions during first experiment otherwise)
6. Put glass coverslip in lower cell chamber, put few drops of water (or red food dye; good for flow visualization and slightly fluorescent so can position channels, but allow longer rinse time after solution connection before starting expt to get true blank signal) on coverslip
7. Align top chip over lower chip using the dimensions of cell chamber and seal/squeeze out liquid and air between layers with back of tweezers
8. Thread control tubing through top compression frame and assemble compression frame
9. Once on microscope (**make all connections slowly)
    h. Start with perfusion of blank through valve
    i. Turn on valves and switch a few times
    j. Switch to blank going to valve waste and connect extra length of capillary (filled with water)
    k. Switch few more times, then when on waste flow direction, put end of capillary in vial of water & leave for remainder of expt (BSA will quickly clog capillaries without flow)
    l. Switch so blank flow is through chamber and connect low concentration standard capillary

m. Connect extra length of capillary (filled with water) to other valve waste & put in vial of water

n. Connect glycerol reagent, CR-A, AUR on glycerol side, CR-B, AUR on NEFA side, in that order

o. Check with microscope to make sure flow is going in correct direction at all inlets

p. Let flow for ~ 10 min before recording starts

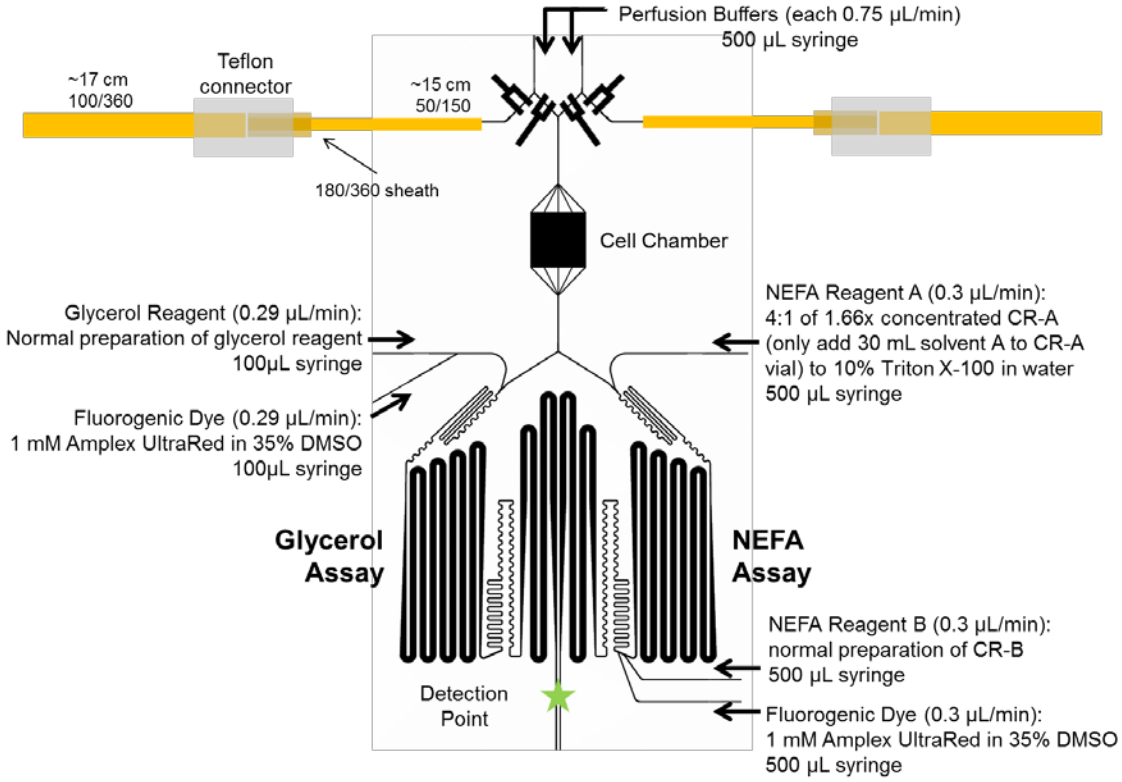

Figure A.1: Set-up and operation diagram for dual assay chip.

APPENDIX B

OFF-LINE ASSAY PROTOCOLS

Fatty Acid Fluorescence Assay Protocol:

- 10 µL standard or sample
- 50 µL Wako Color Reagent A (1.66x concentrated from Wako directions)
- Vortex, RT incubation (duration of starting glycerol assay)
- 6 µL 10 mM Amplex UltraRed (made by adding 340 µL DMSO to 1 mg vial)
- 25 µL Wako Color Reagent B
- Vortex, RT incubation
- Triplicate sampling with 20 µL per well in low volume 384-well plate
- Plate reader settings:
    - Excitation wavelength: 535 nm
    - Emission wavelength: 620 nm
    - PMT voltage: 620 V
    - Light intensity: 10

Glycerol Fluorescence Assay Protocol:

- 10 µL standard or sample
- 4.5 µL 10 mM Amplex UltraRed
- 90 µL Sigma Free Glycerol Reagent
- Vortex, RT incubation

- Triplicate sampling with 20 µL per well in low volume 384-well plate
- Plate reader settings:
    - Excitation wavelength: 535 nm
    - Emission wavelength: 620 nm
    - PMT voltage: 620 V
    - Light intensity: 10

APPENDIX C

COMSOL MODELING OF MICRODIALYSIS PROBE

The following document is the 3D COMSOL set-up for monitoring diffusion of neurotransmitters through a microdialysis probe. As a supplement to a project investigating the neuronal turnover of glutamine (GLN) to glutamate (GLU), a COMSOL model of a microdialysis probe to look at recovery of GLN and GLU was developed. Based on parameters obtained with *in vitro* and *in vivo* experiments, the dialysis membrane diffusion coefficient, and appropriate rate constants for the conversion of GLN to GLU were determined. These values could be used with other models to predict recovery with other conditions. The final model was run on COMSOL version 4.4.

- c_all represents GLN
- r_all represents 'intracellular' GLN
- y_all represents GLU

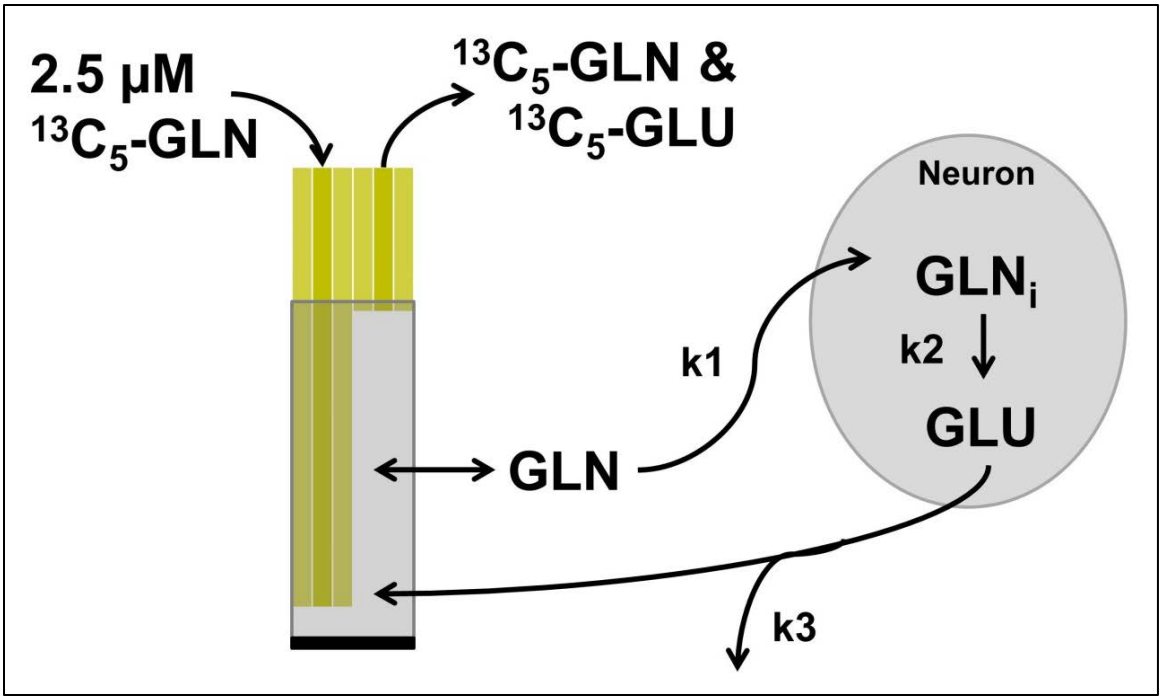

Figure C.1: Experimental reaction scheme modeled with COMSOL. Diffusion of GLN and GLU through microdialysis probe was simulated along with theoretical neuronal turnover of GLN to GLU.

- Global Definitions
    - Parameters

Name	Expression
V	1.667e-11 [m^3/s]
M	0.0002 [m/s]
Dp	8.6e-10 [m^2/s]
Dv	3.2e-10 [m^2/s]
Dm	5.3e-11 [m^2/s]
k1	10 [1/s]
k2	100 [1/s]
k3	100 [1/s]
sc	8
c0	0.0025 [mol/m^3]

- Model 1
    - Definitions
        - Explicit> select domains, rename dialysate
        - Explicit> select domain, rename membrane
        - Explicit> select domain, rename brain
        - Variables 1> selection: dialysate, name: c_all, expression: c1

            selection: dialysate, name: r_all, expression: r1

            selection: dialysate, name: y_all, expression: y1
        - Variables 2> selection: membrane, name: c_all, expression: c2

            selection: membrane, name: r_all, expression: r2

            selection: membrane, name: y_all, expression: y2
        - Variables 3> selection: brain, name: c_all, expression: c3

            selection: brain, name: r_all, expression: r3

            selection: brain, name: y_all, expression: y3
        - Step1> location: 3 (time to make step), from: 0, to: 1
        - Step2> location: 5 (time to make step), from: 0, to: 1
        - Average 1> name: outlet, manually select outlet
    - Geometry (set to mm)
        - Inner Membrane
            - Radius (R): 0.1
            - Height (H): 2.1/sc
            - {0, 0, 0}
        - Outer Membrane

- R: 0.108
- H: 2.1/sc
- {0, 0, 0}

- Outer long capillary
  - R: 0.049
  - H: 2/sc
  - {-0.05, 0, 0}
- Inner long capillary
  - R: 0.02
  - H: 2/sc
  - {-0.05, 0, 0}
- Workplane 1
  - R: 0.02
  - {0.05, 0}
- Bottom Plug
  - R: 0.108
  - H: 0.02/sc
  - {0, 0, 2.1/sc}
- Vial/Brain Region
  - R: 0.308
  - H: 2.4/sc
  - {0, 0, 0}
- Sphere 1

        - R: 0.005
        - {0.115, 0, 0.02}
    - Array 1
        - Size: {4, 1, 75/sc}
        - Displacement: {0.05, 0, 0.03}
    - Rotate 1
        - Keep input objects: ON
        - Rotation: {0, 45, 90, 135, 180, 225, 270, 315}
        - Axis of rotation: {0, 0, 0}
    - Sphere 2
        - R: 0.005
        - {-0.115, 0, 0.02}
    - Array 2
        - Size: {4, 1, 75/sc}
        - Displacement: {-0.05, 0, 0.03}
    - Rotate 2
        - Keep input objects: ON
        - Rotation: {22.5, 67.5, 112.5, 157.5, 202.5, 247.5, 292.5, 337.5}
        - Axis of rotation: {0, 0, 0}
- Materials
    - Don’t enter anything here

- Laminar Flow 1> select dialysate domain (within membrane and inner long capillary)
    - change to incompressible flow
    - Fluid Properties 1> density: 993 kg/m^3, viscosity: 0.000692 Pa·s
    - Wall 1> default settings
    - Initial values 1> default settings
    - Inlet> select boundary, laminar inflow flow rate: V/sc, entrance length: 0.00001, check 'constrain endpoints to zero'
    - Outlet 1> select boundary
- Transport of Diluted Species 1> select dialysate domain, keep 'convection' box checked
    - Convection and Diffusion 1> Velocity Field: Velocity Field, Diffusion Coefficient> select diagonal, and for Dzz, enter Dp/(sc^2) i.e.

Dp	0	0
0	Dp	0
0	0	Dp/sc^2

    - No Flux 1: Default settings
    - Initial values 1> concentration c1: 0
    - Flux 1> check 'species c1', enter M*(c2- c1)

      check 'species r1', enter M*(r1- r2)

      check 'species y1', enter M*(y2- y1)
    - Inflow 1> select boundary, enter: c0
    - Outflow 1> select boundary

- Transport of Diluted Species 2> select membrane domain, uncheck 'convection' box
  - Diffusion> select diagonal, and for Dzz, enter $Dm/(sc^2)$
  - No Flux 1: Default settings
  - Initial values 1> concentration c2: 0
  - Flux 1> check 'species c2', enter M*(c1-c2)

    check 'species r2', enter M*(r2-r1)

    check 'species y2', enter M*(y1-y2)
  - Flux 2> check 'species c2', enter M*(c3-c2)

    check 'species r2', enter M*(r2-r3)

    check 'species y2', enter M*(y3-y2)
- Transport of Diluted Species 3> select brain domain, uncheck 'convection' box
  - Diffusion> select diagonal, and for Dzz, enter $Db/(sc^2)$
  - No Flux 1: Default settings
  - Initial values 1> concentration c3: 0
  - Flux 1> check 'species c3', enter M*(c2- c3)

    check 'species r3', enter M*(r3- r2)

    check 'species y3', enter M*(y2- y3)
  - Reactions 1> select brain region

    c3: k1*y3*step1(t[1/s])

    r3: 0

    y3: -k1*y3*step1(t[1/s])

- Reactions 2> select sphere array 1

  c3: -k2*c3*step2(t[1/s])

  r3: k2*c3*step2(t[1/s])

  y3: 0

- Reactions 3> select sphere array 2

  c3: 0

  r3: k3*r3*step3(t[1/s])

  y3: 0

- Mesh (started w/ physics controlled mesh then changed to the following settings)
  - Size
    - Calibrate for: Fluid Dynamics
    - Fine
  - Size 1
    - Calibrate for: Fluid Dynamics
    - Domains: dialysate
    - Coarse
  - Size 2
    - Calibrate for: Fluid Dynamics
    - Boundaries: dialysate
    - Fine
  - Size 3
    - Calibrate for: Fluid Dynamics

- Boundaries: brain
- Normal

- Corner Refinement
  - Domain dialysate
  - Boundaries: dialysate
  - Minimum angle between boundaries: 240 deg
  - Element Size Scaling Factor: 0.35
- Free Tetrahedral 1
  - Domain: dialysate
- Boundary layers
  - Boundary layer properties (pre-set variables): dialysate domain
    - Boundary layers: 2
    - Boundary layer stretching factor: 1.2
    - Thickness adjustment factor: 5
- Free Tetrahedral 2
  - Remaining

- Study 1
  - Step 1: Stationary> check only ‘laminar flow’ modules
    - Enable ‘Direct’ solver
- Study 2
  - Step 1: Time Dependent> check everything except ‘laminar flow’, set time range, under ‘Values of Dependent Variables’ check ‘values of variables

not solved for' and choose method: 'solution', study: 'study 1, stationary', selection: 'automatic'

- Enable 'Direct' solver
- Changed to 'Fully Coupled' solved instead of segregated
- Time-Dependent Solver 1> Time stepping> Change initial step to 0.5 s and max step to 1 s

- Results
  - Under 'Data Sets' add 3D Cut Line

(mm)	X	Y	Z
Point 1	0	0	0.11
Point 2	1	0	0.11

  - Concentration
    - Slice 1: change c1 to c_all or r_all
  - 1D Plot Group
    - Global
      - Select appropriate solver in data set
      - Enter outlet(c_all)
  - 1D Plot Group
    - Global
      - Select appropriate solver in data set
      - Enter outlet(r_all)
  - 1D Plot Group
    - Global
      - Select appropriate solver in data set

- Enter outlet(y_all)

- 1D Plot Group
  - Line Graph
    - Select Data Set: 3D Cut line
    - Enter c_all in y-axis data ‘expression’
    - Change x axis data parameter to ‘expression’ and enter x
- 1D Plot Group
  - Line Graph
    - Select Data Set: 3D Cut line
    - Enter r_all in y-axis data ‘expression’
    - Change x axis data parameter to ‘expression’ and enter x
- 1D Plot Group
  - Line Graph
    - Select Data Set: 3D Cut line
    - Enter y_all in y-axis data ‘expression’
    - Change x axis data parameter to ‘expression’ and enter x

❖ Experiment 1 - Well stirred matching:

- Additional laminar flow modules are activated in study 1 in brain region
- Transport of Diluted Species 3 has convection box checked, and is linked to Velocity Field (spf2.U) in Convection and Diffusion tab
- Reaction 1 & Reaction 2 in Transport of Dilute Species 3 are deactivated
- Vary membrane diffusion coefficient

❖ Experiment 2 – In Vivo Matching ([Gln]):

- Only Laminar Flow module 1 is activated in study 1
- Transport of Diluted Species 3 is only Diffusion dependent
- Only Reaction 1 in Transport of Dilute Species 3 is activated
- Vary k1 & k2

❖ Experiment 3 – In Vivo Matching ([Glu]):

- Only Laminar Flow module 1 is activated in study 1
- Transport of Diluted Species 3 is only Diffusion dependent
- Only Reaction 1 in Transport of Dilute Species 3 is activated
- Vary k1 & k2

❖ Experiment 4 – In Vivo Matching ([Glu], by adding decay rxn):

- Only Laminar Flow module 1 is activated in study 1
- Transport of Diluted Species 3 is only Diffusion dependent
- Reaction 1 & Reaction 2 in Transport of Dilute Species 3 are activated
- Vary k3

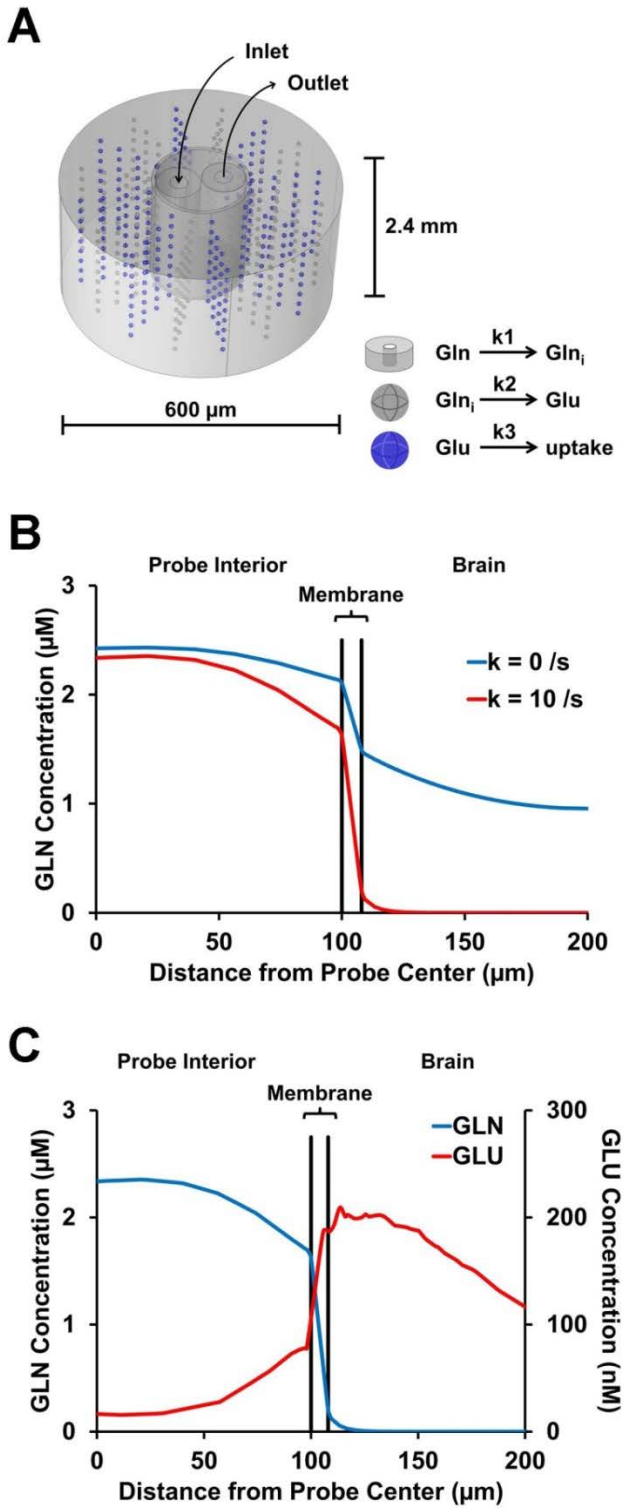

Figure C.2: Modeling of microdialysis probe *in vivo*. (A) Diagram of COMSOL model with reaction domain highlighted in the legend. (B) Flux of infused GLN across dialysis membrane and concentration profile across regions, with varied brain 'consumption' reaction rates. (C) Measurement of concentration profiles for infused GLN, and GLU formed outside the probe (k1 = 10, k2 = 100, k3 = 100 s^{-1}).

APPENDIX D

COMSOL MODELING OF DUAL ASSAY CHIP

The following document is the 2D COMSOL set-up for the dual enzyme assay chip used in Chapters 2 & 4. This model was used to determine experimental flow rates and ensure sufficient mixing of reagents. The final model was run on COMSOL version 4.3b.

- Global Definitions
    - Parameters

Name	Expression
inlet	1.25e-11 [m^3/s]
gly	9.67e-12 [m^3/s]
FA	5.0e-12 [m^3/s]

- Model 1
    - Definitions
        - Step1> location: 0.2 (time to make step), from: 0, to: 1
        - Average 1> name: outlet1, manually select outlet 1
        - Average 2> name: outlet2, manually select outlet 2
        - Average 3> name: pointA, manually select point A (after built)
        - Average 4> name: pointB, manually select point B
    - Geometry (set to mm)
        - Imported from AutoCAD
        - Added point in the middle of channel after flow split, before first inlet

- Mirror point to other side of flow split

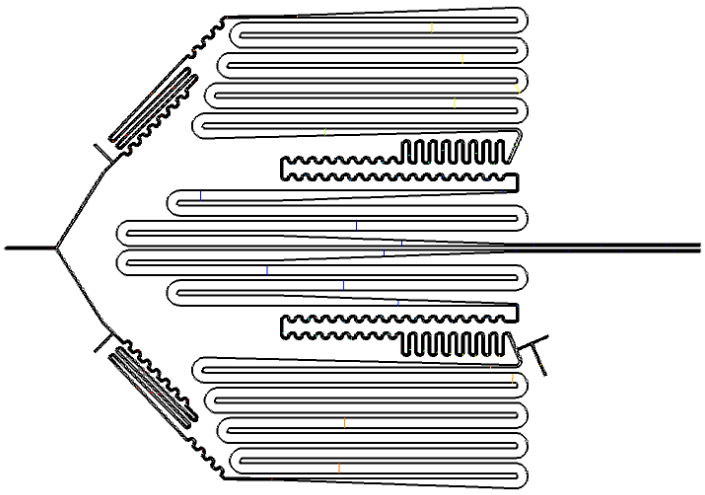

- Materials
  - Water, liquid
- Laminar Flow 1> select entire domain
  - change to incompressible flow
  - check ‘Use shallow channel approximation’
  - Channel thickness: 0.00006
  - Fluid Properties 1> default settings
  - Wall 1> default settings
  - Initial values 1> default settings
  - Inlet 1> select appropriate boundary, laminar inflow flow rate: inlet, entrance length: 0.00001, check ‘constrain endpoints to zero’ (use for all inlets)
  - Inlet 2> select appropriate boundary, laminar inflow flow rate: gly
  - Inlet 3> select appropriate boundary, laminar inflow flow rate: FA
  - Inlet 4> select appropriate boundary, laminar inflow flow rate: FA

        - Inlet 5> select appropriate boundary, laminar inflow flow rate: FA
        - Outlet 1> select boundaries
    - Transport of Diluted Species 1> select entire domain, keep ‘convection’ box checked
        - Convection and Diffusion 1> Velocity Field: Velocity Field (spf)
        - No Flux 1: Default settings
        - Initial values 1> concentration c1: 0
        - Inflow 1> select top inlet boundary, enter: 0.5*step1(t[1/s])
        - Inflow 2> select remaining inlet boundaries, enter: 0
        - Outflow 1> select 2 outlet boundaries boundary
    - Mesh (physics controlled mesh)
        - Calibrate for: Fluid Dynamics, Fine
- Study 1
    - Step 1: Stationary> check only ‘laminar flow’ module
        - Enable ‘Direct’ solver
- Study 2
    - Step 1: Time Dependent> check only ‘transport of diluted species’, set time range, under ‘Values of Dependent Variables’ check ‘values of variables not solved for’ and choose method: ‘solution’, study: ‘study 1, stationary’, selection: ‘automatic’
        - Enable ‘Direct’ solver
        - Changed to ‘Fully Coupled’ solved instead of segregated
        - Time-Dependent Solver 1> Default settings

- Results
    - Under ‘Data Sets’ add 2D Cut Line
    - View velocity (Figure D.1) and concentration plots
    - 1D Plot Group
        - Global
            - Select appropriate solver in data set
    - 1D Plot Group
        - Line Graph
            - Select Data Set: 2D Cut line
            - Change x axis data parameter to ‘expression’ and enter x

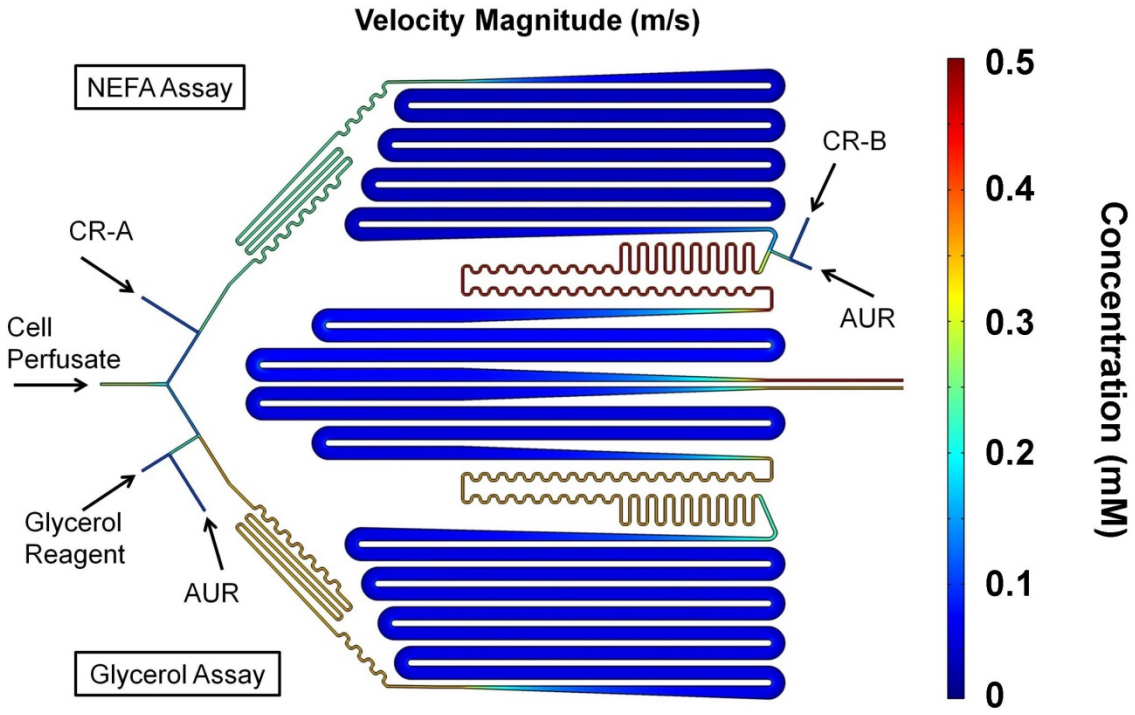

Figure D.1: Velocity plot of flow through dual assay chip.

Measuring Flow Split Ratio with Varying Downstream Inlet Flow Rates

- Use 1D plot group, enter ‘pointA’ and ‘pointB’ as expressions, compare velocities (spf.U), results shown in Figure D.2

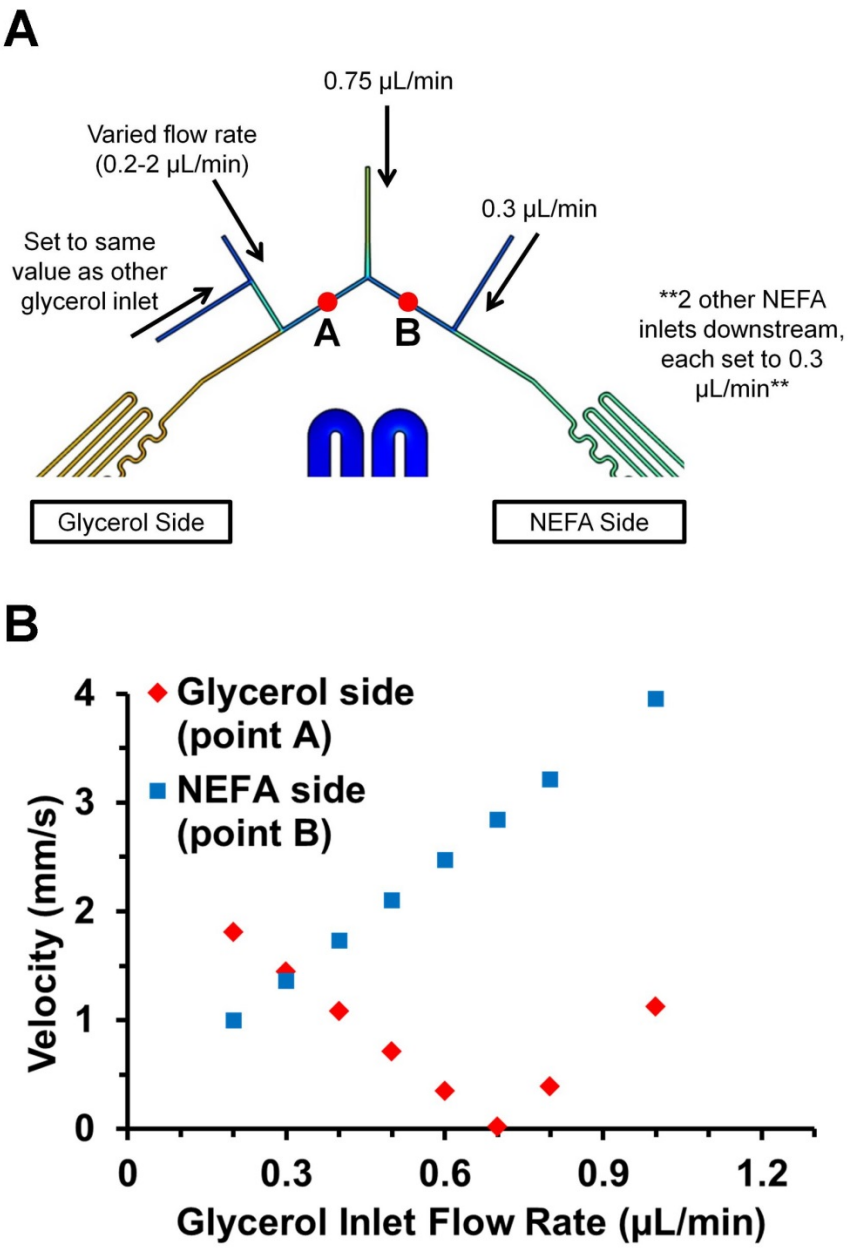

Figure D.2: Flow split analysis of dual assay chip. (A) Diagram of chip and measurement points. (B) Flow velocity at points A & B were monitored while glycerol reagent flow rates were varied.

Measuring Delay Time and Temporal Response

- Use 1D global plot group, enter ‘outlet1’ as expression, measure concentration (c1), repeat with ‘outlet2’, shown in Figure D.3
- Rise time measured as 10-90% of the step change and delay time measured as the time of concentration change to 10% if the step change
    - NEFA Side: 11.5 min delay time, 1.3 min rise time
    - Glycerol Side: 9.2 min delay time, 1.2 min rise time

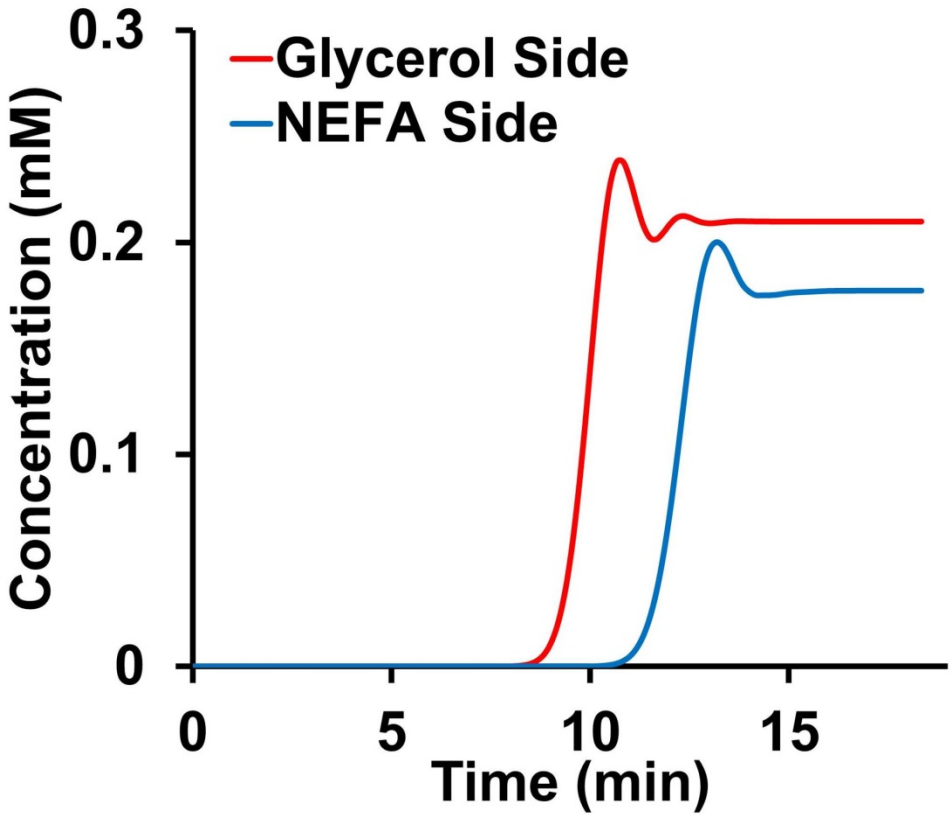

Figure D.3: Step change plot of dual assay chip. Top inlet flow rate changed from 0 to 0.5 mM (other inlets remained at 0 mM, hence the varying maximum concentrations).

Measuring Reagent Mixing After Inlets

- Use 1D line group, select 2D cut line (a few cut lines positioned across channels after inlets), measure concentration (c1), shown in Figure D.4

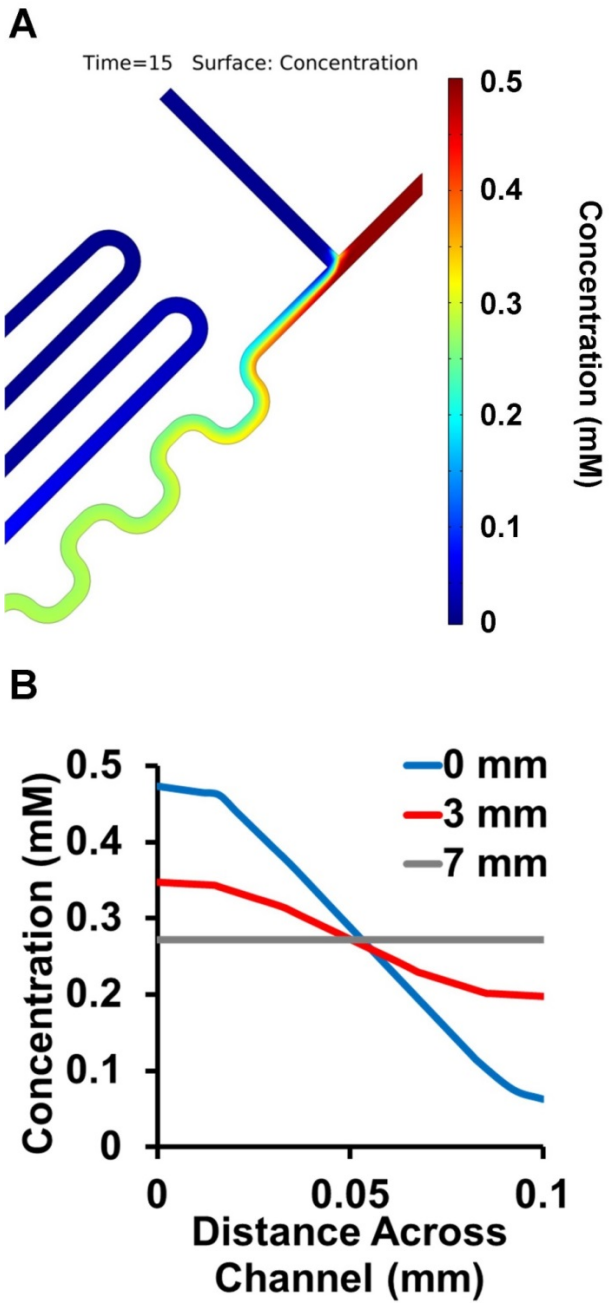

Figure D.4: On-chip reagent mixing efficiency. (A) Pictoral representation of 2 concentrations of a chemical species mixing at a reagent inlet on the dual assay chip. (B) Concentration of the chemical species was measured across the width of the channel at various distances from the reagent inlet.

APPENDIX E

COMSOL MODELING OF MICROFABRICATED PROBE

Modeling Set-up Procedures

The following document is the 3D COMSOL set-up for monitoring diffusion of dopamine through a microfabricated porous membrane, to support a collaborative research project. The porous membrane was etched into the side of a novel fabricated microdialysis probe, which reduces the spatial resolution of *in vivo* neurochemical monitoring. The model helped identify the theoretical porosity and recovery of the probe. The final model was run on COMSOL version 4.4.

- Global Definitions
    - Parameters

Name	Expression
diff	6e-10 [m^2/s]
por	0.3

- Model 1
    - Definitions
        - Variables 1> selection: domain 1, name: c_all, expression: c
        - Variables 2> selection: domains 2 & 3, name: c_all, expression: c2
        - Average 1> name: outlet, manually select outlet
    - Geometry (set to mm)
        - Block1

        - 0.06, 0.023, 4 (W, D, H)
        - {0, 0, 0}
    - Block2
        - 0.06, 0.023, 4 (W, D, H)
        - {0.075, 0, 0}
    - Block3
        - 0.135, 0.023, 0.06 (W, D, H)
        - {0, 0, 3.94}
    - Union1
        - Blocks 1-3
    - Block4
        - 0.06, 0.005, 4 (W, D, H)
        - {0, 0.023, 0}
    - Block5
        - 0.06, 0.005, 4 (W, D, H)
        - {0.075, 0.023, 0}
    - Block6
        - 0.135, 0.005, 0.06 (W, D, H)
        - {0, 0.023, 3.94}
    - Union2
        - Blocks 4-6
    - Block7
        - 1, 1, 4.5 (W, D, H)

- {-0.45, 0.028, 0}

- Materials
  - Water, liquid (Domains 1-2)
  - Poly-Si (Domain 3, Young's Modulus = 160e9 Pa, Poisson's ratio = 0.22, Density = 2320 kg/m^3)
- Free and Porous Media> select domains 2 & 3
  - change to incompressible flow
  - Fluid Properties 1> default settings
  - Wall 1> default settings
  - Initial values 1> default settings
  - Porous Matrix Properties> select domain 3, permeability: 50e-18 m^2, porosity: por
  - Inlet> select boundary, laminar inflow flow rate: 100e-9 [L/min], entrance length: 0.00001, check 'constrain endpoints to zero'
  - Outlet 1> select boundary
- Species Transport in Porous Media> select domains 2 & 3
  - Mobile Fluid, Immobile Solid> select velocity field, bulk density: 2320, porosity: por, fluid diffusion coefficient: diff
  - No Flux 1: Default settings
  - Initial values 1> concentration c1: 0
  - Free Flow> select velocity field, diffusion coefficient: diff
  - Inflow 1> select boundary, enter: 0
  - Outflow 1> select boundary

- Laminar Flow> select domain 1
  - change to incompressible flow
  - Convection and Diffusion> select velocity field
  - Fluid Properties 1> default settings
  - Wall 1> default settings
  - Initial values 1> default settings
  - Inlet> select boundary 1, laminar inflow flow rate: 0.1 [L/min], entrance length: 0.001, check ‘constrain endpoints to zero’
  - Outlet> select boundary 46
- Transport of Diluted Species 1> select domain 1, keep ‘convection’ box checked
  - Convection and Diffusion 1> Velocity Field: Velocity Field (spf)
  - No Flux 1: Default settings
  - Initial values 1> concentration c1: 0
  - Open Boundary> boundaries 1-2, 5, 46
  - Flux> inward flux: 0.02 [m/s] * (c2-c)
  - Concentration> select boundaries 1-5, 46, concentration: 1
- Mesh (physics controlled mesh, changed block 7 to coarser)

- Study 1
  - Step 1: Stationary> check ‘free and porous media flow and laminar flow’ modules
    - Enable ‘Direct’ solver
- Study 2

- Step 1: Time Dependent> check ‘species transport in porous media and transport of diluted species’ modules, set time range, under ‘Values of Dependent Variables’ check ‘values of variables not solved for’ and choose method: ‘solution’, study: ‘study 1, stationary’, selection: ‘automatic’
    - Enable ‘Direct’ solver
    - Changed to ‘Fully Coupled’ solved instead of segregated
    - Time-Dependent Solver 1> Time stepping> Change initial step to 0.5 s and max step to 1 s

- Results
    - Under ‘Data Sets’ add 3D Cut Line 1

(mm)	X	Y	Z
Point 1	0.03	0	2
Point 2	0.03	0.3	2

    - Under ‘Data Sets’ add 3D Cut Line 2

(mm)	X	Y	Z
Point 1	0.105	0	2
Point 2	0.105	0.3	2

    - Concentration
        - Slice 1: change c to c_all
    - 1D Plot Group
        - Global
            - Select appropriate solver in data set
            - Enter outlet(c_all)

- 1D Plot Group
    - Line Graph
        - Select Data Set: 3D Cut line 1
        - Enter c_all in y-axis data ‘expression’
        - Change x axis data parameter to ‘expression’ and enter y
- 1D Plot Group
    - Line Graph
        - Select Data Set: 3D Cut line 2
        - Enter c_all in y-axis data ‘expression’
        - Change x axis data parameter to ‘expression’ and enter y

Results

The following excerpt based on this model was published in Lee, W. H., et al. *Anal. Chem.* **2016**, *88*, 1230-1237.

Comsol modeling and simulation of 1 mM dopamine diffusing through the membrane of microfabricated probe. The microfabricated probe was constructed in COMSOL Multiphysics 4.4 (Burlington, MA) to model its recovery. The fabricated probe has semi-circular fluidic channels; but for ease of modeling, the channels were designed as 60 μm x 24 μm rectangles which gave the same cross-sectional area as the actual probes. The total length of the channels was 8 mm in a ‘U’ shape like the actual probe. The porous membrane was designed as a polysilicon rectangle, 5 μm x 60 μm, overlaid the channels. A large box was connected to the external boundary of the membrane region for simulating the probe in a well-stirred solution.

The ‘Free and Porous Media Flow’ and ‘Species Transport in Porous Media’ physics models were applied to the channel and membrane regions. Navier-Stokes equations modeled the fluid (water) in the open channel with a flow rate of 100 nL/min. Fluid movement in the porous region was defined by the Brinkman equation and a permeability of 50 nm^2 was used. The porosity variable was modified to match experimental data. For the transport of chemical species, the diffusion coefficient of dopamine, 6 x10-10 m^2/s was used†. The exterior probe volume used ‘Laminar Flow’ and ‘Transport of Diluted Species’ physics with a flow rate of 10 mL/min to simulate a well-stirred solution. Images below show cross section of probe at the middle and end of the probe color coded for DA concentration.

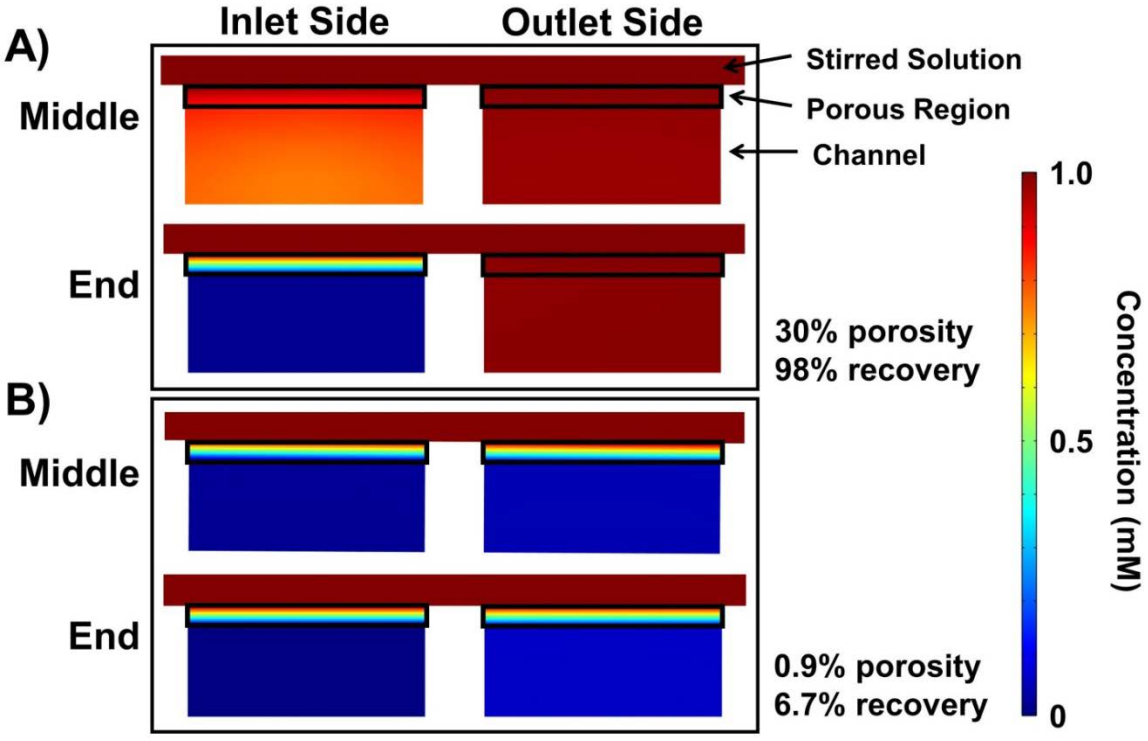

Figure E.1: A) Recovery for probe with 30% porosity and B) for 0.9% porosity.

† Gerhardt, G.; Adams, R. N. Anal. Chem. 1982, 54 (14), 2618–2620.